ABSTRACT

Title of Document: LIVE CELL IMAGING TO STUDY THE ASSEMBLY AND FATE OF AUTOPHAGOSOMES

Dale W. Hailey, Ph.D., 2008

Directed By: Professor Ian Mather, Cell Biology and Molecular Genetics

Autophagy (formerly macroautophagy) is a critical process that occurs in all Eukaryotes. Induction of the pathway results in formation of multilamellar membrane-delimited structures that engulf cytosolic proteins, organelles and intracellular pathogens *en masse*. Capture and catabolism are integral to the diverse roles of autophagy in recycling components, degrading aggregate-prone proteins, removing damaged organelles, depleting cells of organelles and cytosolic mass, and isolating intracellular pathogens. Despite recent attention, fundamental questions about autophagy remain. How do autophagosomes form? What exact roles do they play in non-starvation conditions? To investigate these topics, I developed live-cell imaging approaches to identify substrates and turnover rates of autophagosomes, and to survey intracellular membranes for putative roles in autophagosome formation. The following studies show that autophagosomes utilize lipid derived from the mitochondria during their formation, and that this is a unique aspect of starvation-

induced autophagy. During formation, autophagosomal markers transiently localize to punctae on the surface of mitochondria. A tail-anchored outer mitochondrial membrane protein freely diffuses into the newly forming autophagosome until the two organelles dissociate. Starvation-induced autophagosomes produced in this manner engulf cytosolic contents, are 3-MA-sensitive and persist only transiently in cells before fusing with lysosomes. These findings reveal that the outer mitochondrial membrane serves as a major membrane source for autophagosome biogenesis during starvation. Furthermore, the data define a new intracellular pathway from mitochondria to the autophagosomal/lysosomal system. Following, Chapter 1 provides a general survey of autophagy, Chapter 2 discusses advances in live-cell imaging and its use to identify autophagosome substrates, Chapter 3 discusses monitoring autophagosome turnover by photo pulse-labeling in live cells, Chapter 4 presents data implicating the use of mitochondrial membrane in the biogenesis of autophagosomes, and Chapter 5 reviews the implications of the data herein.

LIVE CELL IMAGING TO STUDY THE ASSEMBLY AND FATE OF AUTOPHAGOSOMES

By

Dale W. Hailey

Dissertation submitted to the Faculty of the Graduate School of the
University of Maryland, College Park, in partial fulfillment
of the requirements for the degree of
Doctor of Philosophy
2008

Advisory Committee:
Professor Ian Mather, Chair
Professor Stephen M. Wolniak
Associate Professor Wenxia Song
Assistant Professor Iqbal Hamza
Professor Tom Porter

Dedication

I want to dedicate this to three people--my wife Rachel Scherr and my parents Susan Worsfold and Warren Hailey.

Rachel has been my wife and dearest friend now for almost twenty years. I watched her write her dissertation, and now she has had the dubious honor of watching me finish mine. She is just what a busy graduate student needs—a tireless juggler of the day-to-day details, who is always a rock of reassurance. She makes me laugh and feel at home anywhere--even in the lab late at night. Thank you R.

Growing up on a farm was the perfect set for me. I didn't know it then, but I have my parents to thank for a childhood rich in sensation. The Rathdrum prairie and Coeur d'Alene lake were full of the tactile things that draw a biologist in. My parents gave me a beautiful place to grow up and a sense of ownership of that space. They wanted me to enjoy Coeur d'Alene and they wanted me to see the "bigger" world. My mom struggled with the local school district to get an eighth grade algebra program in place. My dad put in long hours at the Potlatch log deck to pay for our travels. Thank you Mom and Dad for the innumerable things that you have done for me and the subtle ways you have encouraged me. Now that I'm a parent, I have some sense of how much work that can be.

Acknowledgements

I am of course very much indebted to my advisor at the National Istitutues of Health—Jennifer Lippincott-Schwartz. I worked in her lab during my tenure as a University of Maryland graduate student and she acted as the advisor of the work herein. Jennifer has an uncanny knack for surrounding herself with people who shamelessly adore cell biology. Both her own enthusiasm and the enthusiasm of the people around her is infectious, and I have enjoyed an environment of insight and excitement during my tenure at NIH. Being a biologist requires a measure of awe, and it is truly wonderful to have worked in an environment that supports the notion that we should be amazed. The fact that biology works at all, that we can see into it, should give us pause—a short pause before trying another experiment. I owe Jennifer a tremendous amount for bringing me into a scientific community.

Members of the lab have contributed scientific ideas, persistence, and expertise in addition to their friendship and humour. In particular, I want to thank Peter Kim and Holger Lorenz for lunchtime and hotel lobby autophagy debates. Those conversations initiated much of the work that follows. Kasturi Mitra has also been a bank of knowledge about mitochondria, and of course Rachid Sougrat's EM expertise is irreplaceable.

Many lab members have contributed in less obvious ways, and for those, I want to say that I am deeply indebted to the scientists that are passing or have passed through Jennifer's lab, many of whom are now scattered around the globe. In particular, I want to thank Win Arias for being the most gracious scientist one could

hope to meet, and encouraging me through the years both by his smile and his example.

Beyond the NIH fence, I want to thank members of the University of Maryland. Todd Cooke initially encouraged me to join the graduate program at the University of Maryland despite my serpentine path to graduate school. And Steve Wolniak initially served as my on-campus advisor, and later gave me the opportunity to assist with his fantastic cell biology class. I especially want to thank Ian Mather who became my University of Maryland advisor while spending a sabbatical at the NIH. He is marvelously encouraging and supportive, and his United Kingdom sensibilities always leave me with a smile. I will remember with some sardonic joy dealing with the red tape of mouse transport around the beltway. Ian is always frank and sincere about this academic path. Even without the accent, he is a model of integrity.

Lastly, I want to thank my two sons who are much too young to care about acknowledgements. They have been constant reminders of the bottom line. Why do we study biology? Of course I could trot out the usual suspect--it improves health. While that is true, the boys remind me of another reason. We went to the moon in part to say wow. The bugs and the plants are closer but no less stunning. Jordan shows the symptoms of living with a biologist already, with his gesture and emphatic "I'm keeping that thought in my brain." Maybe we will know something about what on earth that means in his lifetime.

Table of Contents

List of Figures

Chapter 1: The Execution and Output of Autophagy

The following chapter reviews current literature on autophagy, beginning with a review of the history of the field and concluding with current knowledge of the formation of autophagosomes.

Autophagosomes are unique multilamellar organelles that engulf intracellular components. Their captured substrates include freely diffusing proteins in the cytosol as well as large structures like peroxisomes, mitochondria, ER fragments, aggregated proteins, and a variety of intracellular pathogens (Cuervo, 2004; Kirkegaard et al., 2004; Klionsky, 2007). Ultimately autophagosomes fuse with lysosomes, merging the delimiting membranes of autophagosomes with lysosomal membranes. These fusion events deliver the lysosome proton ATPase pump to the outer membranes of the hybrid organelle—the autolysosome--and expose its contents to lysosomal proteases. Contents of autolysosomes are degraded and at least some products produced by catabolism of the substrates are transported back to the cytosol (Figure 1). This recycling activity of autophagy underlies its well-characterized and best-known role—to promote survival during starvation (Klionsky and Emr, 2000).

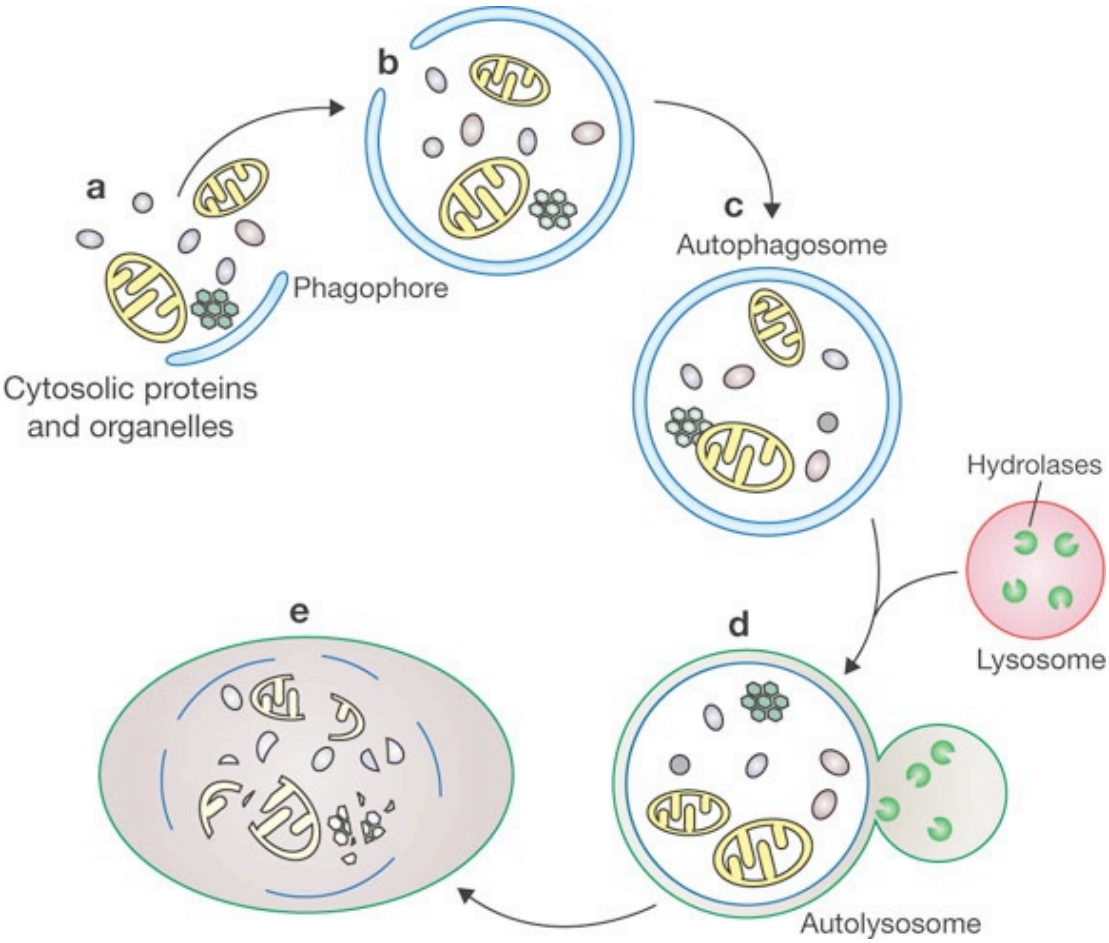

Figure 1: Capture and degradation of cytosolic proteins and organelles by autophagy. Freely diffusing cytosolic components as well as protein aggregates and organelles like peroxisomes and mitochodria (a) are engulfed by autophagosomes *en masse*. (b). How this engulfment is orchestrated is unclear. However, the output is a multilamellar organelle whose outer membrane fuses with the lysosome (c). Fusion of the delimiting membrane with the lysosomal membrane produces an acidic hybrid organelle—the autolysosome (d); subsequently, lysosomal proteases catabolize the captured substrates (e). (from Xie and Klionsky, 2007).

1. Autophagy and cellular metabolism

Starvation is a ubiquitous aspect of life. Constitutive processes required for life consume energy and components. Many organisms can execute programs to restrict metabolic activity when faced with limited nutrient and energy supplies (i.e. formation of quiescent spores in single celled organisms, dormancy and seed generation in plants, hibernation in animals.) However, evolution has strongly selected means to maintain metabolic activity in the absence of continual input from the environment. Most organisms orchestrate reactions that convert chemical energy into stores that can be liberated by regulated enzymatic activities as needed. Glycolysis is one instance of this; not surprisingly, it is one of the most ancient metabolic processes known (Romano and Conway, 1996). However, chronic starvation can severely deplete energy and molecular components, and during these periods, Eukaryotic organisms can activate autophagy. Autophagy, formerly called macroautophagy, retrieves molecules and energy via bulk degradation of intracellular components. Hence its name: auto—"self" and phagy—"eating."

Christian de Duve coined the term autophagy in 1963. Digestion occurs at the organism level in order to deliver energy and components into a living system; by analogy, de Duve described digestion at the cellular level that catabolizes substrates to support cell homeostasis (De Duve and Wattiaux, 1966). Electron micrographs of rat liver tissue in the 1950s and 1960s revealed the presence of unique inducible multilamellar structures that formed in response to starvation. EM studies suggested these structures catabolized cytosolic contents during their maturation (Ashford and Porter, 1962).

In 1967, the hormone glucagon was reported to induce autphagosome formation (Deter et al., 1967). Glucagon, released in response to decreasing blood glucose, induces autophagy in the liver. Consequently, glycogen granules (the animal equivalent of starch) are engulfed and catabolized in the liver to feed metabolic pathways. Regulation by glucagon established a role of autophagy in regulated metabolism. Another metabolic hormone, insulin, was later shown to repress autophagosome formation (Pfeifer, 1977). In low glucose conditions, autophagy is induced by glucagon to liberate glucose from glycogen granules in the liver; conversely, raising blood glucose results in insulin release, and suppression of autophagy

Later studies demonstrated control of autophagy by regulatory kinases involved in metabolic control. The kinase mTOR (mammalian target of rapamycin) integrates many metabolic signals, and its activity continuously suppresses autophagy when amino acids are replete. In the absence of amino acids and in other starvation conditions, mTOR kinase activity decreases, releasing a block on autophagy (Kanazawa et al., 2004). The regulatory control of autophagy by metabolic signaling all point to integration of the autophagy pathway into the metabolic circuitry of organisms.

Early work on autophagy was in part motivated by diabetes research. Prior to the discovery of insulin, starvation was employed as a means to diminish the dire effects of excessive blood glucose in diabetic patients. Exploring the physiological consequences of the "starvation diet" motivated work with nutrient deprived rats. That work first identified the organelles termed autophagosomes. Only a handful of

labs worked on autophagy through the 1980s. Although morphological readouts of autophagy existed (e.g. transmission electron microscopy of liver and other tissues), studying the autophagic process was intractable. In 1982, Seglen and Gordon were the first to publish a biochemical analysis of autophagy, two decades after de Duve's initial morphological description. Seglen and Gordon also identified 3-methyladenine—a small molecule inhibitor of autophagy (Seglen and Gordon, 1982). A smattering of other tools became available, but the field was largely static until the mid 1990s. Because autophagosomes engulf diverse intracellular substrates, even with protocols to efficiently isolate these organelles, there were few biochemical readouts that could be used to screen for autophagy effectors or further develop subcellular fractionation techniques. Some initial biochemical analyses of isolated autophagosomes identified abundant cytosolic substrates. However, these analyses were not successful in identifying the molecular components of autophagosomes.

2. Identification of autophagy genes

In 1992 Kazuhiko Takeshige in Yoshinori Ohsumi's laboratory published the first description of autophagy in the budding yeast *Saccharomyces cerevisiae.* The authors identified mutants in vacuolar proteinases (e.g. PRB1) that accumulated spherical structures within their vacuoles, the functional equivalent lysosomes in higher Eukaryotes. Formation of these intravacuolar structures was induced by a number of conditions including starvation for nitrogen and carbon. The authors reported that the induced structures were analogous to autophagosomes. Because of reduced proteolytic activity in the vacuole, the structures failed to degrade, and as a consequence, the membrane delimited structures accumulated. The authors named

these structures autophagic bodies (Figure 2) (Takeshige et al., 1992). Ohsumi's group was able to leverage these initial visual observations. His group isolated mutants in a vacuolar proteinase deficient background based on their failure to form autophagic vacuoles. The first of these mutants (Atg1) was used to characterize other conditions subsequently employed to identify additional yeast autophagy mutants. Autophagy mutants identified by the Ohsumi group fell into 15 complementation groups—all of which had defects in bulk protein degradation and showed rapid cell death under starvation conditions—a phenotype easily screened for using yeast replica plating. Tsudaka and Ohsumi published findings from the initial screen in FEBS letters (Tsukada and Ohsumi, 1993). Despite the article's relative obscurity, it set the stage for identifying and characterizing the suite of proteins now established as the core components responsible for autophagosome regulation and formation.

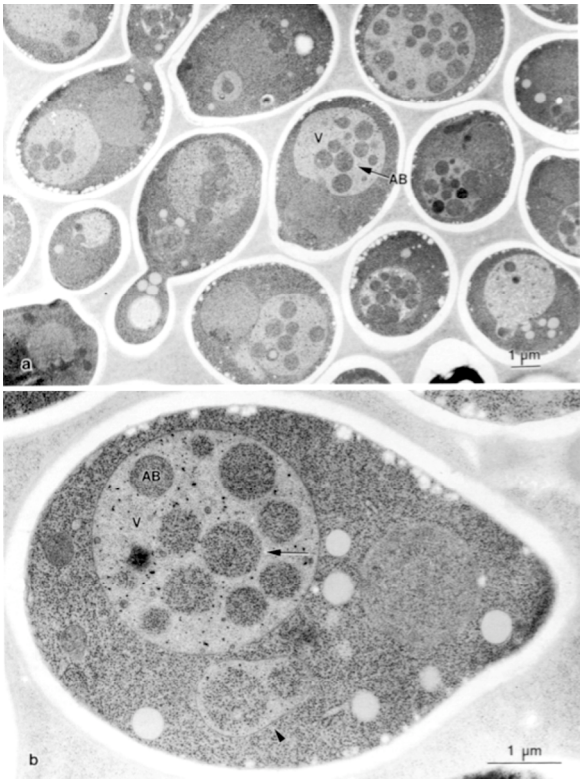

Figure 2: *S. cerevisiae* autophagic bodies in proteinase deficient cells. When starved for nitrogen by growth in SD –N for 2 hours, yeast vacuoles (V) accumulate intravacuolar bodies. These structures, termed autophagic bodies (AB) by the authors, have an electron density like that of the cytosol and are the yeast functional equivalent of mammalian autophagosomes. The phenotype of these cells made possible the first genetic screens that identified autophagy components. (from Takeshige et al., 1992)

Concurrent with the work from Ohsumi's lab, Dan Klionsky's group identified yeast mutants that failed to complete the proteolytic processing of aminopeptidase 1 (API). The API precursor is synthesized in the cytosol and delivered to the yeast vacuole as a 61kD protein. Following its delivery to the vacuole, API is activated by proteolytic processing to generate a 50kD hydrolase. The screen identified mutants that accumulated the 61kD form in the cytosol in order to identify factors required for API delivery to the yeast vacuole (Harding et al., 1995). Findings from Klionsky's lab were published in 1995 and established the Cvt (cytoplasm to vacuole) pathway. In the following year Ohsumi and Klionsky together published a paper reporting on the shared machinery used by the autophagy and the Cvt pathways in *S. cerevisiae*, and described what have come to be called the core autophagy (Atg) proteins (Scott et al., 1996).

Several technological advances accelerated autophagy research as the yeast Atg genes were identified . (1) The green fluorescent protein was described in the 1970s (Prendergast and Mann, 1978) but wasn't popularized as a fluorescent reporter until 1994 (Chalfie et al., 1994). (2) RNAi silencing was discovered in plants in 1992 and first used in an animal (*C. elegens*) in 1998 (Fire et al., 1998). (3) Whole genome sequences also came available. The *S. cerevisiae* genome was completed in 1996, *C. elegans* genome in 1998, and *H. sapiens* genome in 2001. The role these technologies continue to play in the development of the autophagy field is profound. GFP fusions to Atg proteins are ubiquitously used now as autophagosomal markers (Mizushima et al., 2004), RNAi knockdowns are employed to identify previously

unappreciated functions of autophagy, and genomic sequences are used to identify autophagy homologs in higher eukaryotes, to establish RNAi screens, and to engineer mutant autophagy proteins. Fortuitously, homology searches in higher eukaryotes have revealed that autophagic machinery is strikingly well conserved across the Eukaryotic domain at both the structural and functional level. While one could argue that this indicates the ubiquitous experience of starvation by all organisms, an alternative explanation is likely--that autophagy is involved in far more intracellular processes than was previously appreciated.

3. New functions of autophagy in higher eukaryotes

There has been a tremendous interest in autophagy since the initial identification of the Atg genes. Despite being described for decades, its role in general aspects of cell homeostasis beyond the scope of starvation was largely unappreciated until the late 1990s. Autophagy is now implicated in diverse processes and has received considerable attention from the fields of development, cancer and cell death, immunity and neurodegeneration. Following is a survey of the initial observations and studies that implicate autophagic processes in these diverse fields.

Since identification of Atg genes, a number of studies have implicated autophagy in developmental programs. Studies in *Drosophila melanogaster* reveal autophagic structures within developing salivary glands that presumably consume and catabolize cytosol in order to deplete cells of volume and ultimately induce "autophagic cell death", thereby clearing cells for the formation of a lumen (Berry and Baehrecke, 2007). Developmental programs activated by nutrient stress are perturbed in *Arabidopsis thaliana*, affecting leaf senescence and the development of

inflorescences (Doelling et al., 2002). In *C. elegens*, nutrient restriction or high population density lead to an arrest at the dauer larval stage, and dauer formation is abnormal in a number of autophagy mutants (Melendez et al., 2003). Recently autophagy has been implicated in mammalian nervous system development (Figure 3). Ambra1 knockout mice were reported to exhibit defects in regulated cell proliferation of the nervous system (Fimia et al., 2007). Developmental defects observed in autophagy mutants are often attributed to failures in the execution of cell death programs during tissue morphogenesis. However, knockout mice have revealed other defects that demonstrate that the catabolic capacity of autophagy is required during stages of mammalian development. Atg5 knockout mice die shortly after birth following the transition from placental nourishment to suckling (Kuma et al., 2004). The parsimonious explanation is that autophagy plays a transitional role by supplying nutrients to sustain mice pups during nutrient depletion. Interestingly however, the Atg5 knockout mice cannot be recovered by intravenous supplementation immediately following birth. Whether this is because of relying on nutrients supplied through the blood stream is insufficient at this transition or whether some other effect is at play is currently unclear.

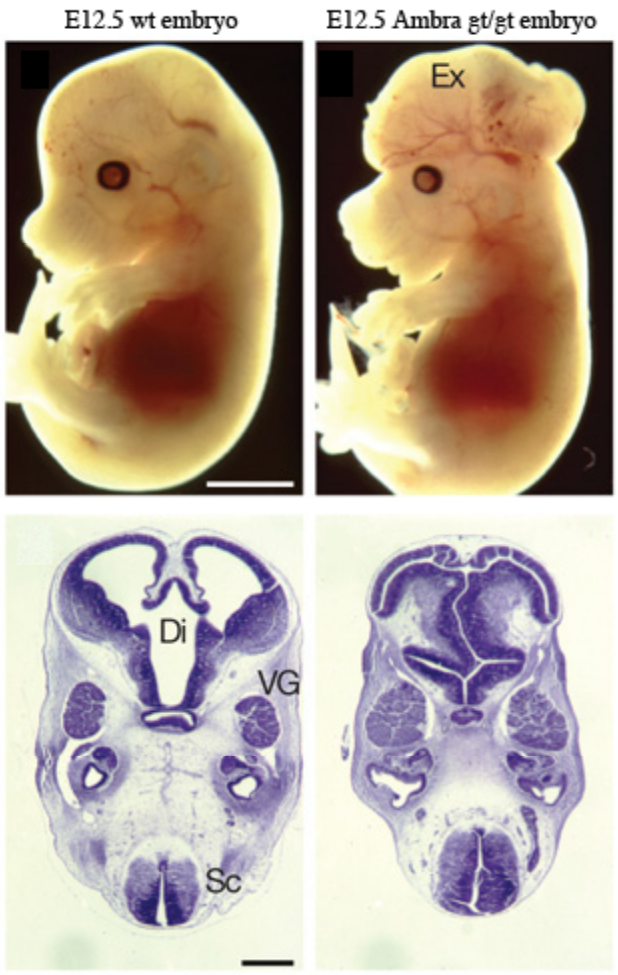

Figure 3: Abnormal development of the nervous system in Ambra1$^{gt/gt}$ autophagy-deficient mice. Insertion of the lacZ gene into the Ambra1 locus disrupted Ambra1 function and provided a reporter for expression of the interrupted gene. The disruption is embryonic lethal (notably, the embryos die at an earlier stage than is observed for Atg5 or Atg7 knockout mice.) Ambra1$^{gt/gt}$ mice show exencephaly (brain development outside the skull) (Ex) (top L versus top R), as well as neuroepithelium proliferation in the spinal chord (Sc) diencephalon (Di) (i.e. interbrain: thalamus, hypothalamus etc.) and fifth ganglia (VG). (bottom L versus bottom R). (from Fimia et al, 2007.)

Autophagy has received a tremendous amount of interest from the cancer field. In 2006, the first joint Keystone meeting on autophagy and apoptosis was held, and it is now fair to say that interest in autophagy has eclipsed interest in apoptosis as a potential cancer target. The role of autophagy in cancer was initially reported in a study from Beth Levine's group. The mammalian homolog of Atg6 (Beclin 1, a component of the regulatory Vps34 Class III PI3 Kinase complex required to initiate formation of autophagosomes) is mutated in a high percentage of breast cancer cell lines. Functional Beclin 1 acts as a tumor suppressor (Liang et al., 1999). This role of autophagy in maintaining death capacity and suppressing tumourogenesis is most likely related to its role in developmental programs, and a number of studies have investigated whether caspase activation and autophagic cell death are coordinated. Although much of the interest in the cancer field has been in potentiating cell death execution by inducing autophagy, there are cases in which autophagy may be oncogenic. Tumors may persist in hypoxic conditions by activating autophagy (Dayan et al., 2006; Pouyssegur et al., 2006), and autophagy can degrade damaged mitochondria and consequently potentially suppress apoptotic signaling (Colell et al., 2007).

The role of autophagy in immunity was first suggested by experiments showing that the Epstein-Barr nuclear antigen (EBNA; the major antigen associated with latent viral infection) required autophagy for loading on MHC Class II molecules. These studies demonstrated a functional role for autophagy in immunity. When autophagy was inhibited, recognition by EBNA specific T-cells was compromised (Paludan et al., 2005). Because autophagosomes have been shown to

capture a number of intracellular pathogens including *Mycobacterium tuberculosis*, *Legionella pneumophila* and *Coxiella burnetii* (Kirkegaard et al., 2004) it is not surprising that it affects delivery of pathogens to the lysosomal environment and thereby affects production of antigens via proteolysis within the lysosome and generation of antigenic peptides from these pathogens. Prior to autophagy's documented role in immunity, innate immunity was ascribed to delivery to the lysosome via the endosomal system.

Lastly, autophagy has received much attention as a potential therapeutic target for treatment of neurological diseases (Rubinsztein et al., 2007). The formation of protein aggregates is a hallmark of many neurological diseases including Alzheimer's, Parkinson's and polyglutamine tract expansion diseases like Huntington's. The capacity for autophagy to degrade protein aggregates has been established in a number of contexts. In autophagy-defective Atg7 knockout mice, large ubiquitin-positive aggregates accumulate, suggesting that autophagy, while inducible, has a constitutive basal activity that clears aggregated or aggregate-prone proteins (Komatsu et al., 2005). In 2004 Ravikumar et al reported that autophagy is induced by polyglutamine tract expanded proteins by trapping the inhibitory kinase mTOR in beta-sheets formed by aggregations of these proteins. Consequently the regulatory kinase mTOR is inactivated and autophagy is derepressed. The authors propose that this process is a general means for cells to respond to accumulations of aggregated proteins in order to degrade these aggregates prior to acute toxicity. Indeed, upregulating autophagy in fly models of Huntington's disease extends the lifespan of neurons expressing the Huntington protein (Ravikumar et al., 2004).

In addition to cytosolic aggregates, autophagosomes are also reported to capture misfolded proteins in membrane compartments. In 2000, Teckman et al published a study of α1-antitrypsin, a protein secreted by the liver. A mutant form of this protein (ATZ) misfolds and aggregates in the ER, causing severe liver damage. Accumulations of mutant ATZ result in the proliferation of autophagosomes that engulf ATZ aggregations in the ER. (Teckman and Perlmutter, 2000). Autophagosomes also proliferate during the progression of Alzheimer's disease, possibly due to overexpression of peptides from the Beta protein that inhibit proteasome activity (Nixon et al., 2005). Autophagic vesicles are rare in normal brain tissue; however, they are commonly observed in brain tissue from Alzheimer's patients.

The ability of autophagy to capture protein aggregates in a number of different contexts has motivated interest in using autophagy as a therapy in protein aggregation diseases. The hope is that by employing the so-called housekeeping function of autophagy, the formation and accumulation of protein aggregates can be suppressed (Rubinsztein et al., 2007). While initial studies like those in the fly models of both Huntington and SBMA (Spinal and bulbar muscular atrophy) are encouraging, neurological diseases are a particular challenge because their etiology remains unclear and may involve decades of accumulated contributions that lead to the final toxicity of diseases.

4. Functional groupings of autophagy proteins

Execution of autophagy in Eukaryotes results in the formation of multilamellar vesicles that engulf cytosolic proteins and organelles *en masse*. The

biogenesis of autophagosomes is clearly distinct from events that underlie formation of most intracellular vesicles. Canonical budding events typically involve recruitment of a protein coat (e.g. a clathrin lattice) to deform a single membrane into a bud. The membrane bud then undergoes a fission event to generate a small volume enclosed by a single membrane. The multilamellar (typically double-lamellar) structure of autophagosomes implicates some other biogenesis program. How exactly autophagosomes form remains unclear--addressed in more detail in chapters 4 and 5. Despite the lack of a clear picture of autophagosome biogenesis at present, autophagy proteins can be subdivided into functional groups (regulation, initiation, expansion and maturation, and fusion) that act sequentially in the process of autophagosome biogenesis.

4.a. Regulation

Rapamycin is currently the best-known regulator of autophagy and the first small molecule regulator used to unravel the pathways regulating autophagosome biogenesis. The regulatory role of mTOR (mammalian target of rapamycin) was reported in 1995 by Fred Meijer's group. Blommaart et al showed that insulin treatment (used to repress autophagy) resulted in phosphorylation of a 31kD protein. The authors identified this protein as the ribosomal protein S6 (Blommaart et al., 1995). S6 is phosphorylated by the p70 S6 Kinase. When phosphorylation of S6 is inhibited by Rapamycin treatment, autophagy is induced. (Rapamycin inhibits mTOR kinase, a positive regulator for p70 S6 kinase dependent phosphorylation of S6.) The authors proposed that autophagy is regulated in an inverse manner to general protein synthesis—a conceptually appealing model for cell growth regulation.

Under replete conditions, cells freely incorporate components into proteins (S6 active) and inhibit intracellular recycling. Under starvation conditions, cells downregulate new protein synthesis (S6 inactive) while retrieving components to maintain critical functions within the cell. Regulation of the S6 ribosomal component therefore acts as a metabolic switch toggling between autophagy and protein synthesis.

The exact role of the Atg regulatory proteins including Atg13, Atg17 and the kinase Atg1 is ambiguous. These proteins are however the most upstream factors involved in autophagosome formation. Assembly of the proteins into a complex activates the Atg1 kinase. In 2007 Lee et al demonstrated that *D. melanogaster* Atg1 kinase inhibits TOR activity. Additionally, siRNA knockdown of Atg1 results in increased S6 phosphorylation. Therefore, Atg1 activity appears to mimic Rapamycin treatment (Lee et al., 2007). How exactly the Atg1 kinase promotes the formation of autophagosomes is not clear; however, it does not appear to be through transcriptional regulation. We and others have observed that autophagosome formation efficiently occurs in the presence of protein synthesis inhibitors like cyclohexamide. This is not surprising given that autophagy is induced during a general repression of protein synthesis. The most likely current scenario is that the Atg1 kinase in some fashion activates the complex responsible for initiating sites of autophagosome biogenesis.

4.b. Initiation

Autophagosome biogenesis is initiated through the activity of a Class III PI3 kinase complex including Atg6 (yeast homolog of Beclin 1) and Vps34 (Cao and Klionsky, 2007; Furuya et al., 2005). Most but not all autophagic inductions fail to

proceed when activity of this complex is blocked. The Class III PI3 kinase complex targets phosphatidylinositol to generate phosphatidylinositol(3)phosphate, here abbreviated PI(3)P. (Note this is not the PIP3 produced by ligand-dependent activation of many cell surface receptors. PIP3 is phosphorylated at three sites, and is associated with growth factor engagement and inhibition of autophagy.)

The Class III (Vps34) PI3 kinase complex has been the source of much interest since it appears to initiate autophagosome formation (discussed more in chapter 4). Mutants in this complex, based on epistasis experiments in yeast, affect the most upstream stage of autophagosome biogenesis (Suzuki et al., 2004). The complex can be inhibited by a number of small molecules, including the first autophagy inhibitor identified by Seglen and Gordon--3 methyladenine.

Proteins that regulate activity of this complex continue to be identified. UV irradiation resistance-associated gene (UVRAG) was identified in 2006 and shown, like Beclin 1, to be a tumor suppressor and positive regulator of Class III PI3 kinase activity (Liang et al., 2006) Recently EndophillinB/Bif-1 was also shown to interact with the complex via interaction with UVRAG, and act as an inducer of autophagy (Takahashi et al., 2007). Interestingly, Bif-1 has a BAR domain that may interact with a precursor membrane to tether the PI3Kinase complex to a precursor membrane. Notably, it remains unclear how exactly the Class III PI3 Kinase complex initiates autophagy. It is likely that the PI(3)P lipid initiates autophagosome formation. However, other scenarios are possible in which other aspects of the complex like the presence of BAR domains modify the initiation site.

4.c. Expansion and Maturation

Initial growth and expansion of autophagosomes requires a well-characterized set of Atg proteins including Atg4, Atg5, Atg7, Atg8, Atg10, Atg12 and Atg16 (Xie and Klionsky, 2007). The first publications describing the function of these Atg proteins described two sets of reactions that first recruit a complex of Atg5, Atg12, and Atg16 to a precursor membrane (Atg12 and Atg5 in this complex are covalently bound) (Figure 4) (Mizushima et al., 1998). Subsequently Atg8 is recruited from the cytosol and retained on the same precursor autophagosomal membrane by a catalyzed covalent bond to the amine group of the lipid phosphotidylethanolamine (PE) (Ichimura et al., 2000). What exactly these proteins do remains unclear; however, they appear to play structural roles in autophagosome biogenesis. The reactions that covalently bind Atg12 to Atg5 and Atg8 to PE are strikingly similar to ubiquitination reactions. Ubiquitin is activated by an E1, conjugated by an E2, and ligated by an E3 ligase to covalently attach ubiquitin to a substrate (Ohsumi, 2001). Notably, Atg12 and Atg8 are ubiquitin-like proteins that undergo near identical reactions as ubiquitin. The outcome of the reactions is recruitment of these proteins from the cytosol onto membrane precursors of autophagosomes. In both mammals and yeast, the Atg5/Atg12/Atg16 protein complex is recruited first, and its recruitment is required for the subsequent recruitment of Atg8 (Mizushima et al., 2001). While the Atg5/Atg12/Atg16 complex rapidly dissociates from autophagosomal membranes at an early stage in biogenesis (see chapter 3 for experimental evidence), Atg8 bound to PE is retained on autophagosomal membranes through their fusion with lysosomes (Kabeya et al.,

2000). These proteins and reactions are strikingly well-conserved from yeast to humans.

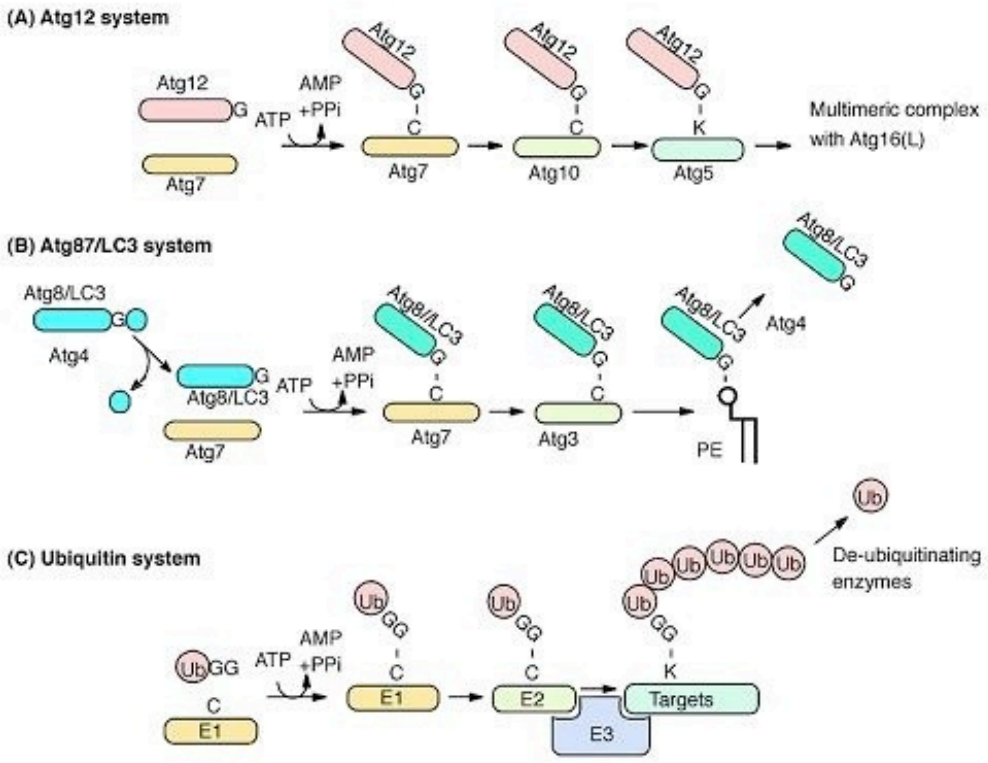

Figure 4: The Ubiquitin-like conjugation systems required for lipidation of the Atg8 and its retention on membranes. The Atg12 system covalently binds the ubiqutin-like protein Atg12 to Atg5 through a series of reactions (A). These reactions chemically mimic the E1/E2/E3 reactions required to ubiquitinate target proteins at lysine residues (C). A second set of E1/E2/E3 reactions covalently binds Atg8 to NH_2 in the head group of phosphotidylethanolamine (PE) (effectively acting like amino group in the lysine-ubiquitin reaction) (B). Both sets of reactions are required for autphagosome formation. (from Ohsumi Y., 2001.)

4.d. Lysosomal Fusion and Degradation

What exactly regulates fusion of autophagosomes with lysosomes is unclear at this time. Thus far, there are no known mechanical processes like v-SNARE/t-SNARE interactions to catalyze the fusion event. Two late endosomal Rab GTPases, Rab7 and Rab9, are reported to colocalize with the Atg8 homolog LC3 in starved mammalian cells. Rab7 also appears on enlarged autophagosome-like structures that contain the pathogen *Coxiella burnetii* (Gutierrez et al., 2004), and the GTP bound state of Rab7 is reported to affect fusion of autophagosomes and lysosomes (Young et al., 2006). Lysosomal status clearly affects the fusion process. Drugs that inhibit lysosomal proteolysis by affecting the pH of the lysosome (e.g. bafilomycin, ammonium chloride, and chloroquine) are widely reported to block fusion with autophagosomes, though the mechanism is unknown (Klionsky et al., 2008b). The status of microtubules also perturbs autophagosomal/lysosomal fusion events, as global microtubule depolymerization by drugs like nocodazole and vinblastine stalls conversion of autophagosomes to autolysosomes (Kochl et al., 2006). This may owe to microtubules providing a scaffold that spatially restrains autophagosomes and lysosomes and promotes membrane contact of the organelles. It is well-established that autophagosomes move along microtubules; notably, the best characterized Atg8 homolog was first named MAP1LC3 for microtubule-associated protein 1 light chain 3. Although the processes that catalyze fusion remain vague, what is clear is that this fusion merges the outer delimiting membrane of the autophagosome with the membrane of the lysosome; consequently, interior membrane(s) and engulfed substrates are exposed to lysosomal proteases. Atg8 signal is rapidly lost from

autolysosomes, both via proteolysis of the interior membrane(s) and cleavage from the surface of the autolysosomal membrane by the enzyme Atg4.

5. The autophagosome biogenesis and destruction program

Our current understanding of the biogenesis and fate of autophagosomes rests on experiments carried out in a wide variety of systems and contexts. The most common tool for exploring the behavior of the autophagy pathway has thus far been starvation. However, a growing number of conditions are used experimentally to induce formation and turnover of autophagosomes. A key question in the autophagy field is whether autophagy is simply autophagy, or whether induction conditions fundamentally affect the execution and output of the process (Figure 5). As the autophagy field develops, it is increasingly clear that fundamental aspects of autophagy must be different in some regards. Developing robust and efficient techniques to examine the biogenesis and fate of these structures is a first step in addressing this question. In the following chapters I investigate this question with techniques adapted from live-cell imaging.

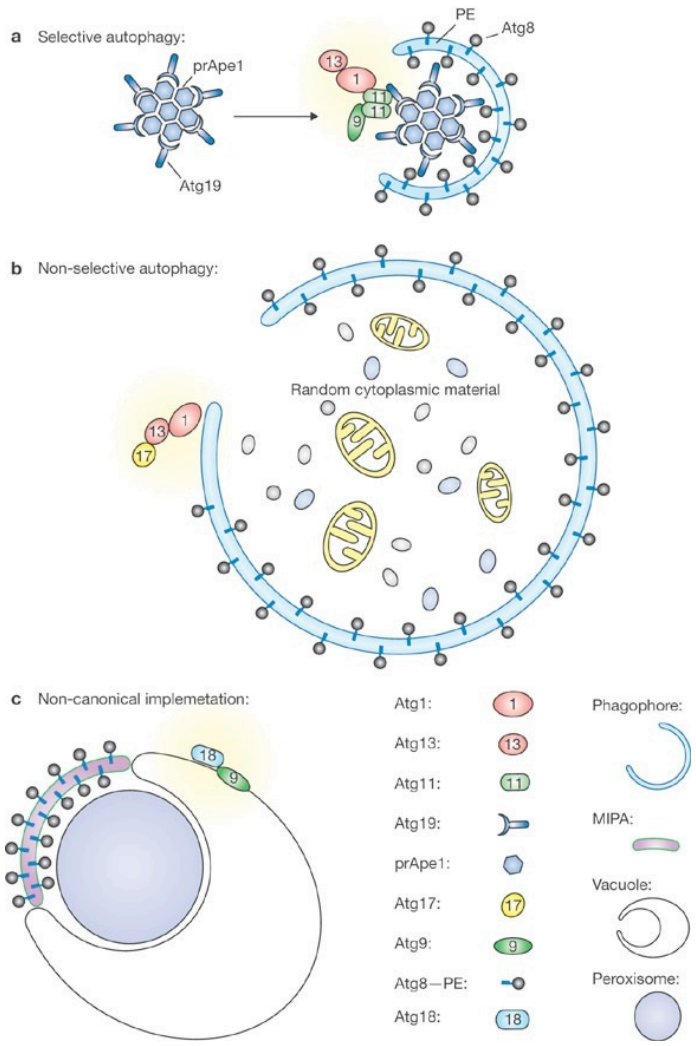

Figure 5: Reported forms of autophagy reveal distinct processes orchestrating autphagosome formation. Delivery of the precursor of Aminopeptidase 1 (Ape1) to the yeast vacuole utilizes autophagy components to selectively envelope a crystalline protein core within an autphagosome-like membrane. This cytoplasm to vacuole targeting (Cvt) pathway is constitutively active (a). Non-selective (and inducible) autophagy requires enveloping a fluid phase. No structural core is present to orchestrate membrane assembly around the core or deform the membrane. (b) Reports in yeast indicate that autophagosomal membranes can "cap" peroxisomes against the yeast vacuole during their engulfment (c). Currently it is unclear whether there is a universal biogenesis program that underlies all of these processes. (from Xie and Klionsky)

Chapter 2: Technological Developments in the Imaging and Labeling of Autophagosomes

The following chapter begins with a general consideration of why imaging methodologies are well-suited for the study of autophagy. I then discuss advances in live cell imaging, first by considering improvements in microscopy systems and second by considering advances in live cell fluorescent labeling technology. Finally I present techniques I have developed that use live cell imaging in order to characterize autophagy proteins and identify autophagy substrates.

1. Labeling subpopulations of proteins by laser targeting

As discussed in Chapter 1, the formation and degradation of autophagosomes involves recruitment of a subset of Atg proteins to precursor membranes, retention of some Atg proteins on those membranes through maturation into autophagosomes, and ultimately, delivery of an Atg protein subset and autophagy substrates to the autolysosome. Monitoring autophagy therefore involves tracking a dynamic set of components as they transit various states within the cell. Tracking the itineraries of proteins as they target and move through membrane systems has been a long standing interest of the lab where this work was done. In the early 1990's Jennifer Lippincott-Schwartz' group at the National Institutes of Health pioneered studies to quantify the kinetics of protein movement between the endoplasmic reticulum and Golgi membrane systems. Those dynamic studies revealed underlying and unexpected aspects of protein secretion. Extensive previous work had intuited models from in

vitro reconstitutions of the secretory pathway and snapshots from electron microscopy and antibody-based studies. The use of GFP-based live cell imaging introduced a new methodology. Initial studies in the lab followed flux of fluorescently labeled transmembrane proteins (e.g. vesicular stomatitis G Protein and galactosyltransferase) between the endoplasmic reticulum and Golgi systems (Cole et al., 1996). Later studies looked at binding of cytosolic effectors (e.g. ADP ribosylation factor 1 and Sar1 GTPase) to membranes (Presley et al., 2002).

One of the most powerful aspects of live cell imaging that underlies much of the work from the Lippincott-Schwartz lab is the ability to selectively label subpopulations of proteins in living cells and follow the dynamic behavior of those populations. Different states of proteins are typically all present within a cell. Hence, an ongoing challenge in microscopy is this: How do you follow a particular state of a protein against the backdrop of the other states? The development of microscopes with the ability to direct highly focused laser beams to discrete regions in a cell, and use of genetically encoded bleachable fluorescent tags made it possible to selectively label (or "unlabel" via bleaching) protein subpopulations (Lippincott-Schwartz et al., 2003). On the face of it, it is a simple advance, but selective photobleaching has broad applications. Effectively, developments in laser targeting and genetically-encoded fluorescent protein labeling make subcellular fractionation of unperturbed living cells possible. The lab continues to advance this approach, now with developments like sptPALM to monitor populations of single molecules in living cells and quantitatively extract subsets of populations with different diffusion rate signatures (Manley et al., 2008).

2. Developing Microscopy Systems with Selective Laser Targeting

Technology to photobleach living cells with laser light was available decades before genetically encoded fluorescent proteins were described. Watt Webb's group published a technical description of spot bleaching in 1976 (Axelrod et al., 1976). Pioneering photobleaching experiments involved targeting a focused laser to a point on a fluorescently labeled membrane. Images were captured to follow reappearance of fluorescence signal in the photobleached spot. This reappearance was analyzed in order to follow movement of non-bleached fluorescent molecules back into the bleached region. Photobleaching and recovery analyses provided a novel readout for the rate of diffusion of a particular fluorescent molecule in its particular cellular context. Webb and others used the acronym FPR (fluorescence photobleaching recovery) to refer to this approach; now FRAP (fluorescence recovery after photobleaching) is more commonly.

While photobleaching experiments were used in cell biology in the 1970s and 80s, microscope manufacturers did not extensively support FRAP experiments until Green Fluorescent Protein tagging became commonplace (Reits and Neefjes, 2001; White and Stelzer, 1999). Arguably, it is fortuitous that GFP can be bleached with a relatively low amount of low energy (490nm) light. Because it is genetically encoded (and genomes are now extensively sequenced), the ability to make nearly any "live" protein fluorescent made FRAP a broadly applicable cell biology tool. Consequently, targeted laser photobleaching was enabled on many microscope systems. Early work from the Lippincott-Schwartz group and others required photobleaching GFP-labeled proteins in entire organelles and structures (e.g. the Golgi, nucleus, cytoskeleton)

(Adams et al., 1998; Ellenberg et al., 1997). Spot bleaching was insufficient for these applications, and systems like the Zeiss LSM510 scanning confocal microscope were developed in part to support laser targeting of large geometrically complicated regions.

Point scanning confocal microscopes like the LSM510 generate sample signal by sequentially scanning a point of excitation light over the sample (Paddock, 2000). It was relatively straightforward to adapt point scanning hardware in order to enable photobleaching of user-defined regions. Point scanning technology has since been added to other types of high-resolution imaging systems specifically to enable photobleaching experiments. On these systems the photobleaching laser is typically targeted to the sample along a dedicated optical path and steered by galvometer-positioned mirrors.

Fitting non-scanning high-resolution systems with photobleaching units has tremendous promise for cell biology. Point scanning systems have an inherent deficit—it takes time to scan a point over a sample and sequentially build an image, and the speed of image acquisition is critical for many cell biology applications. Movement in cells is constant. Motor proteins rapidly move intracellular components including the cytoskeleton and tethered organelles, and simple diffusion of molecules is surprisingly fast: 25 μm^2/sec, 5 μm^2/sec, and 0.35 μm^2/sec for GFP in cytosol, ER lumen, and ER membrane respectively (Snapp et al., 2003). Consider these values in light of the fact that large mammalian cells have diameters in the range of 30-100 μm. Several non-point scanning high-resolution systems dramatically increase acquisition speed by illuminating larger sections of the field at once during image capture

without dramatically compromising resolution. For instance, Nipkow spinning disk systems illuminate the entire sample field and capture emitted signal from all "points" of the sample by passing emitted light through (effectively) a grid of pinholes to a CCD camera chip (Maddox et al., 2003). 100 millisecond exposures are a realistic expectation on these systems. To obtain an image with similar definition and dynamic range on an LSM510 takes five to ten times longer. That difference becomes dramatic for three dimensional imaging. (e.g. a 10um high cell sampled every 500nm requires 20 slices; i.e. 2s (Nipkow) versus 20s (LSM510) per timepoint.)

3. Assessing the Practical Effect of Microscope Developments

In 2005 I participated in beta testing a system designed by Carl Zeiss MicroImaging Inc. specifically built for high-speed photobleaching applications--the Zeiss Live DUO. The DUO system is effectively a high-speed imaging system with an LSM510 module used for targeted laser photobleaching (Figure 6). The imaging system uses novel optics that convert a radially symmetric laser beam into a planar beam with even intensity along its long axis. The system uses that beam to excite a line on the sample, and emitted light from this line on the sample is passed through a "confocal" slit to a sensitive linear offloading camera (Wolleschensky et al., 2006). This line scan technology system makes it possible to achieve image acquisition rates for a field the size of a cell that are comparable to a spinning disk system; for a smaller field or line, the rates can be much faster. I evaluated the Live DUO system using live cell markers previously designed in the lab that are uniquely appropriate

for assessing speed, resolution and photobleaching capabilities, and subsequently used this system for autophagy studies discussed in detail in Chapter 3 and 4.

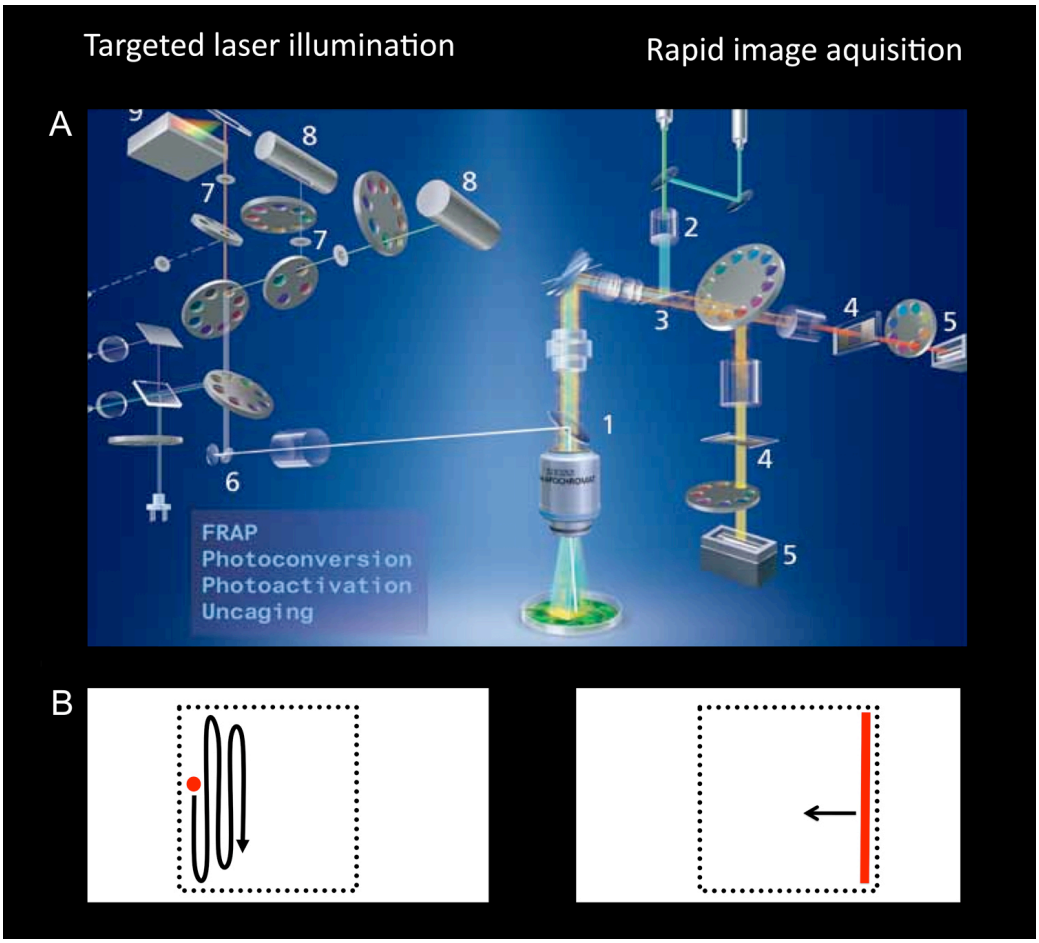

Figure 6: A high-speed high-resolution image acquisition system coupled to a laser targeting module. (A) Components to the left of the sample (LSM510 componenets) can be used to direct a focused laser beam to a defined region of the sample via stearing mirrors and a beam splitting mirror at position 1. Right hand components illuminate the sample via optical generation of a planar laser beam (at position 2) and signal capture with linear offloading cameras at the 5 positions. (B) Representations of the laser scan paths for LSM510 (Left panel) and the DUO (Right panel). Red regions indicate the illuminated area. Black arrows indicate the path of the laser scan. The one dimensional sweep of the laser (Right panel) dramatically increases scan time compared to serpentine scanning on the LSM510 (Left panel).

One common way to evaluate the performance of microscopy systems is by imaging fluorescent beads stably embedded in mounting media (Zucker and Price, 1999; Zucker and Price, 2001). Molecular Probes and Spherotech manufacture such beads in a variety of diameters and with spectral characteristics that crudely mimic most fluorescent proteins. Imaging stationary beads with uniform fluorescence is a common approach to reveal how well and how consistently a system conveys image information from a uniformly excited sample to a detector and finally to a digital file. However, while such information can be used to evaluate for instance how well and consistently a system can resolve discrete features, it is often hard to intuit the practical meaning of resolving capability, maximal image acquisition rates, etc. Beads are photostable stationary objects. Images of protein populations and intracellular structures are on one level simply images of many very small beads (points) of varying intensities that define the feature (Betzig et al., 2006). However, because in living cells the structures are in constant motion and are labeled by non-ideal fluors, imaging them taxes systems in different and often unpredictable ways. In addition to conventional evaluations that are arguably particularly suited to engineers and physicists, biologists need rigorous ways to evaluate the performance of microscopy systems in the context of living cells. What follows are several examples discussing how genetically encoded fluorescent protein fusions expressed in live cells can be used to empirically evaluate microscopy systems.

3.a. Assessing Structural Resolution

One way to investigate the ability of a system to resolve structural detail is to evaluate a structurally complex signal in living cells. In high-resolution images, the endoplasmic reticulum (ER) appears as a complicated meshwork with an appearance akin to netting (Terasaki et al., 2001; Willig et al., 2006). The meshwork is constantly rearranging both via large-scale movements as well as rearrangements in the connection points within the mesh. In order to resolve this meshwork, a system must acquire a sufficient signal with a short exposure against a low noise background. Comparing microscopy systems is always challenging because of differences in the internal hardware. However, one empirical approach is to require a minimum amount of signal loss for a fixed number of consecutive images (e.g., <5% percent photobleaching per 100 frames), and then ask how well the appearance of a demanding structure (e.g. the ER meshwork) can be optimized. Below is an image of labeled ER membrane taken using an LSM510 optimized for <5% photobleaching over 100 single plane images, and an image on the DUO system optimized while requiring the same signal stability (Figure 7, bottom panels). Because minimizing photobleaching using the LSM510 requires decreasing the pinhole and increasing detector gain, captured images inevitably show loss of clear resolution of the ER network. When requiring a comparable level of photobleaching on the LSM 5 DUO system and optimizing imaging parameters, we can retrieve far more structural information for the same amount of photobleaching. The dynamic range of the signal and detail of the ER mesh is strikingly improved. Although structural image analysis is beyond the scope of this thesis, one can easily get a quantitative snapshot of this

improvement by looking at pixel values along a line that intersects the meshwork. In the case of the DUO image, the values of adjacent pixels differ dramatically, whereas the values between adjacent pixels in the LSM510 image do not. It is a relatively straightforward statistical problem to extract the variance in the population of pixel values as a numerical indicator of the resolution of the ER meshwork.

Whether or not such improved structural information is critical to a particular application, it is clear that the LSM 5 DUO system has far more potential to capture dynamic structural information in living cells than the LSM510. This is particularly critical in either long or highly time resolved applications where photobleaching is limiting and the number of captured images is high.

3.b. Assessing Photobleaching

In addition to the LSM 5 DUO's resolving capabilities for live-cell work, I investigated its photobleaching capabilites. A number of issues arise from the fact that, effectively, one part of the DUO system is dedicated to signal capture and a second part is dedicated to laser targeting for photobleaching. The fact that these systems use different optical paths raises several issues. I address two of these issues here. First, how accurately and reproducibly can the photobleaching laser be targeted to a sample? Second, how quickly can the system switch between bleaching and imaging?

The first issue—accuracy and reproducibility of laser targeting—is a straightforward issue to evaluate. In effect this is really a question of how well the user interface controls targeting of the laser, and how reliably the optical components that regulate the intensity and path of the targeted laser deliver it to the user defined

region. Fixed samples in which the actin cytoskelton is labeled with a bleachable fluor (e.g. Fitc αActin) are convenient tools for this test; stained Fluo cells from Molecular probes are convenient tools for this, as they provide a stable relatively uniform field of fluorescence. By capturing an image of a mounted sample, targeting the laser to a defined region in the sample, and then subsequently acquiring an image after the photobleach, the accuracy of targeting can be evaluated. Provided an appropriate laser power is used for photobleaching, a well-defined black box should be present in the first post-bleach image that aligns with the user defined bleach area in the initial sample image. This experiment can be repeated in different regions of the same sample field over time to assess stability of the photobleaching optical path. By doing so, one can easily detect instability the targeting vis a vis misalignment of the bleached region in the sample with the defined bleach box. Such drift indicates instability in the components controlling the laser targeting. The DUO system components maintained accurate targeting over 6^{+} hours. Notably, other systems that we tested showed much less stability (i.e. the defined region fails to align with the actual bleach) and require frequent recalibrations of laser targeting. While recalibration is relatively trivial through a user interface, instability of the photobleaching optical path can affect confidence in photobleaching experiments that rely on fine targeting of structures.

A second issue raised by the use of a separate optical path for laser targeting is the requirement for a switch between photobleaching and image acquisition. The time required to switch from bleaching to imaging modalities is an issue critical for experiments that are now feasible because of high-speed image aquisition .

Bleaching a population of tagged ER transmembrane proteins is relatively straightforward and realistic on systems like the LSM510. However, it is much more challenging to target and monitor a population of cytosolic proteins. Recall that diffusion of most ER transmembrane proteins is on the order of 50 times slower than most cytosolic proteins (Snapp et al., 2003). If it takes a significant amount of time to switch between photobleaching to imaging modalities, a significant amount of cytosolic recovery will already occur before the first image is captured. Furthermore, if images cannot be captured at rapid rates following photobleaching, the dynamics of the recovery will not be clearly revealed in the aquired image series.

The LSM5 DUO system was designed to rapidly switch between bleaching and imaging modes and subsequently rapidly acquire consecutive images. The effect of switch time can be evaluated by looking at how well-defined the bleach box is in the first image taken after bleaching of a population of freely diffusing GFP molecules. Because these molecules very rapidly move back into the bleach region while the system switches from photobleaching mode to imaging mode, longer switch times reveal a loss of sharpness at the defined edges of the bleached region. Additionally, the image acquisition rate affects the spatial signature of the molecules because movement during image acquisition further blurs the boundary (Figure 7). Fast switch times and rapid acquisition of high-resolution images generate robust diffusion data vis-à-vis accurately indicating the movement of molecules into a well-defined well-bleached space. With improvements in acquisition speed coupled with reliable accurate laser targeting, current microscopy systems are better able to utilize

photobleaching both to monitor protein movement and to selectively label protein subpopulations.

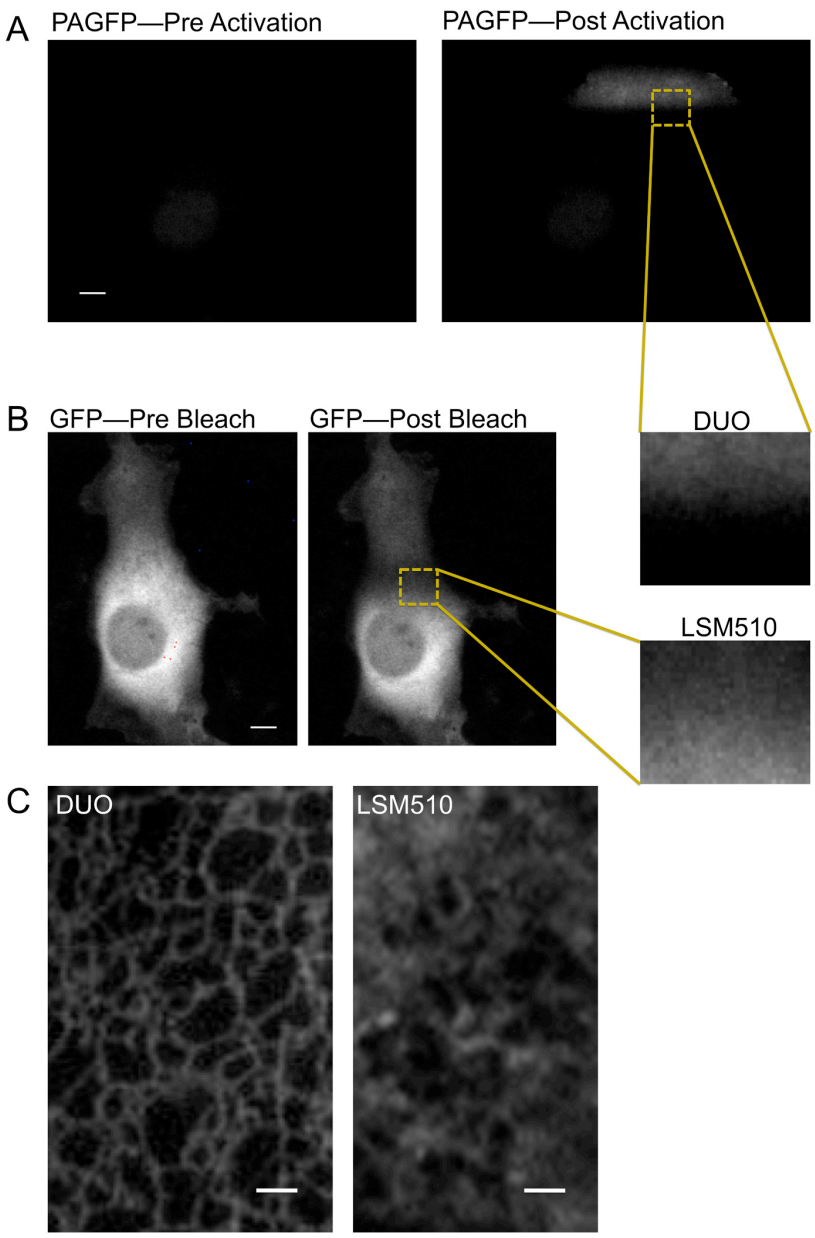

Figure 7: Comparisons of the DUO system with the LSM510 using PAGFP and GFP tagged proteins in live cells. (A) (DUO System) Light from a 405nm diode laser was targeted to a strip in order to activate photoactivatable GFP. The subsequent image was immediately captured with a 100ms exposure. The zoom below indicates definition of the boundary—the

combined effect of the time required for activation, the time required for switching to imaging, and the time required to obtain a signal. (Scale bar 10um.) (B) (LSM510) Light from a 488nm Argon/Krypton laser was targeted to a strip in order to photobleach GFP. For images of comparable resolution, the boundary is much less defined (compare LSM zoom to DUO zoom). (Scale bar 10um.) (C) Images were taken of the ER membrane marker Cd3δ-GFP while requiring an equivalent amount of photobleaching over 100 frames. The complicated meshwork of the ER is much better resolved by imaging on the DUO system. (Scale bars 1.5um.)

The examples above demonstrate use of empirical tests to evaluate the real consequences of improvements in imaging technology. Many modern biological questions are intractable with conventional imaging of fixed samples. Live cell microscopy places new demands on microscopy systems, and the descriptive statistics reported for these systems often do not clearly indicate the real performance of these systems. Tests like these clearly demonstrate that advances in optics, detector sensitivity, and laser design are dramatically improving our ability to utilize live cell microscopy and will continue to do so well into the foreseeable future.

4. Advances in fluorescent protein labeling

Concurrent with advances in imaging technologies, fluorescent protein labeling technologies have dramatically advanced in the last decade and a half. The Green Fluorescent Protein is now used in many contexts that extend its utility far beyond a simple live-cell reporter of positional information. Available fluorescent proteins now cover a wide range of spectra. These include mutants of GFP affecting its chromophore, as well as fluorescent proteins identified in other marine Cnidarians (the phylum containing the sea anemones, corals, sea pansies and other primitize eumetazoans) (Shaner et al., 2005). Spectral variants make it possible to track multiple tagged proteins simultaneously (Ellenberg et al., 1998). Spectral variants can also reveal interactions between tagged proteins via Fluorescence Resonance Energy Transfer, as can assembly of the split YFP (Muller-Taubenberger and Anderson, 2007). Many new fluorescent proteins have unique and useful biophysical and biochemical characteristics. dsRed, (the red fluorescent protein) and its

derivatives maintain fluorescence in low pH environments like the lysosome (Kimura et al., 2007); conversely, some GFP mutants are highly pH sensitive and can be used as pH indicators (Sankaranarayanan et al., 2000). Proteins that can be "turned on" (i.e., photoactivated) are now also available (Patterson, 2008), and one fluorescent protein (Killer Red) is reported to kill nearby proteins by generating light-activated local high concentration of reactive oxygen species (Bulina et al., 2006).

Many advances in fluorescent protein labeling are a product of characteristics of the fluorescent proteins themselves. However, fluorescent protein labeling techniques can also be advanced by taking advantage of how tagged proteins behave in their intracellular environment. Cell biologists are well-placed to develop cell-biology based advances in the use of fluorescent proteins. Below I discuss several approaches to probe first, protein topology, and second, capture of proteins in intracellular structures. These techniques all take advantage of fluorescent protein labeling. Below, the studies are specifically applied to determine topology of an interesting Atg protein and to identify substrates of autophagy.

5. Protein Topology

Fluorescent protein-based microscopy cannot directly visualize protein structure due to the physical limits of resolution and the need to incorporate chromophores into proteins; even novel super resolution imaging techniques are unlikely to ever directly resolve the structure of an appreciable number of proteins. However, as with many approaches to probe realms too small to be directly "seen", we can take advantage of characteristics of proteins to intuit aspects of their

structures. One such characteristic is a protein's spatial relationship with an associated membrane—its topology in a membrane.

Intracellular membranes spatially isolate compartments and provide surfaces to restrain and catalyze reactions. Membranes are critical for life. They isolate incompatible intracellular environments (e.g. the low pH, proteolytic lumen of the lysosome), maintain asymmetric gradients (e.g., calcium gradients across the ER membrane, proton gradients across the mitochondrial membranes), and organize countless biochemical reactions (e.g. ligand interactions with cell surface receptors, clathrin assembly at sites of vesicle formation). The topological relationship of a protein with its associated membrane is a critical feature. It dictates how a protein interacts with its associated membrane, and how the protein interacts with other effectors or substrates whose access is controlled by the membrane. To probe the relationship of a protein-of-interest with its membrane (a characteristic well below the resolution limit of light microscopy) I participated in designing a fluorescent protein-based assay with Dr. Holger Lorenz.

While in the Lippincott-Schwartz lab, Dr. Lorenz was interested in how transmembrane ER proteins targeted for proteasome-mediated degradation in the cytosol are physically extracted from the ER membrane. To monitor this dislocation, he and I engineered Type II transmembrane ER-targeted proteins with multiple fluorescent protein tags and developed an approach to determine the position of those tags relative to the ER membrane. We termed this technique the FPP (Fluorescence Protease Protection) assay—essentially a fluorescent protein-based technique adapted from biochemical protease accessibility experiments (Lorenz et al., 2006).

FPP works via the well-established principle that intracellular membranes can be selectively permeabilized due to their distinct lipid contents. Cholesterol concentrations are dramatically higher in the plasma membrane than other intracellular membranes (Liscum and Munn, 1999). Drugs that permeabilize cholesterol rich membranes (e.g. digitonin) can therefore be used to permeabilize the plasma membrane while leaving other membranes intact (Schulz, 1990). The selective permeabilization of the plasma membrane has two consequences. First, it releases freely diffusing cytosolic proteins through the now leaky plasma membrane. Second, it allows molecules previously outside the cell access to the interior of the cell. Therefore, a protease added after selective permeabilization of the plasma membrane can diffuse into and throughout the cell, contacting proteins at the cytosolic face but not the luminal face or lumen of all intracellular membranes. Consequently, fluorescent proteins accessible to the cytosol lose fluorescence; fluorescent proteins separated from the cytosol by a membrane barrier retain fluorescence. The FPP assay requires digiton, a cytosol-like buffer, and a protease, and the binary fluorescent readout makes it applicable to high-throughput screens of GFP-fusion protein collections. For individual proteins-of-interest, the assay is an efficient means to obtain basic topological information (Figure 8).

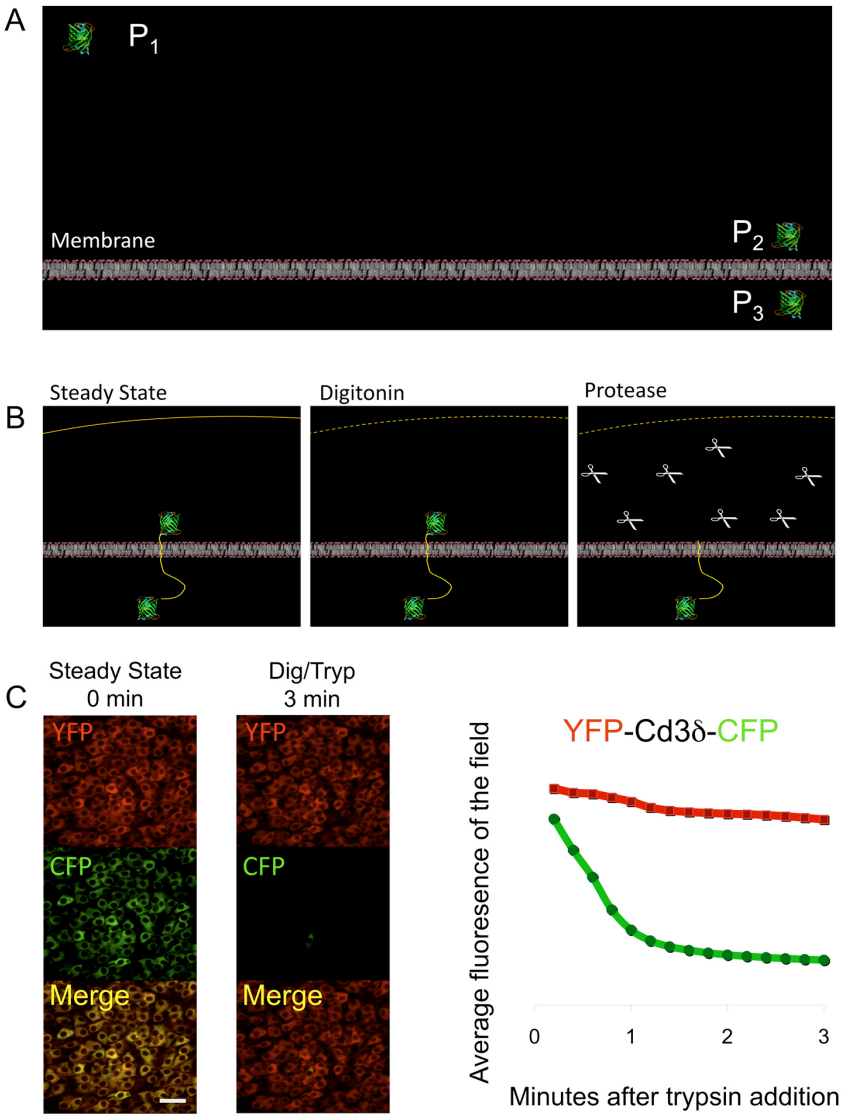

Figure 8: The Fluorescence Protease Protection Assay to resolve protein topology. (A) (Drawn roughly to scale) Light microscopy can at best distinguish signal at P1 from signals P2 and P3. Notably, using cell biology approaches in conjunction with imaging, it is possible to get positional information about P2 relative to P3 and the membrane. (B) Schematic for the FPP assay. Cells expressing fluorescent protein fusion(s) to proteins-of-interest are placed in a cytosol like buffer and selectively permeabilized with digitonin (middle panel). Protease added to the buffer diffuses into the cell, cleaving fluorescent proteins that are not protected by intracellular membranes (i.e. in the lumen of organelles). (C) FPP in practice.

A field of cells stably expressing the multi-labeled ER targeted protein signal sequence-YFP-Cd3δ-CFP was assayed. YFP is targeted to the ER lumen. It's signal persists while the signal from CFP at the cytosolic face disappears. CFP signal at the cytosolic face is depleted within minutes of trypsin (protease) addition (Plot). (Scale bar 100um.)

I applied the FPP technique to complement extensive work from Sharon Tooze's lab probing the strucuture of mammalian Atg9 (mAtg9). Atg9 was first identified as a core autophagy component in *S. cerevisiae* screens (Scott et al., 1996). In yeast it is essential for autophagosome formation and delivery of ApeI to the yeast vacuole via the Cvt pathway (see Chapter I). Atg9 is notable because, unlike other autophagy components, it is a multispanning transmembrane protein; hence it received much attention because it held promise for revealing the membrane source of autophagosomes. Interestingly, in yeast the protein labels mitochondria, intracellular vesicles, and the Pre Autophagosomal Structure (PAS; the site of autophagosome formation) (Mari and Reggiori, 2007). Andrew Young and coauthors in the Tooze lab identified the mammalian homolog mAtg9 by bioinformatics (Young et al., 2006).

As often occurs, algorithms to predict the topology of Atg9 were inconsistent, indicating between 5 to 7 transmembrane domains (TMDs) (Ott and Lingappa, 2002). Both glycosylation site mapping and in vitro synthesis followed by protease treatment of ER microsomes were carried out to determine the likely orientation of the protein in the membrane. To complement this work, the FPP assay was used to probe the topology of RFP-Atg9 expressed in cells. We could not evaluate the C- terminus because fusion of fluorescent proteins to the C- terminus of mAtg9 mislocalized the protein. However, based on FPP, the N- terminus of Atg9 faces the cytosol, consistent with glycosylation and microsome data that argue both the N- and C- termini face the cytosol. Hence the protein most likely spans the membrane six times.

This and other initial descriptions of Atg9 have not clearly established the function of Atg9 in mammalian autophagy. While the yeast deletion blocks autophagy, autophagosomes still form in RNAi knockdown in mammalian cells, although the structures are smaller (Young et al., 2006). However, Atg9 continues to be an interesting member of the Atg proteins, and studies to elucidate its function are ongoing. It is likely that additional Atg9 homologs exist in mammals, one with a mitochondrial targeting motif (Heidi McBride, personal communication).

Application of FPP to the mAtg9 study illustrates both advantages and drawbacks of the assay. Obtaining information about the position of protein termini is relatively trivial, and, because the assay is carried out in cells with a full complement of endogenous proteins to coordinate membrane insertion, the assay can address concerns about proper protein folding in *in vitro* assays like microsome translation. Investigating positions other than the N-and C- termini in multispanning proteins requires inserting a fluorescent protein within the polypeptide of the protein, and there is significant risk that a large internal insertion will disrupt the native structure of the protein. That said, truncation and deletion of internal domains is commonly used to investigate protein structure and function. The utility of the FPP assay may improve significantly if techniques that utilize binding of fluorescent molecules to small peptide regions (e.g. FLASH) are further developed (Adams and Tsien, 2008; Luebke, 1998). For now, the assay is a quick way to determine the subcellular location of protein termini of transmembrane proteins--a constraint that is often useful in intuiting structure and revealing likely regions for protein interactions.

6. Capture of proteins in intracellular structures

Selective permeabilization is a useful technique for another aspect of autophagy studies—assessing capture of substrates. As discussed above, the high concentration of cholesterol in the plasma membrane makes it possible to selectively permeabilize the plasma membrane. Freely diffusing cytosolic proteins can then rapidly diffuse out of the cell while proteins associated with or inside intracellular membranes are retained. Because autophagosomes are the only reported organelles that readily engulf intracellular cytosolic contents, they are uniquely efficient at trapping diverse populations of freely diffusing cytosolic proteins. Conventional vesicle budding events occur constitutively in cells, but those events either capture contents from the lumen of intracellular organelles or from the extracellular space. Most other movements of large cytosolic molecules into membrane delimited intracellular spaces require regulated transfer events to actively move specific proteins.

To assess the ability to visualize substrate capture, I expressed exogenous GAPDH-YFP (Glyceraldehyde 3-phosphate dehydrogenase and LDH (Lactate dehydrogenase) fused to the yellow fluorescent protein) in starved *Rattus norvegicus* cells that stably express the live cell autophagy marker CFP-LC3 (CFP fused to microtubule-associated protein 1 light chain 3, the *Rattus norvegicus* homolog of Atg8). GAPDH and LDH are abundant cytosolic proteins. GAPDH is commonly used as a protein loading control. Both are reported substrates of autophagy (Fengsrud et al., 2000b; Hoyvik et al., 1991). GAPDH-YFP and LDH-YFP signals appear as cytosolic signals and fluorescence microscopy cannot discriminate

subpopulations in autophagosomes from the background cytosolic signal. Following treatment with digitonin, the majority of these signals disappear by escape from the cytosol via diffusion out holes in the membrane made by intercalation of digitonin. However, a fraction of GAPDH-YFP and LDH-YFP are retained. This retained protein is present in punctae, most of which label with the CFP-LC3 autophagy marker. The retention of a subpopulation of these enzymes indicates that it is possible to selectively release diffuse cytosolic proteins in order to reveal underlying subpopulations trapped in autophagosomes. Notably, although I used an exogenous protein, one could also permeabilize cells with digitonin and subsequently fix and stain with appropriate antibodies to substrates of interest. CFP signal withstands paraformaldehyde fixation and can be amplified if necessary using GFP antibodies.

While digitonin is a valuable tool to release captured cytosolic substrates by allowing diffusing cytosolic proteins to pass through the plasma membrane, digitonin is also toxic to the cells. Most cellular architecture is preserved during digitonin treatment, but exchange of cell cytosol with permeabilization buffer depletes critical cytosolic factors. Countless reactions that depend on these factors will slow or stop. Cell cytosol extracts can be used as buffer, but that requires significant resources.

Identifying captured substrates in live cells is an alternative approach to identify autophagosomal substrates. Freely diffusing cytosolic proteins in live cells sample the entire cell volume in a short period of time. We can use this fact to photobleach these proteins. By repetitively targeting a small region of the peripheral cytosol with a photobleaching laser, proteins that diffuse and hence transit the targeted region are bleached, revealing the trapped subset that cannot enter the

targeted region and hence retain signal (Snapp et al., 2003). The outcome is effectively the same as digitonin treatment. However, because the cells are live, the retained signal can be subsequently followed by live-cell imaging (Figure 9). Notably, as time passes, additional YFP-GAPDH signal will appear as the protein is translated, complicating this monitoring.

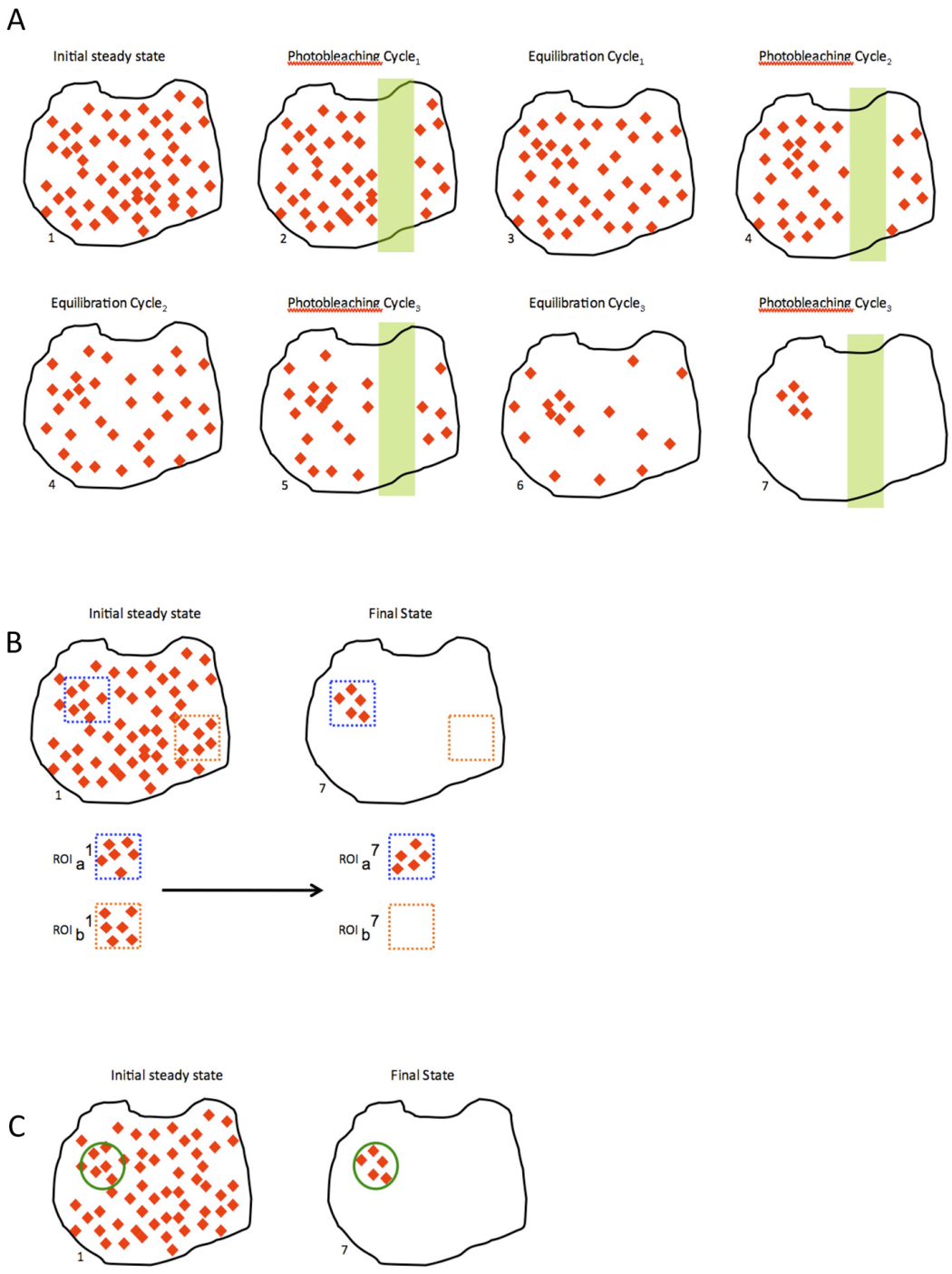

Figure 9: Photobleaching to selectively deplete signal and reveal subpopulations of proteins captured in organelles (Schematic). (A) Repetitively photobleaching a region of the cytosol rapidly depletes freely diffusing fluorescent proteins. (red diamonds: fluorescent proteins;

green rectangle: photobleached region.) Following bleaching (e.g. panel 2), diffusing proteins re-equilibrate (e.g. panel 3). Subsequent bleaching will bleach signal from those proteins that have moved into the bleach region. Iterating this process depletes signal from diffusing proteins to reveal proteins that cannot freely diffuse. Their capture retains them outside the bleach zone (panel 7). (B) Prior to selective bleaching, confocal imaging will not reveal distinctions between trapped and non-trapped flurophores. Bleaching reveals how proteins transit the underlying architecture of the cell. (C) A second marker can be used to assess the mechanism of retention. Conveniently, many fluorescent proteins have unique spectra that enable bleaching of one marker in the presence of a marker protein (e.g. the green label to identify the membrane responsible for capture of the red protein).

The selective "labeling" of autophagosomal substrates is one instance where advances in microscopes, fluorescent protein labeling and cell biology can converge to reveal additional functional data about autophagy. It is possible to follow the fate of only the captured substrates over time by photoactivating the cytosol, selectively photobleaching the freely diffusing population, and then monitoring the fate of the remaining signal. Effectively, photoactivation allows one to pulse-label captured substrates (Patterson, 2008). The use of a photoactivatable protein here means that new protein synthesis in the cytosol will not contribute to signal, as those proteins are not activated. In the following chapter I describe a similar approach to follow the fate of the autophagosomal membrane itself via monitoring the Atg8 homolog LC3 as a reporter for those membranes.

The assays above all illustrate advantages of using genetically encoded fluorescent protein labeling in live cells. Notably, live cell imaging is not simply a tool for watching cell or organism behavior over time. The fact that dynamic movements take place within live cells can be used to reveal the architecture of the cell (e.g. protein topology, protein capture, etc.) that is otherwise difficult or impossible to directly visualize. Fixed cells can be labeled, but once cellular components are cross-linked we can no longer take advantage of the fact that cell membranes affect movement of proteins within the spaces they delineate. Live cell imaging lets us ask not just where something is, but where it can go, and the ability to answer that question can dramatically inform our observations (Figure 10). By analogy, this is like charting a river system by puting a dye in the water rather than mapping the shoreline. Arguably, autophagy is a process dedicated to generating

boundaries in order to restrict and/or degrade portions of the cell. Experimental designs that leverage the intersection of microscopy development, fluorescent protein development, and cell biology information are well positioned to explore the autophagic process.

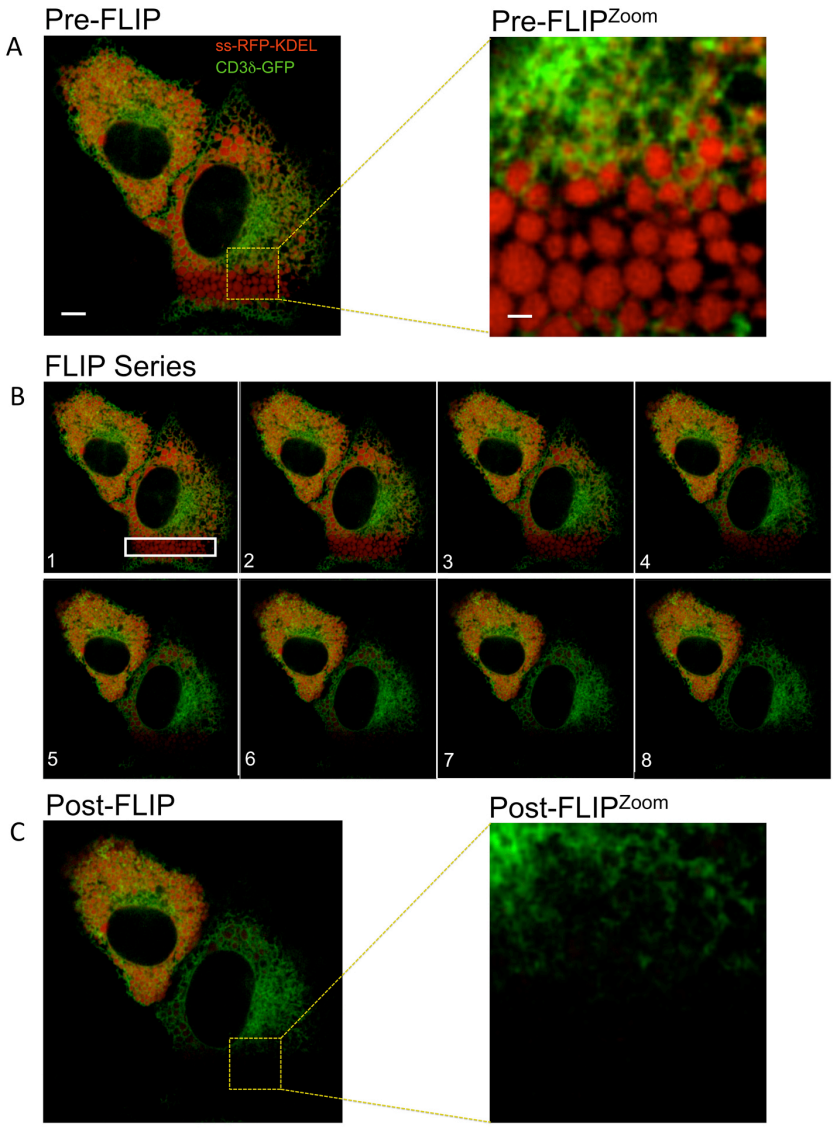

Figure 10: Probing cellular architecture using living cells. (A) Dual channel imaging to assess localization of two proteins that appear to label separate compartments—a reticular

network (the ER) and a vesicular compartment (see Zoom of yellow box, right panel). (Scale Bar left, 10um. Scale Bar right, 2um.) (B) Repetitive photobleaching (FLIP) to assess compartment continuity. Depletion of signals via bleaching the proteins with simultaneous 490 and 561 nm light depleted both signals. (Numbers indicate iterations, white box indicates targeted region). (C) All red signal was rapidly lost. Red molecules must therefore transit the entire volume of the cell. Note there is no loss of red signal from the untargeted upper left cell. Despite the vesicular appearance, ss-RFP-KDEL is contained in one continuous compartment in the cell. In fact, this is the lumen of the compartment also marked by the green signal, Cd3δ-GFP. Cd3δ-GFP is not depleted on this time scale; diffusion in the ER membrane is dramatically slower than the lumen. The vesicular appearance is a consequence of swelling of the endoplasmic reticulum via ER stress. A static image of these cells is clearly misleading.

Chapter 3: Using Photoactivatable Proteins to Monitor Autophagosome Lifetime

The following chapter was previously submitted and accepted for inclusion in a Methods In Enzymology volume on Autophagy edited by Dan Klionsky (Title: Using Photoactivatable Proteins to Monitor Autophagosome Lifetime, Authors: Dale Hailey and Jennifer Lippincott-Schwartz). The photo pulse-label technique discussed here is used in Chapter 4 as one means to compare starvation to other conditions that induce autophagy.

Many conditions are now known to cause autophagosome proliferation in cells and organisms including amino acid and serum starvation, ER and oxidative stress, and pathogen infection. Autophagosome proliferation is also observed in disease states and developmental programs. The widespread use of GFP-Atg8 fusion molecules has provided a simple way to visualize the proliferation of autophagosomes in cells. However, GFP-Atg8 markers do not reveal the underlying cause of autophagosome proliferation. Two processes regulate the number of autophagosomes present in cells: (1) formation of the structures and (2) their turnover through fusion with lysosomes. Here we describe the use of photoactivatable proteins to decouple the processes of autophagosome formation from autophagosome turnover. Photoactivatable proteins fused to Atg8 homologs make it possible to pulse-label existing populations of autophagosomes in living cells. The fate of those pulse-

labeled autophagosomes can then be monitored to determine autophagosome lifetime. This assay is applicable to both engineered tissue culture models and transgenic organisms expressing photoactivatable proteins fused to Atg8 homologs.

1. Introduction

Since Atg8 was first characterized in *S. cerevisiae* in the mid 1990s, its related homologs in higher eukaryotes (collectively referred to as Atg8 below) have been used to directly visualize autophagic vesicles in cells and tissues, replacing monodansylcadaverine staining as a standard autophagosome marker. During autophagosome formation, the C terminus of Atg8 is processed and covalently bound to phosphotidylethanolamine in membranes (Ichimura et al., 2000). The resulting shift of Atg8 from the cytosol to autophagosomal membranes provides a convenient, easily assayed readout for cellular conditions that proliferate autophagosomes. However, because Atg8 and its homologs persist on autophagic structures from their inception through fusion with lysosomes (Tanida et al., 2005), Atg8-positive structures can accumulate either because of increased rates of autophagosome formation or decreased rates in their degradation (Klionsky et al., 2008a). Many conditions cause Atg8-positive structures to proliferate, including amino acid starvation, serum deprivation, ER stress, proteasome inhibition, calcium dysregulation, mitochondrial damage and some viral and protozoan infections (Ding and Yin, 2008; Kirkegaard et al., 2004; Kuma et al., 2004; Lum et al., 2005). Autophagosomes also accumulate during developmental programs and the progression of diseases including Alzheimer's and Huntington's (Fimia et al., 2007; Levine and Kroemer, 2008). With such diverse conditions reported to induce Atg8-

positive structures, a straightforward method is needed to evaluate the role these structures play in cell homeostasis--in particular, a reliable means to determine whether autophagosome proliferation indicates increased formation or alternatively a failure of the structures to degrade. The assay presented here decouples autophagic induction from degradation in order to reveal turnover rates of Atg8-positive autophagosomes in a straightforward manner.

Catabolism of autophagic substrates was initially assessed by radiolabel pulse-chase experiments. These experiments provided a direct readout for autophagic activity. A number of approaches have since been developed to analyze the fate of autophagic substrates (Tasdemir et al., 2008). Autophagy is most commonly described as a nonselective degradation process that turns over small fractions of diverse protein populations by bulk capture. To confidently assess autophagic turnover of a substrate population, protein populations often must be tracked over long periods of time. Assessing the effects of drugs over such time periods increases the risk of confounding off-target effects. Additionally, pulse-labeling of autophagic substrates is often laborious and difficult to apply in a high-throughput fashion. We present an alternative method to assess the lifetime of autophagosomes by using a photoactivatable fluorescent protein-based assay. This technique requires substitution of GFP in well-characterized GFP-Atg8 fusion proteins with either photoactivatable GFP (PAGFP) or other genetically encoded photoactivatable fluorescent proteins in order to pulse label a population of autophagosomes and quantify their lifetime.

2. Photoactivatable fluorescent protein labeling

Fluorescent protein (FP) labeling is a ubiquitous cell biological tool that enables researchers to monitor a protein-of-interest in living cells or organisms. Fluorescent protein fusions must be shown to phenocopy the activity of the untagged endogenous protein-of-interest. Once characterized, they are invaluable for their ease of use and diverse utility. Fluorescent protein fusions minimize artifacts of sample preparation and enable researchers to monitor dynamic processes in living cells. Autophagy is particularly well suited to studies using fluorescent protein fusions since core autophagy components are recruited from the cytosol to autophagosome membranes upon induction (Xie and Klionsky, 2007).

Conventional fluorescent proteins behave like fluorescent dyes. They absorb a defined range of wavelengths of light (the excitation spectra) and emit lower energy, longer wavelengths (the emission spectra). In the case of GFP, maximum excitation occurs around 490 nm and maximum emission occurs around 525 nm. For most commonly used fluorescent proteins, excitation and emission spectra are a consistent property of the fluorescent protein. The spectra change little in response to environmental factors such as pH, temperature, proximal redox potential, etc. The chromophore of GFP (the portion of the protein that absorbs light energy and reemits light) maintains a stable structure under most conditions, and the consequent stable spectral behavior of GFP is in fact critical for its use in many quantitative imaging applications (Zimmer, 2002).

Recently, a number of fluorescent proteins have been characterized that can undergo alterations in chromophore structure. These structural alterations are induced

by exposure to high-energy light and result in irreversible changes in the spectral properties of the chromophores. So-called photoactivatable proteins behave much like caged compounds that can be light-activated (Lippincott-Schwartz and Patterson, 2008; Lukyanov et al., 2005). Once photoactivated, the spectral properties of a targeted fluorescent protein population are distinct from the unactivated population. Therefore, a set of proteins can be highlighted. With appropriate imaging configurations, this highlighted population can then be uniquely followed. Proteins outside of the activated region as well as proteins folded and/or translated after the photoactivation will be spectrally distinct and can be distinguished from activated proteins (Lippincott-Schwartz and Patterson, 2008).

By substituting the photoactivatable protein PAGFP for GFP in GFP-Atg8 fusions, autophagosomes can be pulse-labeled. A brief pulse of 400nm light can be used to highlight a population of autophagosomes present at a given time. Fluorescence from this population is lost as the pulse-labeled autophagosomes fuse with lysosomes. Following lysosomal fusion, decreased pH and proteolysis abolish fluorescence of activated PAGFP-Atg8. An autophagosomal population can therefore be monitored in live cells at the microscope to quantify how quickly the pulse-labeled autophagosome population disappears. By knowing how long Atg8-positive structures persist within cells, the role autophagosomes play in active catabolism of substrates can be deduced. Using this approach, it is relatively simple to determine whether a condition or drug treatment accumulates autophagic structures via inducing autophagosome formation or alternatively blocking autophagosome degradation. This

assay can be used in diverse research models ranging from tissue culture cells to whole organisms.

Here we present an example of this photo-chase assay using a *Rattus norvegicus* tissue culture cell line referred to below as NRK144. This NRK (normal rat kidney) line stably expresses PAGFP-LC3 (the photoactivatable protein PAGFP fused to microtubule-associated protein 1 light chain 3, the best-characterized mammalian Atg8 homolog). (Kabeya et al., 2000). We discuss considerations in choosing a photoactivatable protein and present an example of how the photo-chase assay is carried out.

2.a. Choosing the biological system

In this paper we use a stable tissue culture line as a simple tool to evaluate the behavior of autophagosomes. We note that based on studies of the GFP-LC3-expressing mouse line and many other reports, autophagy is a tissue-specific context-dependent process (Mizushima et al., 2004). Many questions will need to be addressed in more complicated systems. However, initial studies to explore regulatory controls, mechanistic aspects of autophagy and drug effects may be more tractable in tissue culture models. There are important caveats to using these systems. Overexpression of Atg8 homologs has been reported to induce formation of Atg8-positive structures that may generate aggregates of Atg8 or induce formation of autophagosomes (Kuma et al., 2007). Anecdotally, cells transiently expressing Atg8 homologs also have nonhomogenous responses, possibly due to the range of Atg8 levels or variable stress responses to transfection reagents. To minimize these issues,

we have used cell lines that stably express photoactivatable protein fusions to Atg8 homologs.

Once an expression system is established, growth conditions can be adjusted to minimize basal autophagy. In order to assess the lifetime of autophagosomes formed in response to a condition of interest, there should be very few Atg8-positive structures present in untreated cells. Serum concentration, media pH, and confluency all affect the basal level of autophagosome formation. We find that increasing serum concentrations from 10 to 12% and decreasing cell confluency decrease basal autophagosome formation, consistent with serum factors suppressing autophagy (Furuta et al., 2004). Additionally, autophagosome formation is a known response to a range of pathogen infections. If there is any question about whether cells are free of mycoplasm or other intracellular pathogens, cells should be cleaned with a broad range antibiotic such as BM Cyclin (Roche, Cat# 10 799 050 001). Establishing conditions that minimize the number of autophagosomes present in the cells under basal conditions ensures that induced autophagic structures represent autophagosomes formed in response to the induction being studied.

2.b. Choosing an appropriate photoactivatable protein:

In the following example we use PAGFP as the photoactivatable genetically encoded marker. PAGFP was the first published photoactivatable protein—a variant of wild-type GFP (Patterson and Lippincott-Schwartz, 2002). Since PAGFP was reported in 2002, the catalog of photoactivatable proteins has grown. To choose the best available photoactivatable protein, we advise surveying the current literature. The properties of many of these proteins are now being optimized for biological

applications. At the time of this publication, a review by Patterson provides a convenient comprehensive overview of the current catalog of photoactivatable proteins (Patterson, 2008). Although some of the new photoactivatable proteins show much promise, there are two notes of caution.

First, most photoactivatable proteins have not to date been used extensively. Atg8 fusions must function in both cytosolic and membrane-bound forms (Kabeya et al., 2000). When properly intercalated into autophagosome membranes, these fusion proteins are locally concentrated and are sterically constrained. This environment may promote oligomerization, and it is especially important to confirm that novel Atg8 fusion proteins are fully functional. New fluorescent protein Atg8 fusions should be evaluated empirically by careful comparison with either endogenous Atg8 or the well-characterized GFP fusions to Atg8. Of course it must be kept in mind that the C terminus of Atg8 is proteolycially processed by Atg4 for subsequent lipidation; fluorescent protein fusions therefore must be at the N terminus.

Second, some spectral properties of photoactivatable proteins are undesirable for the photo-chase assay. The assay utilizes the fact that fluorescence from the activated population is readily quenched as lysosomes fuse with pulse-labeled autophagosomes. The effective disappearance of pulse-labeled autophagosomes enables one to quantify the lifetime of autophagosomes. Accordingly, photoactivatable proteins that fluoresce in low pH (lysosomal) environments are not appropriate; lysosomal fusion will not abolish fluorescent signal from these proteins. (Note that a second fluorescent protein-based technique to quantify autophagosome

turnover utilizes different pH sensitivities and is previously reported (Kimura et al., 2007).

With these caveats in mind, choosing the optimal photoactivatable protein involves three considerations: Are the spectra appropriate for the particular application? Are the photoactivation properties optimal? Is the photoactivated fluorescent protein sufficiently photostable to allow repetitive imaging during the monitoring of fluorescence?

2.c. Spectral Considerations

Photoactivatable proteins currently fall into two categories—those that "turn on" and those that undergo a spectral shift (Patterson, 2008). Proteins that turn on are effectively invisible prior to activation. Visualizing these proteins requires using one excitation and emission set. Consequently, a large range of available spectra can be used to simultaneous image a second fluorophore. However, photoactivatable proteins that turn on are difficult to detect prior to activation. Using these proteins, it can be challenging to identify transfected cells or cells of interest in a mosaic tissue. It is also difficult to evaluate the state of the cells prior to activation (i.e., whether autophagosomes have been formed).

A second class of photoactivatable proteins are those that undergo a profound spectral shift upon photoactivation. Most described proteins in this category undergo a green to red (GFP- to RFP-like) shift. Because these proteins are fluorescent prior to activation, cells expressing these proteins can be readily identified. This can expedite locating cells expressing a transfected marker or cells in an organism expressing a transgene. However, because they fluoresce in two spectral ranges, they may limit

applications that require monitoring additional tagged proteins-of-interest or other fluors.

Selecting an appropriate photoactivatable protein also requires considering autofluorescence within cells. We observe that starvation conditions increase autofluorescence in many tissue cultures lines. Ideally, spectra of photoactivatable proteins should have minimal overlap with intracellular autofluorescence. This is particularly important since autofluorescence frequently appears in lysosomes. To evaluate the contribution of autofluorescence, nonactivated cells should be imaged with identical imaging parameters under identical culture conditions as those that will be used to track photoactivated autophagosomes. Although we have not observed this in the NRK144 line, one should also address whether the photoactivation induces autofluorescence by photoactivating cells that do not express the photoactivatable protein, and subsequently monitoring these cells. Ideally no signal should be visible in either case. If significant autofluorescence is detected , narrowing the band pass of the emitted signal may help restrict its contribution.

As indicated above, in the example described in this chapter, we use photoactivatable GFP (PAGFP) fused to LC3. PAGFP is derived from GFP. It differs by a few amino acids which specifically affect the chromophore (Patterson and Lippincott-Schwartz, 2002); structurally PAGFP-LC3 is nearly identical to the commonly used GFP-LC3. Whereas unactivated PAGFP can be visualized with filters customized to its blue-shifted excitation spectra, for practical purposes it behaves like a switchable protein. It is turned on by light in the 400 nm range, and following activation can be monitored with commonly used GFP or FITC imaging

configurations. Similar to GFP, its fluorescence is rapidly destroyed at low pH. Its fluorescence is therefore lost once pulse-labled autophagosomes fuse with lysosomes.

2.d. Photoconversion Considerations

2.d.i. Calibrating laser targeting

To "highlight" a population of photoactivatable fluorescent proteins, the proteins are exposed to a brief pulse of light. For most photoactivatable proteins thus far reported, exposure to 400 nm range light efficiently activates the proteins. Relatively inexpensive low wavelength 405 nm diode lasers are now available on many microscopy systems. These lasers are ideal for photoactivation experiments. On scanning confocal systems, light from a 405 nm diode laser is typically directed along the imaging light path; it is therefore not usually necessary to calibrate targeting of the photoactivation laser. A number of non-scanning high-resolution microscopy systems (i.e., spinning disk, line-scan and deconvolution systems) are now also configured for photoactivation. On these systems, the light path of the photoactivation laser is separate from the imaging light path. Therefore laser targeting must be calibrated. To calibrate targeting, a region is defined and exposed to 405 nm light and an image is immediately captured. The defined region is then compared to the actual bleached region in the captured image. Most systems have software adjustments that allow the user to easily offset the laser targeting if the position of the bleached region does not match the defined region. Note that these offsets are specific for the wavelength. For this calibration we recommend using a fixed sample stained with a ubiquitous probe such as FITC-αActin.

2.d.ii. Optimizing photoactivation

Low wavelength light can photo-oxidize cellular components and generate reactive molecules, particularly in tissue culture cells that we typically culture in relatively high oxygen environments (Baier et al., 2006). Ideally, the 405 nm light pulse used to photoactivate fluorescent protein fusions should be minimized as much as possible without excessively compromising signal in order to avoid phototoxicity. For optimal photoactivation, one would like as little signal as possible from the fluorescent protein prior to photoactivation, followed by a robust amount of signal following photoactivation. The difference between these points is the "fold activation", and the ideal photoactivation produces the best "fold activation" for the least light exposure.

Because the amount of energy needed to effectively activate a population of photoactivatable proteins depends on specific biological considerations and hardware configurations, we suggest empirically optimizing photoactivation conditions. To optimize photoconversion, cells expressing the photoactivatable fluorescent protein are repetitively targeted with a low level of photoactivation light. Each iteration will result in an increase in signal until the process of photobleaching overtakes the process of photoactivation. (400 nm light will photobleach the majority of fluorescent proteins.) Plotting the total fluorescence of the photoactivated protein against the iteration number will generate a plot with a maximum that indicates the maximum fluorescence and the associated optimal number of iterations for photoactivation (Figure 11). This optimization procedure is easily carried out with photoactivatable protein fusions to Atg8 homologs. Prior to autophagic induction, these proteins are

essentially cytosolic. The entire cell can therefore be targeted by the photoactivation light, and subsequently total cell fluorescence can be monitored.

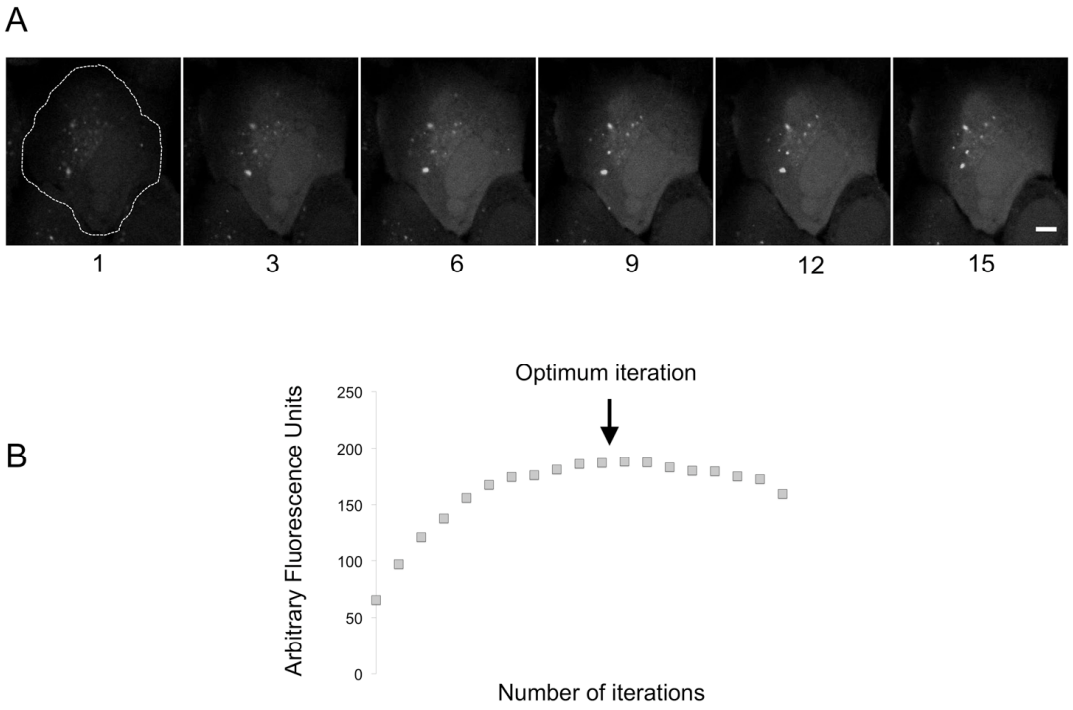

Figure 11: Example of an experiment to optimize photoactivation parameters. (A) A live cell stably expressing PAGFP-LC3 was repetitively exposed to light pulses from a 405 nm diode laser. The white dashed line indicates the targeted region. An image (using parameters for the GFP signal) was captured prior to each exposure. Numbers below the images indicate the iteration number. (Scale bar 10um) (B) Mean fluorescent intensity was quantified within the targeted region for each image to track the increase in fluorescence as a function of the number of exposures to the 405 nm pulse. The highest fluorescence occurred at the 11^{th} repetition. Loss in sequential frames indicates that photoactivation is nearly complete and photobleaching is then the dominant effect. Therefore, for the given laser intensity, 11 cycles of 405 nm exposure will produce the maximum fold activation of PAGFP-LC3. Note that this may need to be decreased if phototoxicity is observed. Scale bar: 20 μm.

3. Experimental example: Setting up a sample and optimizing photoactivation

In the example presented here, we begin by seeding NRK144 cells into a chamber with a coverglass bottom. Following are step-by-step instructions to set up the chamber and optimize photoactivation. This example assumes use of an inverted microscope and imaging system capable of targeting low wavelength laser light to a user-defined region of interest.

3.a. Setting up chambers

1. Grow a T25 flask of NRK144 cells to 90% confluency in DMEM/10% FBS.
2. Transfer 350 μL of 37°C DMEM/10%FBS to each well of an 8-well Nunc LabTek chamber (Nalge Nunc International, Cat# 155411).
3. Remove the medium from the T25 flask and rinse twice with 37°C phosphate buffered saline (PBS).
4. Remove PBS and add 2 mL 37°C 0.05% Trypsin/0.53 mM EDTA (CellGro, Cat# 25-051-Cl); wait for cells to lift (<2 min).
5. Transfer 1.0 mL of trypsinized cells to a sterile 1.5 mL microcentrifuge tube to simplify handling in Step 6 below.
6. Transfer 10 μL of trypsinized cells from the microcentrifuge tube to each well in the LabTek chamber. Move the pipette back and forth while dispensing the cells into the DMEM to assure even cell distribution.
7. Return the chamber to a 37°C/5% CO_2 incubator and culture 16 hours.

3.b. Optimizing photoactivation

1. Warm CO_2-independent medium (Gibco, Cat# 18045-088) to 37°C

2. Remove the LabTek chamber with cells from the incubator and place the chamber on the surface of a T25 flask filled with 37°C water to maintain temperature while out of the incubator.
3. Replace the DMEM with the preheated CO_2-independent medium.
4. Transfer the chamber to a preheated 37°C microscope stage.
5. Locate a field of cells using transmitted light.
6. Take a transmitted light image to identify the location of the cells and an image with GFP parameters to assess the pre-activation PAGFP-LC3 signal. This should be close to background (black). Note: PAGFP does have some emission in the GFP range prior to photoactivation; adjust the intensity of the excitation light and the gain on the system to minimize this signal.
7. Draw a bleach box around the field of cells to define a bleach region.
8. Set up bleach parameters: Typically this involves setting the percent power, duration of exposure, and number of iterations for the targeted laser. Both of these settings should be significantly below saturation levels (see below).
9. Set up a time lapse with the following sequence:
    a. Capture an image using a configuration appropriate for the GFP signal.
    b. Photoactivate by targeting 405 nm light to the user-defined bleach box.
    c. Repeat for 20 cycles.
10. Run this series. Initially, fluorescence should increase with each iteration.
11. Identify the number of iterations where optimal fluorescence occurs. This roughly indicates the number of iterations required at the selected power level, scan zoom, etc. for optimal photoactivation.

12. Note$_1$: If no increase in fluorescence is observed, either the laser power is excessive and bleaching following photoactivation is already occurring in the first iteration, or there is insufficient laser power for photoactivation. Modulate the bleach settings (i.e., laser power, duration of exposure, or number of iterations) and repeat the above experiment.
13. Note$_2$: Although low wavelength lasers are typically used to photoactivate, photoactivation can also be achieved using non-coherent light sources such as mercury and mercury-xenon lamps. Low wavelength filters such as those for DAPI will typically work. However, on most microscope systems it is difficult to regulate the sample exposure using non-laser sources. This may affect reproducibility and the ability to control phototoxicity.
14. Note$_3$: If phototoxicity is observed, we find that defining the targeted region such that the cell nucleus is not exposed reduces potential phototoxic effects of photoactivation. This also expedites photobleaching cytoslic activated PAGFP-LC3 (discussed below).

4. Photobleaching

Once photoactivation parameters have been optimized, it is important to establish imaging parameters that minimize photobleaching of the photoactivated signal. Because the autophagosome photo-chase assay assumes that disappearance of signal from pulse-labeled autophagosomes indicates fusion of pulse-labeled autophagosomes with lysosomes and subsequent degradation, it is important to know that loss of signal is not due to photobleaching during image acquisition. Photobleaching of fluorophores depends on properties of the fluorophores as well as

specific imaging configurations. Again, we advise using an empirical assay to assess the effect of photobleaching. Following photoactivation with the parameters identified above, a field should be repetitively imaged using identical image capture settings as those that will be used in the actual experiment. To determine how many iterations to use, consider the appropriate time sampling and experimental duration to confidently assess turnover rates. If autophagosome loss is predicted to occur over the course of two hours, 10 minute time points are appropriate to generate a curve defined by a total of 12 points from the 12 captured images. Given this scenario, photobleaching resulting from the collection of 12 images then needs to be assessed.

Photobleaching can be evaluated by setting up a time series to repetitively capture signal from the photoactivated field. For the purpose of assessing photobleaching, the delay between sequential frames can be reduced from 10 minutes to 5 seconds. This dramatically reduces the experimental duration to roughly 1 minute. Following capture of this time series, the fluorescence of the photoactivated field can be assessed. This photobleaching assay is carried out prior to inducing autophagy and is completed in a narrow time frame. Loss of photoactivated signal due to degradation of photoactivated proteins is therefore negligible. Fluorescence of the field at the start and end of this time series should consequently be nearly unchanged. If this is not the case, the imaging parameters should be changed. A number of parameters can be optimized to minimize photobleaching during image acquisition. Minimizing photobleaching is easiest to achieve by maximizing the amount of light emitted from the sample that reaches the detector. Objectives and filters with efficient light throughput dramatically help. Long pass filters may be

useful, provided they do not pass signal from autofluorescence or other fluorophores present in the sample. Also, decreased noise in detectors will improve signal to noise. We note that the photo-chase assay only requires resolution sufficient to identify PAGFP-Atg8-positive structures. Therefore, increasing the pinhole on scanning confocal microscopes or using a lower magnification lens may be desirable since better resolution generally comes at the expense of signal. Finally, we note that whereas time sampling should be sufficient to average out fluctuations, excessive sampling will unnecessarily bleach the sample. We therefore advise minimizing the number of images captured during the assay.

5. Experimental example: Assessing photobleaching

1. Using the photoactivation parameters established above, photoactivate a field of cells.
2. Set up a time-lapse series with the total number of images based on the anticipated time duration for autophagosome turnover. We suggest starting with 15 data points.
3. Run the time series below for 20 cycles:
    a. Capture an image using a configuration appropriate for the GFP signal.
    b. Pause for 5 seconds.
    c. Repeat the sequence.
4. Following image capture, measure the total fluorescence by drawing a region of interest around the activated cells in the first field. Determine whether the fluorescence in sequential frames decreases.

5. If little or no bleaching is measured, proceed. If the sample exhibits appreciable bleaching, modify the GFP image capture parameters as discussed above.

6. Carrying out the photochase assay

6.a. Inducing autophagy

Autophagy is commonly induced by replacing growth the medium with buffered solutions that lack critical nutrients. Media formulations that induce autophagy include Hanks Buffered Saline, Earle's Balanced Salt Solution, serum free media, and DPBS (Tasdemir et al., 2008). Incubation of cells in these minimal media leads to robust formation of starvation-induced autophagosomes. Punctate structures that label with PAGFP-LC3 are typically evident within one hour following medium replacement with these formulations. Stresses other than starvation are also known to produce autophagosomes. Some of these stresses are induced by broadly affecting cell homeostasis (i.e., H_2O_2 incubation); others are induced by targeting specific molecular processes (i.e., kinase inhibitors). The current catalog of small molecule inducers of autophagy is relatively short. However, ongoing autophagy drug screens are likely to uncover many more pharmacological modulators of the process (Zhang et al., 2007).

When evaluating the role small molecules play in autophagosome proliferation, it is important to bear in mind that the autophagy pathway responds to a broad range of cellular stresses, and commonly-used solvents such as DMSO can subtly affect cell homeostasis. To minimize off-target effects of drugs or solvents, the duration of treatments should not be excessive, and solvent controls should always be

run in parallel in adjacent wells seeded from the same cell stock. Ideally solvent controls should show no induction of autophagy relative to cells in optimal growth conditions.

Treating cells either with media formulations or small molecules can be easily performed using commercially available microscope chambers with coverglass bottoms. Above we described seeding 8-well LabTek chambers. Low volume microscope chambers such as these are convenient because they minimize required reagents. Having multiple chambers on a single slide is also convenient for drug titrations and parallel controls since all chambers are exposed to the same seeding and handling conditions. The chambers have removable plastic lids that maintain sterility during transfer and are accessible for media exchange and drug addition at the microscope.

The condition and density of cells is an important factor in photo-chase experiments. Because cell density can affect the autophagic response to stresses, cell density should be controlled to ensure it is not excessively high when the experiment is carried out. For the NRK144 line we find that basal autophagy is minimized when the cells are roughly 90% confluent. For autophagic inductions known to be rapid, growth medium can be replaced with either incomplete medium or medium containing a compound of interest on the day of the experiment with cells at 90% confluency. For inductions that require prolonged treatment, treatments should be started at a lower cell density to prevent overgrowth during the treatment. Similarly, if expression of a transgene is being tested, the transgene should be introduced at a cell density that accommodates cell growth while the gene is expressed.

Note that preliminary testing of drugs, media formulations, and culture conditions can be done using GFP-Atg8 expression systems and standard GFP imaging on conventional microscopes. There is very little structural difference between PAGFP and GFP (Patterson and Lippincott-Schwartz, 2002); in our experience with NRK-derived cell lines, PAGFP-LC3 and GFP-LC3 fusions are functionally identical.

7. Experimental example: Generating starvation-induced autophagosomes

1. Warm DPBS to 37°C.
2. Remove the seeded LabTek chamber from the incubator (set up as above) and place it on the surface of a T25 flask filled with 37°C water to maintain temperature.
3. Wash cells twice with DPBS using 500 μL per wash.
4. Remove and replace with 350 μL of DPBS.
5. Transfer the chamber to a 37°C incubator for two hours.
6. Transfer the chamber to the stage of an inverted microscope maintained at 37°C.
7. Locate a field of cells with transmitted light.

8. Pulse-labeling induced autophagosomes

Once autophagy is robustly induced, autophagosomes can be pulse-labeled by photoactivating PAGFP-Atg8 in the cells. Above we outlined a simple protocol to optimize photoactivation parameters. These parameters are now used to activate PAGFP-Atg8-positive autophagosomes. Figure 12 presents a schematic outline of the steps described above to pulse-label a population of autophagosomes. Note that

when 405 nm light is targeted to cells of interest, both membrane-bound PAGFP-Atg8 and cytosolic PAGFP-Atg8 are activated. The cytosolic PAGFP-Atg8 pool can be incorporated into autophagosomes that form later. To pulse label only autophagosomes, it may therefore be necessary to bleach the fluorescence from the cytosolic PAGFP-Atg8 pool following the photoactivation. Activated PAGFP, like GFP, can be photobleached by 490 nm light. Cytosolic PAGFP-Atg8 rapidly transits the volume of the cell and can be selectively bleached by repetitively targeting a small region of the cytosol.

To deplete activated cytosolic PAGFP-LC3 in the NRK144 line, we bleach a 5x5-micron box in the cytosol with 488 nm light every 10 seconds for 2 minutes. Note this will also bleach labeled autophagosomes in the bleach region; keeping the bleach box small minimizes the number of autophagosomes affected. The bleaching parameters depend on laser power, cell shape, etc. and are best tested empirically. Following the photobleaching step, the signal in the bleached region of interest should be roughly equivalent to the signal in this region of interest prior to photoactivation. Because autophagosomes recruit cytosolic PAGFP-LC3 to their membranes and thereby enrich signal on the membrane relative to the cytosol, one should confirm that photobleaching parameters are sufficient to rule out sub-detectable levels of cytosolic activated PAGFP-LC3 labeling autophagosomes formed after pulse-labeling. Non-induced cells can be photoactivated and subsequently photobleached using identical parameters.

Figure 12: Schematic representation of the steps needed to pulse-label an existing autophagosome population using photoactivation. Cells are first induced (1); induction leads to recruitment of PAGFP-Atg8 molecules (in gray) from the cytosol onto autophagosome membranes. Cells are next photoactivated with 405 nm light (2; targeted region indicated by gray box). This step activates both membrane bound and cytosolic PAGFP-Atg8 (activated PAGFP-Atg8 is shown in black.) Subsequently, signal from activated cytosolic PAGFP-Atg8 is photobleached by repetatively targeting a small region of the cytosol with 490 nm light (3; targeted region indicated by gray box). A population of autophagosomes is now pulse-labeled (4). New autophagosome formation will incorporate either activated and bleached PAGFP-Atg8 or non-activated PAGFP-Atg8; therefore, newly formed autophagosomes will not be detected.

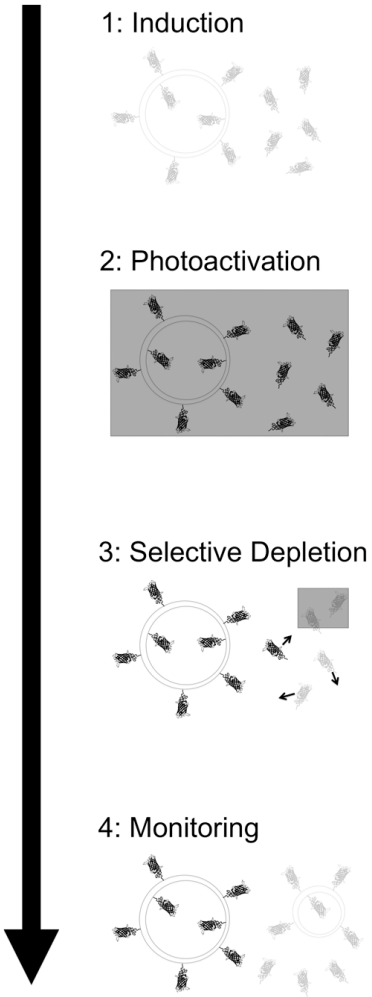

Subsequently, autophagy can be induced. If photobleaching is sufficient, no labeled autophagosomes should be detected during the course of the incubation. (For more details about FLIP--fluorescence loss in photobleaching--approaches to deplete signal, see the FLIP section of Snapp et al. (Snapp et al., 2003).

Following selective bleaching of the activated cytosolic PAGFP-Atg8 pool, a distinct set of autophagosomes is pulse-labeled (Figure 13). Autophagosomes that form after this time can incorporate either newly synthesized and unactivated PAGFP-LC3, or cytosolic activated and bleached PAGFP-LC3. In either case, these molecules do not fluorescently label new autophagosomes. Therefore, the fate of the labeled autophagosomes can now be uniquely tracked by monitoring the disappearance of this population as a function of time.

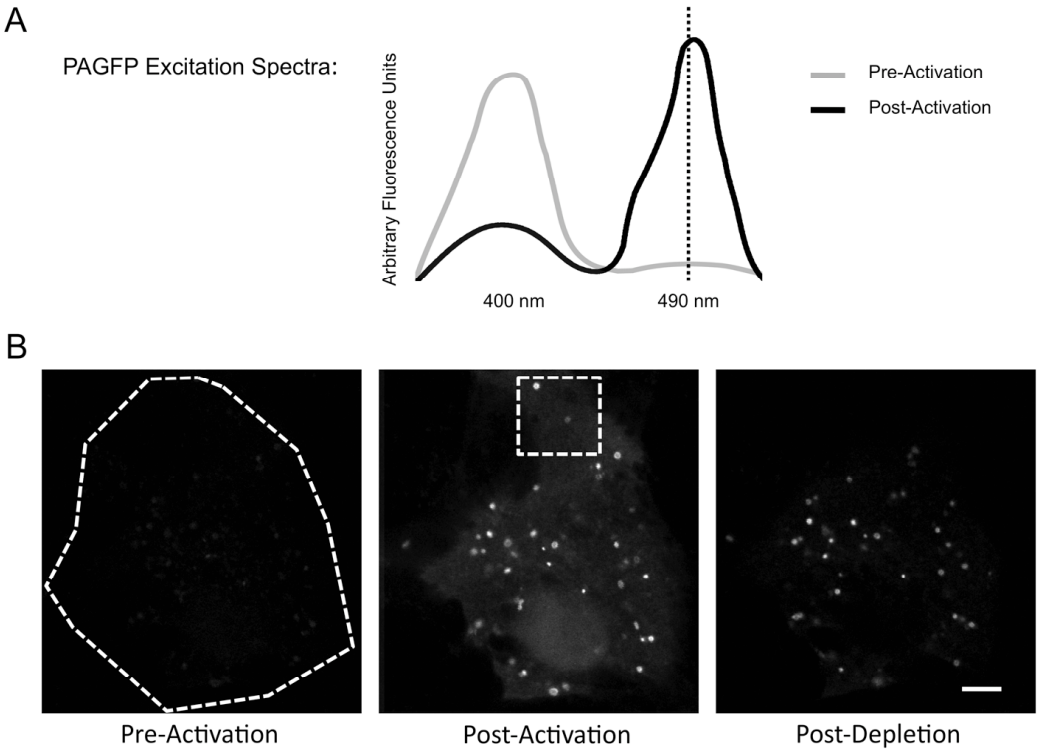

Figure 13: PAGFP spectra and pulse-labeling of a PAGFP-LC3 positive autophagosome population. (A) Prior to photoactivation, the excitation spectrum of PAGFP is centered near 400 nm. Following photoactivation, the excitation spectrum shifts such that its peak absorbance is like that of GFP. Therefore, before photoactivation, signal captured from PAGFP using GFP imaging parameters is minimal; the fluorophore does not efficiently absorb light in the 490 nm range. Following photoactivation, the fluorophore efficiently absorbs 490 nm range light and consequently emits a signal. (B) An induced cell was first photoactivated by targeting the outlined region with 405 nm light (left panel). The cytosolic activated signal was then bleached by repetitively targeting a small region of the cytosol (middle panel; dashed box) with 490 nm light. This depleted signal from the cytosolic activated PAGFP-LC3. At this stage an existing population of autophagosomes was pulse-labeled (right panel). Scale bar: 15 μm.

9. Determining the half-life of pulse-labeled autophagosomes

Determining the lifetime of pulse-labeled autophagosomes following pulse labeling simply involves imaging the pulse-labeled structures at the microscope. Above, we discussed a simple protocol to assess potential photobleaching during image acquisition. Because autophagosomes move dynamically (Jahreiss et al., 2008), it is unrealistic to expect to track individual autophagosomes over their lifetime. Instead, capturing images at distinct time points and quantifying the number of pulse-labeled autophagosomes present at each point provides a reasonable statistical picture of the rate of turnover of the pulse-labeled population. Because photobleaching is an issue (see above) we do not advise attempting to capture three-dimensional stacks to track the total number of autophagosomes in a cell at a given time. Instead we suggest taking a single plane with a pinhole set to capture 2 microns of information. For the NRK144 line, this provides sufficient resolution to easily resolve autophagosomes and a broad enough sampled volume to generate clear reproducible data. Figure 14 shows a panel of time points taken following pulse-labeling of an autophagosome population.

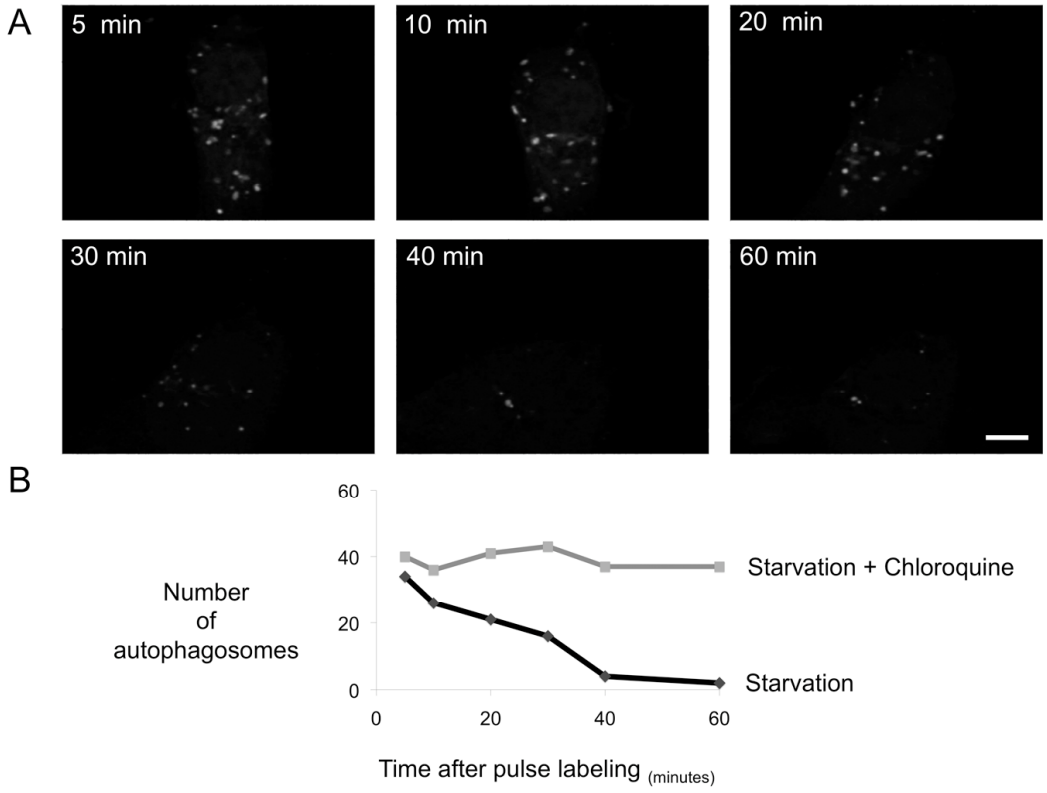

Figure 14: Monitoring the fate of a population of autophagosomes. Following photoactivation and selective depletion, a pulse-labeled population of autophagosomes was imaged every five minutes for one hour (A). Single plane images were captured using parameters previously shown to result in no appreciable photobleaching. (B) PAGFP-LC3-positive autophagosomes were counted in sequential images. The number of autophagosomes observed in each image was plotted as a function of elapsed time (black line). The autophagosome population exhibited a half-life of approximately 25 minutes. Autophagosomes in a cell treated with chloroquine did not degrade in this time frame. Following chloroquine treatment, an autophagosome population was pulse-labeled and tracked using identical photoactivation, bleaching, and imaging conditions (gray line). Scale bar: 25 μm.

The ease and confidence with which pulse-labeled autophagosomes can be counted is dependent on cell type; for example, this affects autophagosome size and number. We have chosen to work with NRK-derived cells in part because these cells generate easily resolvable and quantifiable autophagosomes. For large-scale analyses, when possible we advise establishing a system that generates easily quantifiable signals. Reasonably discrete autophagosomal signals may also expedite automating quantification. A number of software algorithms can be applied to count autophagosomes (e.g., Metamorph TopHat, Improvision Volocity segmentation). While these analyses remove bias, they should always be evaluated against counting by eye to confirm that the algorithms used do not either misidentify or discount significant numbers of autophagosomes.

10. Controls

To demonstrate that loss of signal from pulse-labeled autophagosomes is in fact due to fusion of the structures with lysosomes, the photo-chase assay can be repeated in the presence of lysosomal inhibitors. Many lysosomal inhibitors (i.e., bafilomycin A_1, chloroquine, ammonium chloride) act by increasing intralysosomal pH and consequently inactivating pH-dependent lysosomal proteases (Tasdemir et al., 2008). Although the mechanism is unclear at this time, increase in intralysosomal pH is reported to perturb fusion of lysosomes with autophagosomes (Klionsky et al., 2008b; Yamamoto et al., 1998). Consistent with this, we observe that disappearance of starvation-induced autophagosomes in the NRK144 line is completely blocked by lysosomal inhibition with chloroquine. Persistant PAGFP-LC3 labeled autophagosomes do not appear to be lysosomes that fail to quench PAGFP-LC3

signal, as almost all of these stuctures do not label with the lysosomal marker LysoTracker Red DND-99. (Note that in our experience the lysotracker label functions despite pH elevation by chloroquine.; however, a non pH sensitive marker like LAMP1-RFP could also be used.) This control is important to demonstrate that activated PAGFP-Atg8 is not released from autophagosomal membranes in a manner independent of their conversion to autolysosomes. Although there is debate about whether Atg4 activity (Tanida et al., 2004) might remove LC3 from autophagosomal membranes prior to lysosomal fusion, notably, at least activated signal on the inner membrane will persist irrespective of Atg4 activity.

To further confirm that pulse-labeled autophagosomes disappear via lysosomal fusion, one can also track individual autophagosomal structures to visualize their fusion with lysosomes. Lysosomes can be easily labeled using lysotropic dyes such as LysoTracker Red DND-99; these dyes are trapped in low pH environments due to their inability to cross lysosomal membranes once they are protonated. If pulse-labeled autophagosomes are degraded or quenched once in the lysosomal environment, very little if any overlap of the autophagosome marker with the lysosome marker should be observed. The activated PAGFP-LC3 signal in NRK144 cells persists on autophagosomes through fusion with lysosomes. Upon lysosomal fusion, the signal is rapidly lost.

A final point: the controls above address whether the disappearance of the PAGFP-Atg8 signal on autophagosomes is the result of fusion with lysosomes. The photo-chase assay described here indicates the fate of autophagosomes up to the point when lysosomal fusion occurs. However, we note that this assay does not address the

future fate of the structures once they convert to autolysosomes and lose the Atg8 signal.

11. Conclusions

The photo-chase experiment we describe here is a straightforward approach to study how autophagosomes in cells or tissues contribute to cell homeostasis. Simply observing increased numbers of autophagosomes does not indicate that the autophagy pathway is catabolically active. This fact has been a challenge in the field since early autophagic studies in the 1960s (De Duve and Wattiaux, 1966). In order for autophagic substrates to be degraded, they must be exposed to lysosomal hydrolases. The photo-chase assay described here addresses whether fusion with lysosomes occurs by quantifying how quickly fluorescently pulse-labeled autophagosomes disappear in response to lysosomal fusion events. Unlike assays that quantify the catabolic activity of autophagosomes by substrate analyses, the photo-chase assay evaluates the fate of the autophagosomal structures themselves. Because of this, the assay is a sensitive readout for autophagic catabolism. Additionally, because it is carried out in live cells expressing a transgenic marker, it does not require excessive cell handling or large amounts of reagents needed for standard pulse-labeling.

The assay presented here uses photoactivatable GFP (PAGFP). Since the initial description of PAGFP, many new photoactivatable proteins have been reported, and the photo-chase assay will likely benefit from these new proteins. These proteins already address phototoxicity and detection issues by more efficiently activating and exhibiting a higher fold signal increase. Additionally, some of these proteins have both pre- and post-activation fluorescent signals; in the future, the

photochase assay may be adapted to simultaneously track turnover of a pulse-labeled population while also tracking formation of new autophagosomes (labeled with the unactivated fluorescent protein).

Autophagy is a very promising field for biomedical applications. It's so-called "housekeeping" function is a promising target to address diseases caused by general accumulations of deleterious proteins or organelles, and it's role in cell death is a potential cancer therapy target (Hoyer-Hansen and Jaattela, 2008). Many screens for effectors of autophagy are either recently completed or underway. Approaches to determine how these newly identified effectors function are needed. The photo-chase assay is one approach to rapidly address this challenge. Using the photo-chase assay and complimentary approaches described in this volume and elsewhere (Tasdemir et al., 2008), we can delineate what autophagosome proliferation functionally means.

Chapter 4: Mitochondria supply membranes during the biogenesis of autophagosomes

The following chapter was co-submitted with work discussed below from Richard Youle's lab. (Title: Mitochondria supply membranes during the biogenesis of autophagosomes. Authors: Dale W. Hailey, Peter Kim, Kasturi Mitra, Rachid Sougrat, and Jennifer Lippincott-Schwartz.) The findings presented here are further discussed in Chapter 5 in light of the ongoing debate about how autophagosomes form. Relevant Materials and Methods and References appear in these sections at the end of the thesis.

Starvation-induced autophagosomes engulf cytosol and/or organelles for re-supplying depleted nutrients within cells. The origin of autophagosomal membranes remains unclear. Using live cell imaging approaches to label autophagosomes and other organelles, we find that the membranes of autophagosomes formed under starvation utilize the outer mitochondria membrane. During autophagosome formation, the early autophagosomal marker, mApg5, transiently localizes to punctae on the surface of mitochondria followed by the late autophagosomal marker, LC3. A tail-anchored outer mitochondrial membrane protein diffuses between the outer mitochondrial membrane and newly forming autophagosomes until the two organelles dissociate. Starvation-induced autophagosomes produced in this manner engulf cytosolic contents, are 3-MA-sensitive and persist in cells for less than 40

minutes before fusing with lysosomes. This involvement of outer mitochondrial membrane in autophagosomal formation is unique to starvation. ER stress-induced autophagosomes show no mitochondrial membrane utilization, exhibit different turnover kinetics, and do not sequester cytosolic components. These unexpected findings suggest mitochondria serve a key role in starvation by contributing membrane to the formation of autophagosomes.

1. Introduction

During starvation, many organisms retrieve molecules and energy via bulk degradation of their own intracellular components. This process has been termed macroautophagy, or simply autophagy—"self eating". Execution of autophagy involves formation of multilamellar organelles that engulf cytosolic contents including proteins, protein aggregates, and entire organelles *en masse*. Lysosomes subsequently fuse with autophagosomes, delivering lysosomal proteases that degrade captured substrates within this hybrid structure called an autolysosome. Transporters and permeases within the membrane of the autolysosome then move components released by catabolism back to the intracellular environment (Xie and Klionsky, 2007).

The requirement for autophagy during starvation has been demonstrated across the eukaryotic domain. In the absence of functional autophagy, *S. cerevisiae* cells die more readily when cells are deprived of nitrogen and carbon (Scott et al., 1996; Tsukada and Ohsumi, 1993). Similarly, nitrogen-starved *Arabadopsis thaliana* autophagy mutants exhibit increased rates of leaf senescence and chlorosis (Doelling et al., 2002). In placental mammals, autophagy is activated after birth following the

switch from placental nourishment to suckling. Mice lacking functional autophagy die shortly after birth (Kuma et al., 2004).

Despite intense interest in the autophagy field, the source of autophagosomal membranes is not clearly established (Juhasz and Neufeld, 2006). Proteomic studies of isolated autophagosomal membranes have identified peripheral proteins but no clear signature for a membrane origin (Overbye et al., 2007). Other studies of autophagosome biogenesis have implicated membrane contribution from a number of sources including the ER, TGN, and mitochondria (Axe et al., 2008; Reggiori et al., 2005; Young et al., 2006). These observations and the reported role of autophagy in diverse stress responses raise the question of whether processes regulating the formation of autophagosomes might be determined by induction conditions. A key question in the autphagy field is therefore how starvation-induced autophagy relates to other forms of autophagy.

In addition to starvation, the autophagic pathway is activated by mitochondrial damage, hypoxia, ER stress, pathogen infection, and execution of developmental programs (Kirkegaard et al., 2004; Levine and Klionsky, 2004). Many autophagic inductions are regulated by the mTOR kinase—a kinase that integrates a range of metabolic signals including amino acid levels (Meijer and Codogno, 2004). However, other inductions bypass mTOR regulation (Williams et al., 2008). Additonally some molecular machinery is clearly specific to particular autophagic activities. Atg19p and Atg20p are dispensable for nitrogen starvation-induced autophagy in yeast. However, these proteins participate in delivery of the vacuolar

protease Ape1p to the vacuole that requires core autophagy machinery (Yorimitsu and Klionsky, 2005).

Here we have undertaken a morphological and kinetics approach to look in detail at numerous characteristics of starvation-induced autophagosomes in a mammalian tissue culture cell model. We have examined autophagosome formation and turnover rates, their differential function, and their membrane origin under different induction conditions. Our findings suggest starvation-induced autophagosomes, but not autophagosomes induced by ER stress, utilize the outer membrane of the mitochondria for their formation. We discuss why this occurs and its potential role in lipid circulation within cells.

2. Results

2.a. Characterizing how starvation-induced autophagosomes form

To follow formation and fate of autophagosomes, we isolated a clonal NRK (Normal Rat Kidney) cell line stably expressing cyan fluorescent protein (CFP) fused to LC3 (line NRK58B). LC3 (formerly MAP1LC3, the rat homolog of *S. cerevisiae ATG8*) is a canonical marker for autophagic vesicles. It is covalently attached to phosphatidylethanolamine (PE) that tethers LC3 to autophagic membranes (Kabeya et al., 2000; Mizushima et al., 2004). CFP-LC3 in line NRK58B freely diffused between cytosolic and nuclear pools under replete growth conditions; very little CFP-LC3 was observed on autophagic membranes (<10 autophagosomes per cell) (Figure 17A, B, see 0 time point). Replacement of growth media with DPBS (PBS supplemented with glucose, sodium pyruvate, calcium and magnesium), HBSS or serum-free media induced a starvation response. CFP-LC3 was robustly recruited

from the cytosol onto autophagosomal membranes (Figure 15A). NRK58B cells exhibited very reproducible induction kinetics when maintained at <90% confluence. After a three-hour starvation, cells contained between 20-60 CFP-LC3-labeled autophagic structures. (Figure 15A, B).

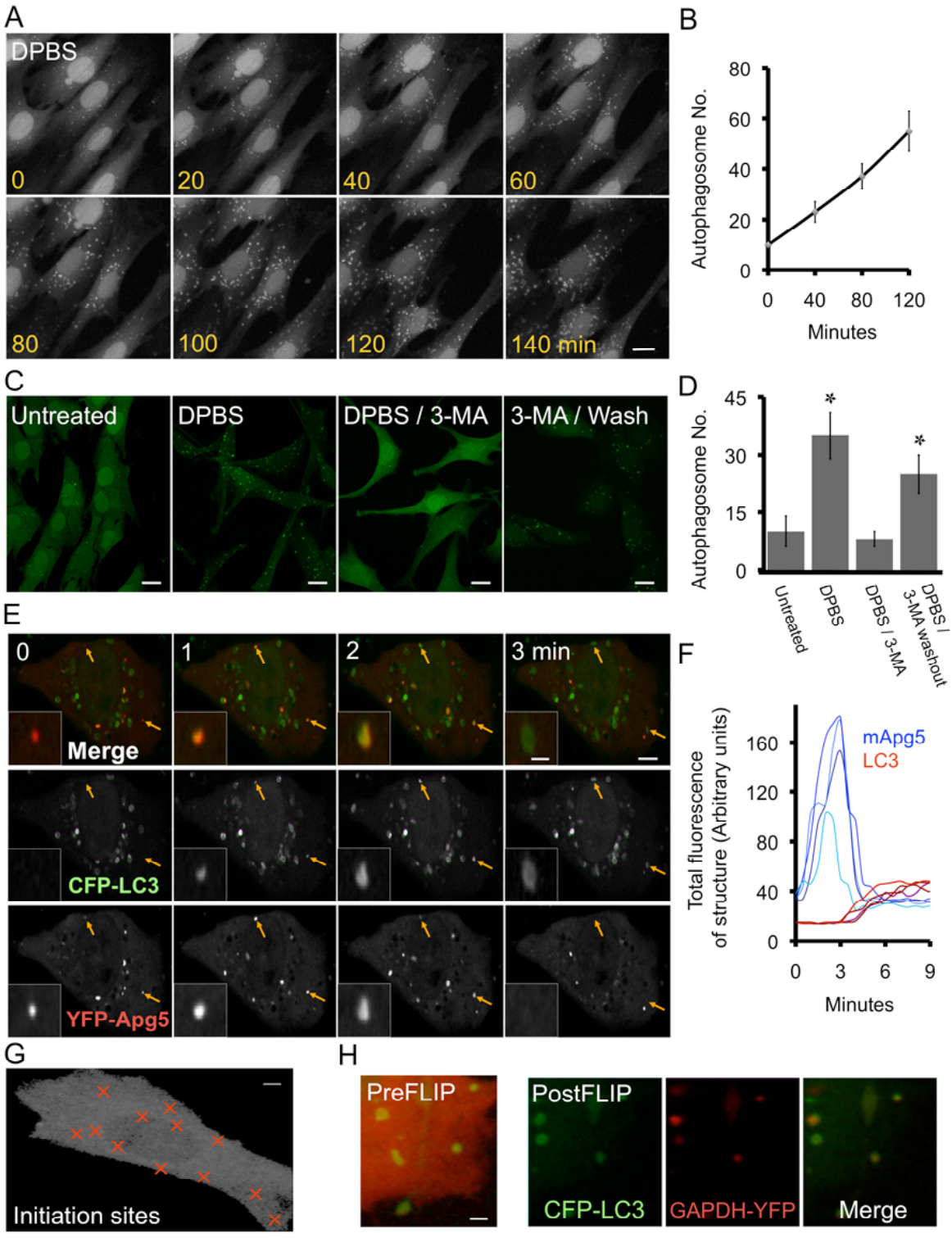

Figure 15: Characterizing the formation of starvation-induced autophagosomes. (A) Time-lapse live-cell imaging of starved NRK58B cells. CFP-LC3 positive structures rapidly

proliferated following switch to starvation media. Note concurrent depletion of cytosolic and nuclear pools of CFP-LC3. Growth media (time 0) was replaced with starvation media (subsequent panels). (Scale bar: 20um) (B) Quantitation of CFP-LC3 positive structures. Autophagosomes were counted in sequential time-lapse frames and plotted as a function of time in starvation media. (C) Treatment with ClassIII PI(3) kinase inhibitor 3-methyladenine. Robust formation of CFP-LC3 structures required activity of the kinase. Identical wells were untreated, starved, or starved in the presence of the 3-methyladenine (3-MA) for 2 hours (three left panels). Subsequently, starved cells treated with 3-MA were washed, incubated in DPBS and imaged 2 hours later (right-most panel). 3-MA treatment abolished recruitment of CFP-LC3 to membranes and depletion of cytosolic and nuclear pools (2^{nd} from right). Washout of 3-MA restored the ability of cells to induce autophagosomes during starvation. (Scale bar: 20um) (D) Quantitation of 3-MA treatments (average of 20 cells). Asterix indicates treatment statistically different from untreated cells by Student t-test. p value < 0.001. (E) Time-lapse live-cell imaging of NRK58B cells expressing YFP-mApg5. During starvation, YFP-mApg5 punctae appeared. These punctae subsequently recruited CFP-LC3 and released YFP-mApg5. Arrows indicate two examples. Inset indicates zoom of autophagosome by lower right arrow. (Scale bars: 2um inset ; 10 um panel) (F) Quantitation of YFP-mApg5 and CFP-LC3 signals in time-lapse frames. Dramatic accumulation of YFP-mApg5 always preceded CFP-LC3 recruitment. YFP-mApg5 persisted <4 min and abruptly released. (G) Mapping sites of autophagosome formation. The transient appearance of YFP-mApg5 which precedes CFP-LC3 recruitment were scattered throughout the cytosol during starvation. (Scale bar 5um) (H) Identifying capture of cytosolic proteins in starvation-induced autophagosomes. Freely diffusing signal was depleted by repetitive photobleaching outside the panel region. This depletion revealed a subpopulation of GAPDH-YFP captured within CFP-LC3 labeled structures. (Scale bar 2um.)

The activity of the Vps34/Beclin 1 Class III PI3 kinase complex is one of the most upstream events in autophagosome formation (Furuya et al., 2005). 3-methyladenine (3-MA) is a potent inhibitor of this kinase complex (Petiot et al., 2000). When NRK58B cells were incubated with DPBS in the presence of 10mM 3-MA for three hours, recruitment of CFP-LC3 onto punctae was abolished; CFP-LC3 existed solely as a freely diffusing pool (Figure 15C, D). Subsequent washout of 3-MA restored the ability of these cells to induce autophagy in response to starvation (Figure 15C, D). These results indicated, that starvation-induced, CFP-LC3-labeled structures require Class III PI3 kinase activity.

To assess the requirement for core autophagy machinery upstream of LC3 recruitment, we monitored behavior of mApg5. mApg5 is downstream of the Class III PI3 kinase complex and has been reported in electron microscope (EM) studies to label cup-shaped autophagosomes (Mizushima et al., 2001). mApg5 is regarded as a marker for an early stage in autophagosome biogenesis. We evaluated whether CFP-LC3-positive structures in the NRK58B line exhibited initial recruitment of YFP-mApg5 to structures prior to the appearance of CFP-LC3 on those structures. YFP-mApg5 was transfected into NRK58B cells imaged using dual channel spinning disk confocal microscopy. The appearance of CFP-LC3 on membranes was always preceded by initial appearance of YFP-mApg5 (Figure 15E,F). YFP-mApg5 on maturing autophagic vesicles appeared as a sudden dramatic burst in fluorescent signal followed by abrupt signal loss (Figure 15E). The YFP-mApg5 signal persisted

for ~3 minutes. This recruitment and release always coincided with subsequent accumulation of CFP-LC3 (Figure 15E,F). Hence, upstream core autophagy machinery was associated with autophagosomal membranes prior to CFP-LC3 recruitment.

Because of the transient nature of the YFP-mApg5 spots and their appearance at early stages in autophagosome assembly, we could use the intracellular locations of these spots to map sites of autophagosome assembly. YFP-mApg5 spot mapping suggests that autophagosome assembly occurs at diverse sites throughout the cell rather than at a tightly localized site of assembly (Figure 15G), inconsistent with formation at spatially restricted organelles like the Golgi and trans golgi network.

We next investigated whether autophagosomes generated by starvation in the NRK58B cell culture system capture diffuse cytosolic components. Glyceraldehyde 3-phosphate dehydrogenase (GAPDH) and lactate dehydrogenase (LDH) are long-lived cytosolic proteins that were previously reported to be autophagy substrates (Hoyvik et al., 1991; Sneve et al., 2005). To evaluate whether these cytsolic substrates were captured by starvation-induced autophagosomes, exogenously expressed GAPDH-YFP (Figure 15H, preFLIP) or YFP-LDH (data not shown) were visualized in starvation-induced NRK58B cells. Fluorescent signals from freely diffusing, cytosolic GAPDH-YFP or YFP-LDH molecules were depleted by repetitive photobleaching targeted to a small region of cytosol. This revealed subpopulations of these proteins present in punctae within the cells (Figure 15H, postFLIP). The punctae co-localized with either lysosomal markers (not shown) or

CFP-LC3 (Figure 15H), indicating that DPBS-induced, CFP-LC3-positive autophagosomes in the NRK58B line trap freely diffusing proteins from the cytosol.

3. Lifetime and fate of starvation-induced autophagosomes

We next characterized the fate of starvation-induced autophagosomes first by assessing whether these autophagosomes readily fuse with lysosomes and then by asking, once formed, how long starvation-induced autophagosomes persist after formation. To visualize fusion of autophagosomes with lysosomes, autophagosomes and lysosomes were simultaneously imaged. Starved NRK58B were subsequently labeled with the lysosomal marker, LysoTracker Red DND-99 (LysoTracker). High-speed imaging revealed frequent fusion events between CFP-LC3-labeled autophagosomes and LysoTracker-labeled lysosomes (Figure 16A, see yellow arrow). Upon fusion, LysoTracker signal accumulated in CFP-LC3-labeled autophagosomes. Soon thereafter, CFP-LC3 signal from these structures was lost (Figure 16A, see yellow arrow at 3 min). Due to this loss, starved cells showed little overall overlap of CFP-LC3 with LysoTracker (Figure 16A) or other lysosomal markers, including YFP-Lgp120 (yellow fluorescent protein fusion to the LAMP1 rat homolog) (not shown).

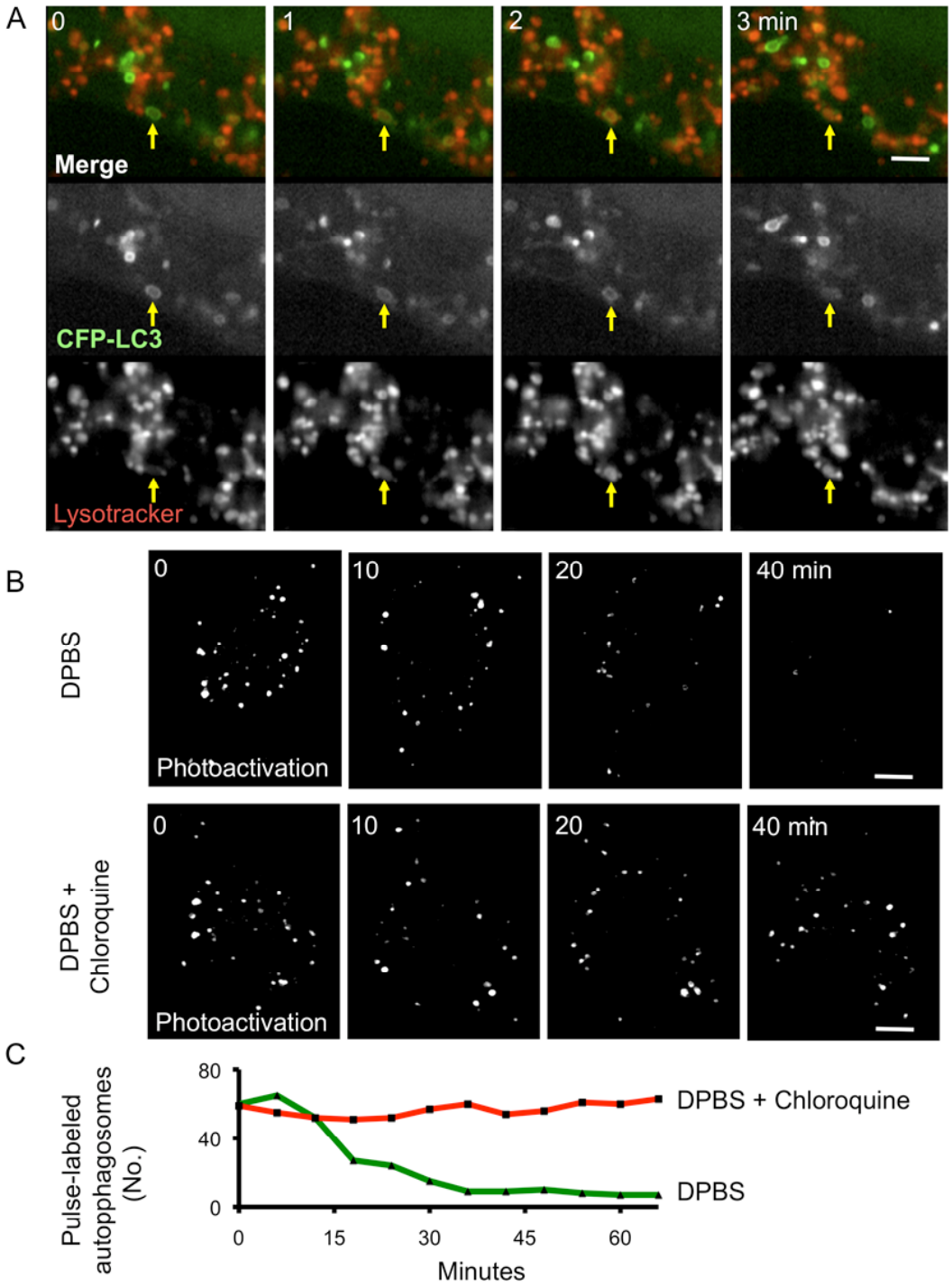

Figure 16: Characterizing the fate of starvation induced autophagosomes. (A) Visualizing fusion of autophagosomes with lysosomes. NRK58B cells were starved and subsequently labeled with a cell permeant vital lysosomal marker. Live-cell imaging revealed fusion

events between autophagosomes and lysosomes that caused accumulation of lysosomal marker and coincident loss of CFP-LC3 signal from the hybrid organelle, the autolysosome (arrow). (B) Visualizing turnover of autophagosomes by photo pulse-labeling and live cell imaging. Following a 2 hour starvation, PAGFP-LC3 cells were photoactivated and depleted of cytosolic activated signal to pulse label an existing population of autophagosomes (Top left panel). Live cell imaging revealed time dependent disappearance of the pulse-labeled population (top panels), which was blocked by addition of chloroquine. (C) Quantitation of the lifetime of the structures. Note the turnover of starvation induced autophagosomes was surprisingly efficient: $t_{1/2}$ of ~25 minutes. (Scale bars for panels A and B: 5um.)

To quantify the rate of autophagosome turnover, we designed a photoactivation experiment to follow the fate of induced autophagosomes. PAGFP (photoactivatable variant of GFP) is a variant of GFP; it's excitation is irreversibly altered when it is exposed to ~405-nm light. Activated PAGFP is excited by 488-nm laser light; non-activated PAGFP is effectively dark (Patterson and Lippincott-Schwartz, 2002). To pulse-label autophagosomes, NRK cells stably expressing PAGFP-LC3 were starved by DPBS treatment and photoactivated. This photoactivation converted PAGFP-LC3 present both in the cytosol and on autophagosomes. To follow only signal present on existing autophagosomes, non-membrane bound PAGFP-LC3 was depleted by repetitively photobleaching a small region in the cytoplasm. This selective photobleaching allowed us to uniquely label a population of autophagosomes; new autophagosomes could incorporate only newly synthesized (non-activated) or activated and bleached PAGFP-LC3. We tracked the fate of this pulse-labeled population of autophagosomess using live-cell imaging (Figure 16B, C). Starvation-induced autophagosomes exhibited near complete turnover within 40 minutes. Loss of PAGFP-LC3 signal was not due to photobleaching or release of PAGFP-LC3 from autophagosomes prior to lysosomal fusion, as the turnover was completely blocked by treatment with chloroquine (Figure 16B, C), an aminoquinoline that increases intralysosomal pH, inactivates pH-dependent lysosomal proteases, and blocks lysosomal fusion with autophagosomes (Tasdemir et al., 2008).

From these live cell studies we conclude that starvation-induced autophagosomes require ClassIII PI3Kinase activity, exhibit subsequent mApg5 and

LC3 recruitment, capture cytosolic cellular components, and degrade in a lysosomal dependent fashion. Furthermore, these autophagosomes assemble at sites scattered throughout the cell and rapidly mature and degrade, requiring a large lipid flux from the autophagosomal membrane source to autolysosomes.

3.a. Comparing starvation-induced autophagosomes to those induced by ER stress

To ask whether properties of autophagosomes induced by starvation are universal or unique to starvation, we conducted parallel experiments on NRK58B cells under conditions known to induce ER stress. Thapsigargin (an ER calcium pump inhibitor) is commonly used to deplete ER luminal calcium stores (Tadini-Buoninsegni et al., 2008). Abundant chaperones like BIP, calreticulin and calnexin require calcium for their activities; depletion of ER calcium generally perturbs the ER folding environment (Brostrom and Brostrom, 2003). Other studies have demonstrated that thapsigargin can induce autophagosome formation (Ogata et al., 2006; Sakaki et al., 2008). Treatment of the NRK58B line with thapsigargin robustly generated CFP-LC3 labeled structures (Figure 17A, B). Formation of thapsigargin-induced CFP-LC3 structures was sensitive to 3-MA; simultaneous treatment with thapsigargin and 10mM 3-MA suppressed the formation of CFP-LC3-positive structures (Figure 17C), indicating that these structures are not LC3 aggregates reportedly observed under conditions of LC3 overexpression. However, in contrast to starvation-induced autophagosomes, thapsigargin-induced structures did not capture diffuse cytosolic components. When GAPDH-YFP was expressed in NRK58B cells and autophagy was induced by thapsigargin, GAPDH-YFP was not retained in CFP-

LC3-positive structures (Figure 17E, F). Recent reports have suggested that autophagosomes induced by ER stress capture predominately ER membrane. Hence these structures could exclude cytoslic proteins like GAPDH-YFP. Thapsigargin-induced autophagosomes also exhibited strikingly longer half lives than starvation-induced autophagosomess (Figure 17G). What underlies these differences? One possibility is that the biogenesis of starvation-induced autophagosomes is fundamentally different. We next considered whether autophagosome formation under starvation conditions has properties that are unique to starvation. To that end, we surveyed putative membrane sources of starvation-induced autophagosomal membranes.

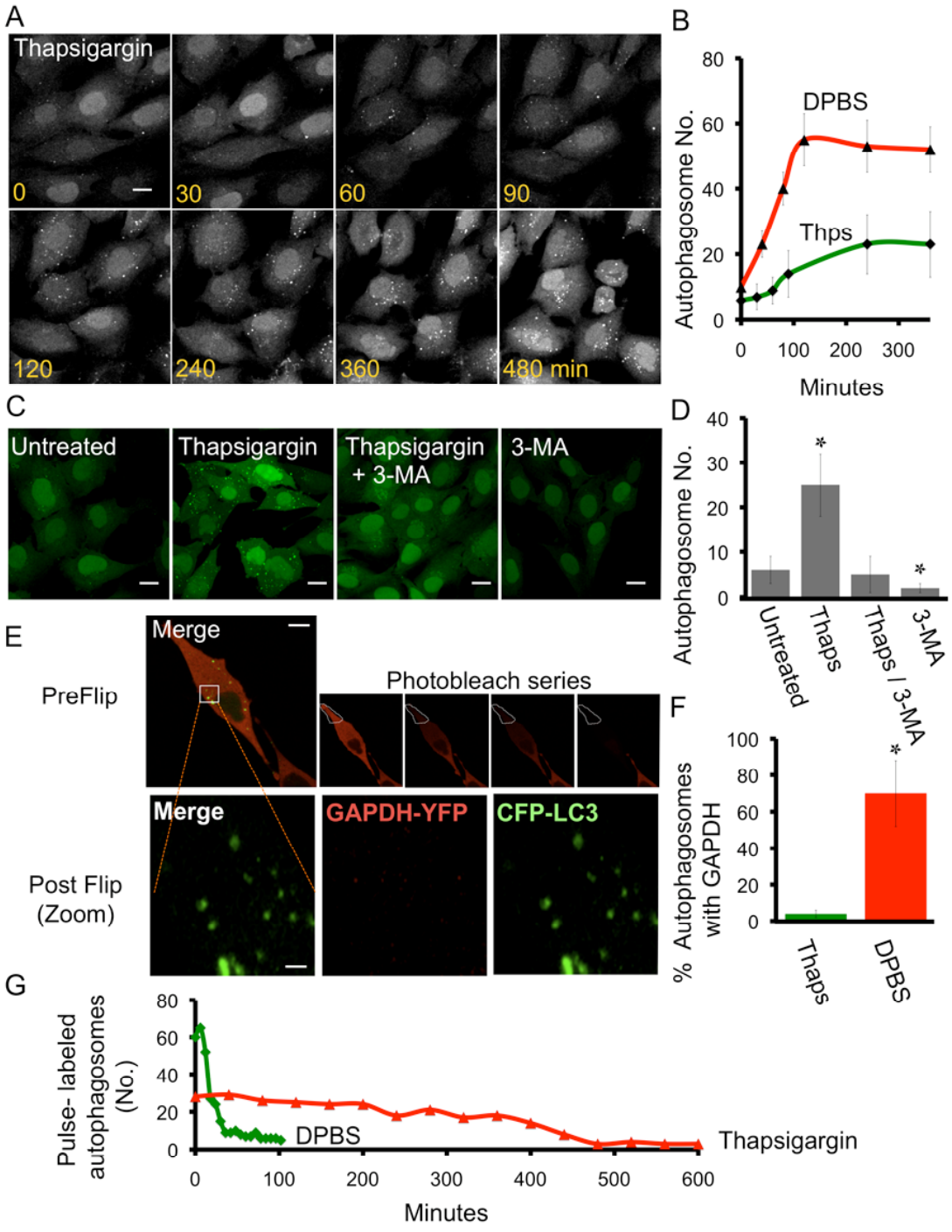

Figure 17: Comparing formation and fate of Thapsigargin-induced autophagosomes. (A) Time-lapse live-cell imaging of thapsigargin treated NRK58B cells. Autophagosomes proliferated immediately following treatment. Note cytosolic and nuclear pools of CFP-LC3 were not depleted. Growth media (time 0) was replaced with media containing thapsigargin

(subsequent panels). (Scale bars: 20um.) (B) Quantitation of CFP-LC3 positive structures. Autophagosomes rapidly proliferated in response to thapsigargin treatment but reached a lower steady state number (green line) than in starvation (red line). CFP-LC3 positive structures were counted in sequential time-lapse frames. (C) Treatment with ClassIII PI(3) kinase inhibitor 3-methyladenine. 3-MA treatment abolished thapsigargin-induced recruitment of CFP-LC3 to membranes. Note that cytosolic and nuclear signal increased relative to untreated and 3-MA alone. (Scale bars: 20um.) (D) Quantitation of 3-MA treatments. 3-MA robustly inhibited autophagosome formation to levels comparable to the untreated control. (Quantitation of 20 cells). Asterix in bar graphs indicates treatment statistically different from untreated cells by Student t-test; p values < 0.001. (E) Assaying for capture of cytosolic proteins in thapsigargin-induced autophagosomes. Depletion of freely diffusing cytosolic GAPDH-YFP did not reveal punctae (i.e. cytosolic proteins within thapsigargin induced autophagosomes.) Top right four panels show depletion of GAPDH-YFP signal by repetitive photobleaching within the white ROI. Bottom panels show zoom of inset outside the targeted photobleach region. Following photobleaching, no GAPDH punctae remained. (Scale bar upper panel: 20um; lower panel: 4um.) (F) Quantitation of GAPDH-YFP captured in autophagosomes. Very few thapsigargin-induced autophagosomes showed GAPDH-YFP capture, compared with a majority of starvation-induced autophagosomes. Asterix indicates treatment statistically different from untreated cells by Student t-test; p values < 0.001. (G) Comparison of the lifetime of the thapsigarin-induced structures versus starvation-induced structures. As in Figure 16C, PAGFP-LC3 positive autophagosomes were pulse-labeled and tracked with live cell imaging. Thapsigargin-induced autophagosomes exhibited a dramatically longer $t_{1/2}$ (~6 hours) than starvation-induced autophagosomes (~25minutes).

3.b. Identifying the membrane source of starvation-induced autophagosomes

We looked for the autophagosomal membrane source using a fluorescent protein-based approach, reasoning that if intracellular membrane systems were utilized in the formation of autophagosomes, chimeric markers robustly expressed might be transferred from those membranes to induced autophagic vesicles. We transiently expressed a battery of YFP-fusion proteins targeted to different intracellular membrane systems in NRK58B cells. In addition to previously characterized markers for the ER (CD3δ-YFP), Golgi apparatus (GalT-YFP), TGN (TGN38-YFP), early endosomal system (EEA1-YFP) and plasma membrane (YFP-GPI), we designed a marker for the mitochondrial outer membrane (YFP-cb5^{TM}). YFP-cb5^{TM} consists of YFP fused to the N-terminus of the tail anchor of mitochondrial targeted cytochrome b5. Under growth conditions, YFP-cb5^{TM} colocalized completely with mitochondrial markers (MitoTracker Red and Mito-RFP, red fluorescent protein fused to the targeting sequence of cytochrome c oxidase subunit VIII to target the mitochondrial matrix).

For each marker, autophagy was induced 16 hours post transfection by replacement of growth media with DPBS. After a 2-hour incubation, potential delivery of the chimeric marker from its respective targeted intracellular membrane system to autophagosomes was assessed. Live cells were imaged by dual-channel high-resolution confocal microscopy using interlace line scanning to eliminate motion artifacts. While other surveyed membrane systems showed little or no overlap with CFP-LC3-positive autophagosomes, the overlap of the mitochondrial outer membrane

marker was striking (Figure 18A). This overlap could not be attributed to the density of the mitochondrial signal, as overlap with the matrix mitochondrial marker was dramatically less (Figure 18B). The mitochondrial outer membrane marker YFP-cb5^{TM} was present on nearly 80% of CFP-LC3 positive autophagosomes formed after 2 hours of DPBS treatment. Other markers exhibited strikingly less overlap (<20% for all other YFP fusions) (Figure 18C).

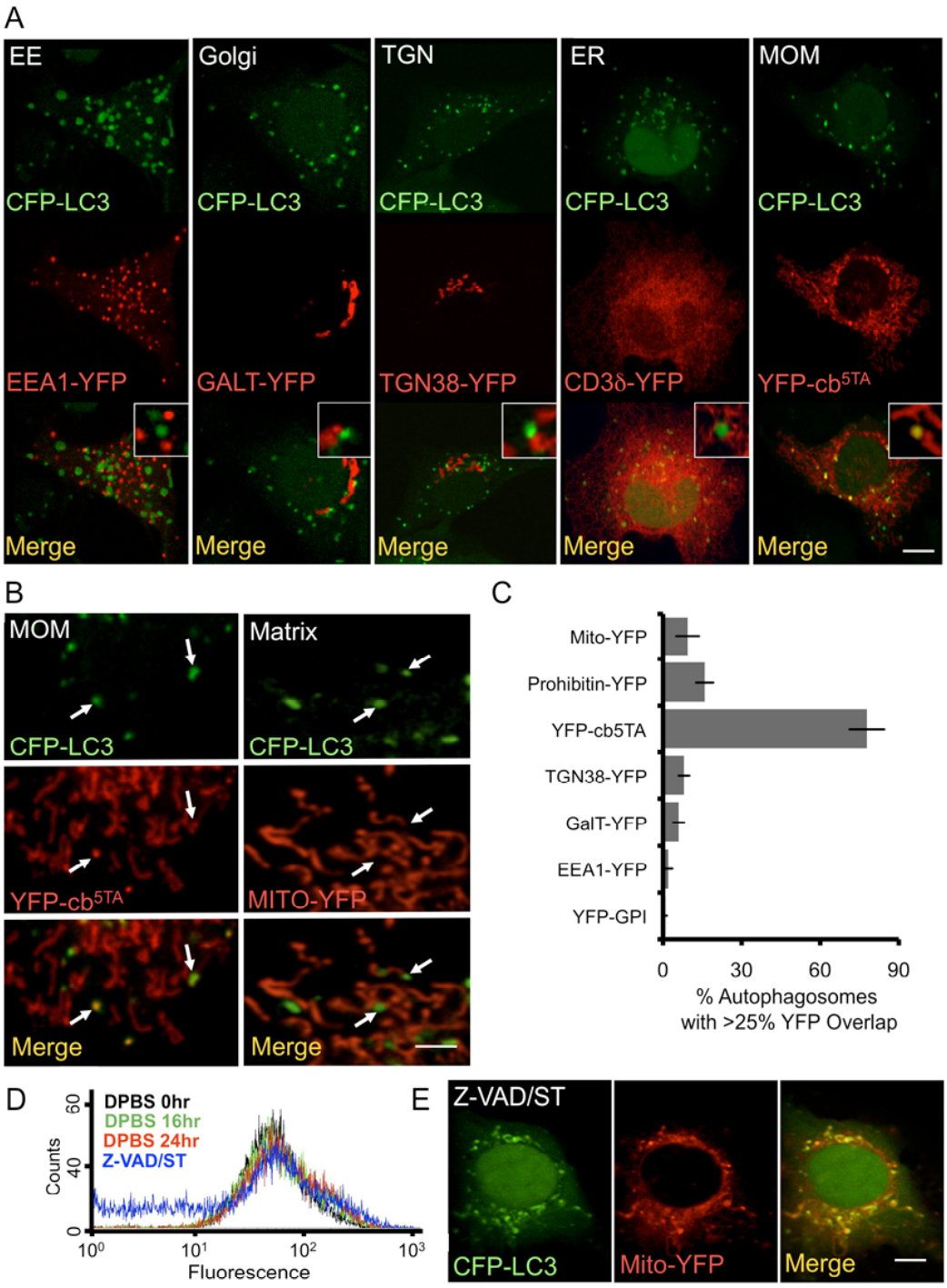

Figure 18: Screening for and evaluating exogenous membrane-targeted markers on autophagosomes. (A) Expression of chimeric-YFP membrane markers in starvation induced NRK58B cells. Chimeric YFP markers targeting intracellular membrane systems were expressed in NRK58B cells (shown here left to right: early endosomal system, Golgi, Trans

golgi network, ER, and mitochondrial outer membrane.) The mitochondrial outer membrane marker YFP-cb5^{TM} uniquely colocalized with induced autophagosomes. (Scale bar 15um.) (B) Comparison of CFP-LC3 signal overlap with mitochondrial outer membrane (MOM) signal and mitochondrial matrix signal. High-resolution imaging of NRK58B cells expressing MOM and matrix markers revealed robust overlap of CFP-LC3 signal with the outer membrane but not the matrix marker (see arrows). (Scale bar: 4um.) (C) Quantitation of overlap of CFP-LC3 signal with membrane marker signal. For each marker, autophagosomes with greater than 25% CFP signal overlap with YFP signal were counted; this number was divided by the total number of autophagosomes to determine percent overlap in each cell analyzed. Twenty cells were evaluated and values were averaged. Overlap with the mitochondrial outer membrane marker was strikingly high (~80% versus <20% for all other markers). (D) Assessment of whether mitophagy might underlie overlap. Cells were either starved or treated with Z-VAD-FMK/Staurosporine and stained with a potential insensitive mitochondrial marker. Subsequent flow cytometry revealed loss of mitochondrial mass in response to Z-VAD-FMK/Staurosporine treatment (left hand panel; left hand trailing blue line) but not DPBS treatment. (E) Fluorescence microscopy confirmed mitophagy in Z-VAD-FMK/staurosporine treated cells; treated cells showed extensive Mito-YFP signal in autophagosomes. (Scale bar: 10um.)

3.c. Investigating the basis for autophagosome/mitochondria overlap during starvation

Mitophagy—the capture and degradation of mitochondria by autophagosomes—is well established in eukaryotes (Mijaljica et al., 2007). We therefore next examined whether overlap of the YFP-cb5^{TM} mitochondrial outer membrane marker with the autophagic marker was due to induction of mitophagy. We assessed co-localization of other mitochondrial components (mitochondrial matrix and inner membrane) with CFP-LC3 after autophagic induction. Mitophagy predicts more overlap of matrix and inner membrane mitochondrial markers with CFP-LC3-positive structures compared to an outer membrane marker. However, both matrix (Mito-YFP) and inner membrane markers (Prohibitin-YFP) showed dramatically less autophagosome-associated signal (9% and 14% respectively) (Figure 18C). Notably, we also looked at a lipid marker for the inner membrane (nonyl acridine orange staining of cariolipin), the inner membrane space-targeted protein Opa1, and the matrix targeted Oct1 protein. These proteins also did not appear on autophagosmes. The dramatic discrepancy between the overlap of the outer membrane marker and markers for other structural elements of the mitochondria indicated engulfment of mitochondria in autophagosomes was not the principle event occurring during DPBS incubation.

Consistent with this, when we compared DPBS incubation with conditions reported to induce mitophagy, we found there were significant differences. Caspase-inhibited cells treated to induce mitochondrial damage (Staurosporine/Z-VAD-FMK treatment) induce mitophagy (Colell et al., 2007). In these conditions NRK58B cells

formed autophagosomes that contained both mitochondrial matrix and inner membrane (Figure 18E). Furthermore, flow cytometry revealed loss of mitochondrial mass in a significant fraction of the population of treated cell (Figure 18D). By contrast, incubation in DPBS, even for prolonged periods, produced neither loss of mitochondrial mass nor apparent capture of entire mitochondria. (Figure 18D).

We next considered other scenarios that could deliver mitochondrial outer membrane marker YFP-cb5^{TM} to starvation-induced autophagosomes. At high-resolution, isolation membranes of autophagosomes could be distinguished from sequestered substrates. Cells transiently expressing GAPDH-RFP were starved and photobleached to deplete signal from freely diffusing GAPDH-RFP. GAPDH-RFP captured within autophagic vesicles was then imaged. Line profiles of GAPDH-RFP within autophagosomes exhibited single bell-shaped intensity profiles, consistent with soluble protein trapped in the lumen of the autophagosomes. By contrast, YFP-cb5^{TM} (like CFP-LC3) showed two well-delineated intensity peaks at the limiting membranes of many autophagic vesicles (Figure 19A). YFP-cb5^{TM} in autophagosomes was present on the outer membranes of these organelles, therefore, and not captured within their lumen.

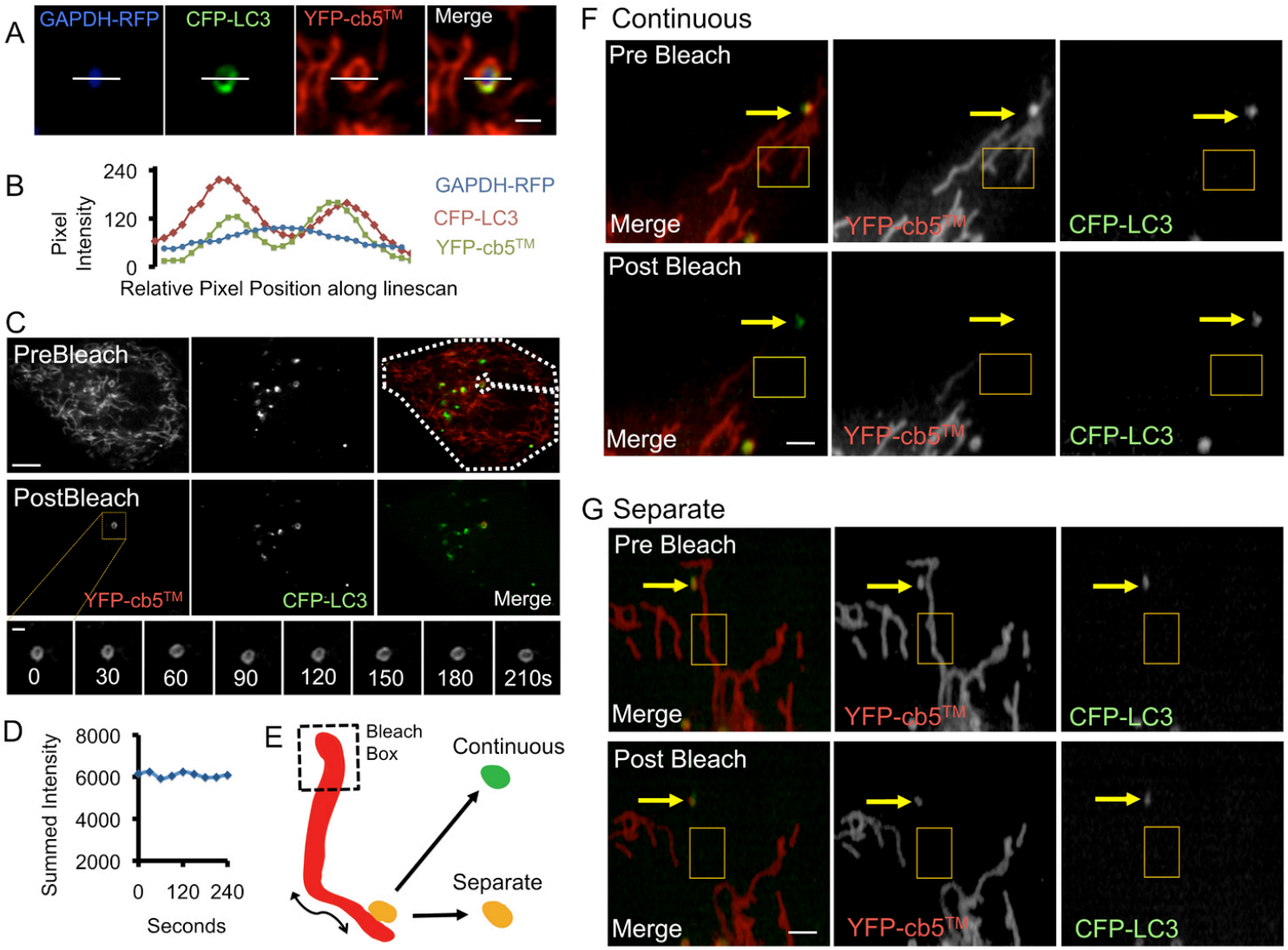
A
GAPDH-RFP
CFP-LC3
YFP-cb5TM
Merge
B
240
120
0
Pixel Intensity
Relative Pixel Position along linescan
GAPDH-RFP
CFP-LC3
YFP-cb5TM
C
PreBleach
PostBleach
YFP-cb5TM
CFP-LC3
Merge
0
30
60
90
120
150
180
210s
D
8000
6000
4000
2000
Summed Intensity
0 120 240
Seconds
E
Bleach Box
Continuous
Separate
F Continuous
Pre Bleach
Post Bleach
Merge
YFP-cb5TM
CFP-LC3
G Separate
Pre Bleach
Post Bleach
Merge
YFP-cb5TM
CFP-LC3

Figure 19: Examining the behavior of the mitochondrial outer membrane marker. (A) Assessment of the association of YFP-cb5^{TM} with the autophagosomal membrane. NRK58B cells were cotransfected with YFP-cb5^{TM} and GAPDH-RFP and starved. Signal from freely diffusing GAPDH-RFP was depleted by photobleaching to reveal CFP-LC3/YFP-cb5^{TM}/GAPDH-RFP positive autophagosomes. High-resolution images of these structures revealed YFP-cb5^{TM} present on the membrane, not trapped in the lumen. (Scale bar 1.5um.) (B) Linescan evaluation of CFP-LC3/YFP-cb5^{TM}/GAPDH-RFP signal in autophagosomes. CFP-LC3 and YFP-cb5^{TM} pixel values along a transecting line (shown in a) exhibited two delineated peaks (membrane). In contrast GAPDH-RFP pixel values along this line exhibited a bell-curve like signal (lumen). (C) Assessment of the stability of YFP-cb5^{TM} on autophagosomal membranes. YFP-cb5^{TM} positive autophagosomes were identified and YFP-cb5^{TM} signal was subsequently bleached in the remainder of the cell (photobleached region indicated by hashed line, top right panel). YFP-cb5^{TM} did not robustly exchange on and off autophagosomes (time series, lower panel). (Scale bar: 10um upper panel; 1.5um lower.) (D) Quantitation of YFP-cb5^{TM} signal persistence. Total intensity of the autophagosome in (C) was quantified for each frame. This value did not significantly decrease over time, indicating there was no significant release or exchange with bleached YFP-cb5^{TM} over the course of 4 minutes. (E) Assaying for association of autophagosomal and mitochondrial membranes (Model). Photobleaching the distal end of a mitochondrial element depletes all YFP-cb5^{TM} signal diffusing throughout the membrane. A YFP-cb5^{TM} positive autophagosome whose membrane is continuous with the MOM also loses YFP-cb5^{TM} signal. A YFP-cb5^{TM} positive autophagosome that is near but not continuous with the MOM retains YFP-cb5^{TM} signal. (F) Assaying for association of autophagosomal and mitochondrial membranes. Autophagosomes that appeared to be associated with mitochondrial elements were identified. Distal ends of associated mitochondrial elements were targeted with 405nm and 490nm light (yellow box). For a subset of autophagosomes, distal photobleaching

depleted signal both from the mitochondria and the associated autophagosome (see loss of all signal, middle panels). (Scale bar: 2um.) (G) Autophagosomes that were spatially close but not associated retained signal after photobleaching of proximal mitochondrial elements (see retention of signal, bottom row, middle panel). (Scale bar: 2um.)

We next investigated the characteristics of the YFP-cb5^{TM} present on autophagic vesicles. YFP-cb5^{TM} signal was photobleached within individual cells to deplete all signal except that present on isolated autophagic vesicles. YFP-cb5^{TM} showed persistent signal on isolated structures for >3 minutes (Figure 19C, D). Therefore, YFP-cb5^{TM} once targeted to membranes appears to stably associate with these membranes and does not readily exchange off these membranes.

3.d. Membrane continuity between outer mitochondrial membrane and newly formed autophagosomes

Given the stable association of YFP-cb5^{TM} with the membranes of autophagic vesicles, we next asked whether mitochondrial outer membrane and autophagosomal membranes are continuous at some point during autophagosome formation. We frequently observed CFP-LC3/YFP-cb5^{TM} positive structures present along mitochondrial tubular elements that also labeled with YFP-cb5^{TM}. Because of the limits of optical resolution, high-resolution images alone could not reveal whether YFP-cb5^{TM} positive autophagic vesicles were in close proximity or whether the structures actually shared membrane with associated mitochondria. We used high-speed, high-resolution imaging coupled with targeted laser bleaching to discriminate between these two possibilities. Mitochondrial elements with associated autophagic vesicles were identified. Small regions at the distal ends of associated mitochondrial elements were simultaneously photobleached with 405nm and 490nm laser lines of diode lasers. If continuity was present, we predicted YFP signal from both the mitochondria and associated autophagosomes would be depleted; without continuity, only the mitochondrial YFP signal would be depleted (Figure 19E). Rapid diffusion

in and out of targeted photobleached regions predictably depleted YFP-cb5^{TM} signal along the entire length of targeted mitochondrial elements. Strikingly, this photobleaching also depleted YFP-cb5^{TM} from regions of CFP-LC3 overlap outside the photobleached region (Figure 19F). Post-translational insertion of YFP-cb5^{TM} directly into the membranes of autophagosomes and close spatial proximity to mitochondrial elements cannot account for these results. The apparent exchange between mitochondrial elements and regions of CFP-LC3 overlap instead indicates that membrane continuity must exist between the maturing autophagosomal structures and associated mitochondrial elements to allow rapid diffusion of YFP-cb5^{TM} between these structures. Most structures do not exhibit this behavior and it was not observed with large (>1000nm) CFP-LC3/ YFP-cb5^{TM} positive structures (Figure 19G). Membrane continuity with the mitochondria therefore appears to be a transient event that occurs early in the formation and maturation of CFP-LC3 positive autophagosomes.

These photobleaching experiments support YFP-cb5^{TM} delivery to autophagosomal membranes first via delivery to the outer mitochondrial membrane. The experiments suggest that during autophagosome formation, autophagosome membranes are continuous with the mitochondrial outer membrane; hence YFP-cb5^{TM} appears in autophagosome membranes and is trapped in these membranes once continuity with the mitochondria outer membrane breaks.

3.e. Autophagosome formation occurs along mitochondria

Utilization of the mitochondrial outer membrane in autophagosome formation predicts that autophagosomes will first appear along mitochondrial elements. Using

high-speed live cell imagined we observed GFP-LC3 punctae appearing in association with mitochondria. Over short time periods, these structures retained association with mitochondria despite highly dynamic mitochondrial movements (Figure 20A). Recruitment of LC3 requires upstream autophagic components. Therefore we next looked to see if autophagy machinery required for LC3 recruitment also appeared along mitochondria. The mApg5/Apg12/Apg16 oligomeric complex (described above) transiently associates with a target membrane—a prerequisite for recruitment of LC3. Mutants that block incorporation of mApg5 into this complex block recruitment of LC3 and autophagosome formation (Mizushima et al., 1998; Pyo et al., 2005). When GFP-mApg5 expressing NRK cells were starved, highly dynamic GFP-mApg5 punctae appeared along mitochondrial elements (Figure 20B). Like GFP-LC3 punctae, these tracked with mitochondrial elements during dynamic movements.

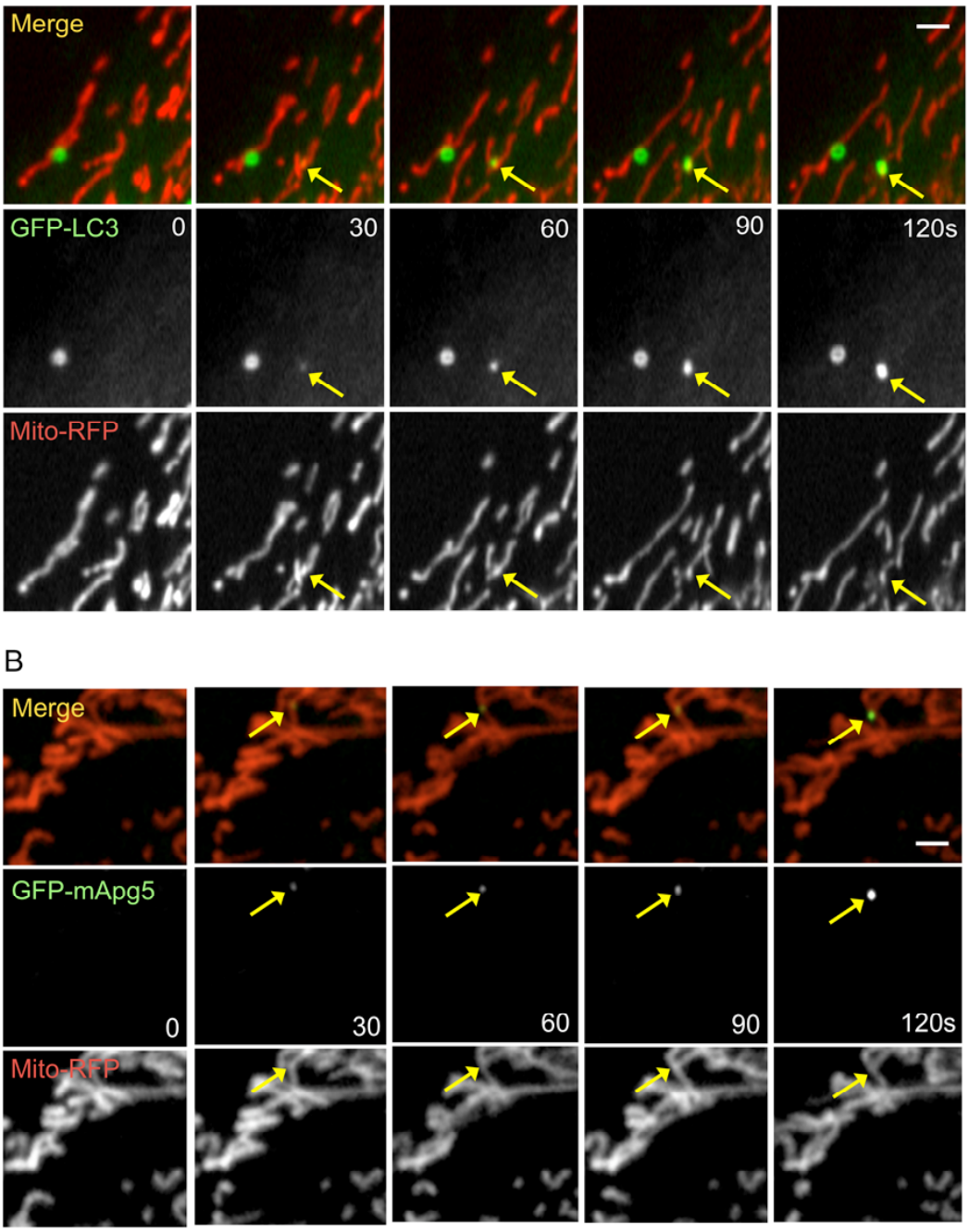

Figure 20: Monitoring the association of starvation-induced autophagosomes and mitochondria. (A) Live-cell imaging of GFP-LC3 labeled autophagosomes and associated mitochondrial elements. NRK cells were transfected with the mitochondria matrix marker Mito-RFP and autophagosome marker GFP-LC3. High-resolution high-speed imaging of starved cells showed autophagosomes grow during tight association with mitochondrial

elements. (B) Live-cell imaging of GFP-mApg5 labeled autophagosomes and associated mitochondrial elements. NRK cells were transfected with Mito-RFP and GFP-mApg5 and subsequently starved. High-speed high-resolution imaging showed autophagosome inception occurs along associated mitochondrial elements. (Scale bars: 4 um.)

To utilize outer mitochondrial membrane without compromising mitochondrial mass, we expected autophagic vesicles would exclude inner mitochondrial membrane and matrix. To further evaluate whether mitochondrial membrane is utilized during autophagosome formation, DPBS induced NRK58B and wild type NRK cells were studied using transmission EM (TEM). TEM of both cell types revealed the presence of multilamellar structures. These structures were never observed in unstarved cells. Most of these structures appeared as isolated organelles, some however were closely apposed or continuous with mitochondrial elements (Figure 21A, panel 1). Notably, for associated spherical, tubular, or ovoid structures, sectioning for EM minimizes observable connectivity because most planes of a cut will not intersect both structures and the point of contact. The mitochondrial-associated structures we observed excluded mitochondria inner membrane and matrix and showed a luminal electron density like that of the cytoplasm—consistent with engulfment of cytosol. Dimensions of these structures correlated well with the dimensions of CFP-LC3 positive structures observed by confocal microscopy. Immuno-EM studies also revealed autophagic structures associated with mitochondrial elements (Figure 21A, panel 2).

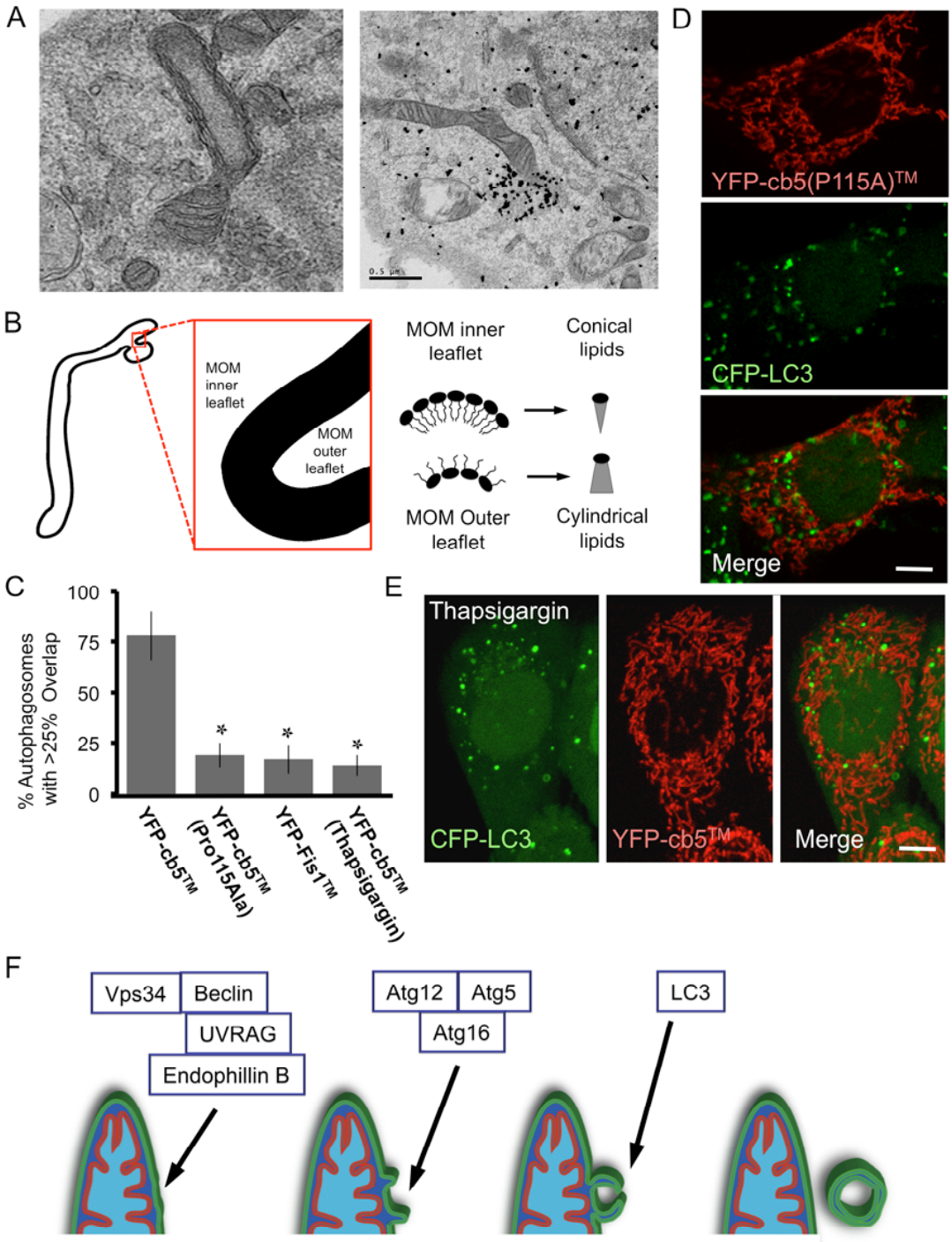

Figure 21: (A) Electron microscopy of starved cells. NRK cells were starved for four hours and subsequently processed and imaged with 100keV TEM (Left panel). Electron micrographs revealed the presence of multilamellar structures tightly associated with mitochondrial elements that exclude mitochondrial matrix. While rare in starved cells, these

structures were never observed in unstarved cells. Immuno EM of starved NRK58B cells labeled with gold-conjugated antibodies against CFP revealed clusters of gold particles that were observed tightly associated with proximal mitochondrial elements. (B) Probing mechanisms for exclusion of proteins from membranes used in autphagosome formation. A sharp point of membrane curvature selects for different lipids on the inner and outer leaflets of the membrane being curved. Such a curvature could block the diffusion of many proteins via preferences for particular lipid environments. (C) Quantitative comparison of the two forms of the outer membrane marker and an additional tagged tail anchor fragment of the Fis1 protein. Mutating Proline115 to Alanine in the $cb5^{TM}$ transmembrane domain forces the transmembrane domain to cross both leaflets and abolishes its delivery to autophagosomes (Quantitation in C, first three bars; Image in D). The paucity of other markers like Fis1 supports a unique mechanism for delivery of the YFP-$cb5^{TM}$ marker due to its particular membrane association. (Asterix indicates significant difference from the YFP-cb5 overlap based on Student t-test. p value <0.001. (Scale bar in D: 10 um.)). (E) ER stress induced autophagosomes do not utilize outer membrane. A four hour treatment of NRK58B cells with 25nM thapsigargin induced autophagosomes that did not acquire the YFP-$cb5^{TM}$ marker. (Scale bar: 10 um.) (Quantitation in C, last bar). (F) One potential model to explain utilization of mitochondrial membranes in autophagosome biogenesis. See Text for description.

TEM micrographs and live cell fluorescence microscopy are consistent with the interpretation that mitophagy does not underlie the robust appearance of the mitochondrial outer membrane marker on autophagic vesicles. Rather, our data suggest that autophagic vesicles form at the surface of mitochondria. Kinetic experiments support the idea that this formation process utilizes components of the mitochondrial outer membrane. Consistent with this, Beclin 1 (mammalian homolog of yeast Atg6p) has been reported on mitochondrial membranes (Liang et al., 1998), and work from the Youle lab demonstrates that targeting of Beclin 1 to mitochondria is critical for starvation-induced autophagy.

3.f. Restricting protein delivery from mitochondria to newly forming autophagosomes

If mitochondria serve as a membrane source for autophagosome formation, why aren't mitochondrial components observed in autophagosome membranes? The paucity of transmembrane proteins in autophagosomal membranes argues that any autophagosomal assembly process (short of *de novo* assembly) must account for exclusion of proteins (Fengsrud et al., 2000a). Membrane partitioning events occur during many cellular processes. We propose partitioning events limit transfer of mitochondrial proteins to autophagic membranes. To test this idea, we altered the Venus-cb5^{TM} MOM marker. Previous studies of cb5 identified a proline in the transmembrane domain that allows for formation of a kinked helix (Takagaki et al., 1983). Based on crosslinking and photochemistry studies, this kinked helix form can intercalate into only the outer leaflet of a targeted bilayer. Conversion of a specific proline to alanine in the cb5 transmembrane domain forces the domain into a linear

helical coil that then spans both leaflets. This alanine mutant YFP-cb5^{TM}(P115A) expressed in NRK58B cells efficiently targeted to the mitochondria. However, in DPBS-treated cells it did not appear on induced autophagosomes (Figure 21C, D). The degree of colocalization with autophagosomes was equivalent to the degree of overlap observed for both mitochondrial matrix markers and transmembrane markers associated with the outer membrane (<20%) (Figure 21C). Exclusion of the YFP-cb5^{TM}(P115A) mutant from autophagosome membranes supports one potential mechanism that may generally exclude mitochondrial proteins from autophagosomes. Proteins associating only with the outer leaflet of a membrane can more readily traverse points of sharp curvature in that membrane (Schmidt and Nichols, 2004). (Notably, we also did not find other outer membrane proteins (i.e. Tom20, Beclin 1, Mfn1, Mfn2, of Fis1) on autophagosomes.) The inability of many transmembrane proteins or proteins in large complexes to transit through a point of sharp membrane curvature (potentially a site of autophagosome biogenesis) could underlie the paucity of integral membrane proteins observed in proteomic analyses of autophagosomal membranes. Additionally, the closely apposed membranes of autophagic vacuoles could exclude proteins present in the inner-membrane space.

3.g. Utilization of the mitochondrial outer membrane in autophagosome biogenesis is not universal

As discussed above, dysregulation of intracellular calcium by the SERCA ATPase inhibitor thapsigargin also induces CFP-LC3-positive structures in the NRK58B line. The formation and fate of these structures was discussed above (Figure 17A-G). To address whether mitochondrial membrane is used by these

autophagosomes as well, we applied the same methodology to study overlap of YFP-cb5^{TM} and CFP-LC3 in thapsigargin-treated NRK58B cells. Autophagosomes were identified and assessed for overlap of the mitochondrial outer membrane marker. Strikingly, overlap of the MOM marker with autophagosomes was not observed when autophagosomes were induced by thapsigargin (overlap <10%) (Figure 21C, E). Despite requiring activities of shared core autophagy machinery, DPBS- and thapsigargin- induced structures do not share capture of the mitohchondrial membrane marker. Although there is discrepancy in the literature, recent reports suggest that thapsigargin-induced autophagosome formation is regulated by pathways independent of pathways regulating amino acid starvation-induced autophagosomes. Our observations suggest that utilization of different membranes in autophagosome formation may underlie these differences.

4. Discussion

Whether autophagosomes form *de novo* or from pre-existing cytomembranes is a long-standing debate, and the origin of autophagosome membranes remains unclear (Juhasz and Neufeld, 2006). Here we present data to suggest that mitochondrial membranes contribute to the formation of autophagosomes during starvation. We show that autophagosome inception occurs along mitochondria.; the early autophagosomal marker mApg5 transiently localizes to punctae on the mitochondria. LC3 subsequently replaces mApg5 at these sites where LC3 positive autophagosomes transiently associate with mitochondria as they grow. We show that a tail-anchored outer mitochondrial membrane protein labels the delimiting membranes of autophagosomes, and that its delivery to autophagosomal membranes

is via the mitochondria membrane. We show this marker can be depleted from autophagosomes by photobleaching associated mitochondrial elements; the membranes of these organelles are therefore transiently shared. Consistent with live cell fluorescence microscopy data, electron microscopy reveals autophagic structures associated with mitochondria that exclude mitochondrial matrix and inner membrane. These data strongly implicate involvement of mitochondrial membranes in the formation of autophagosomes.

4.a. Support for mitochondrial involvement

A number of recent reports implicate mitochondria involvement in autophagosome formation. Some autophagy proteins (i.e. a proteolytic fragment of Atg5, and the yeast protein Atg9p) localize to mitochondria, and several mitochondrial localized proteins (i.e. smARF , SIRT1, Bif-1/EndophillinB) positively regulate autophagy (Lee et al., 2008; Reef et al., 2006; Takahashi et al., 2007). Bif-1 (a mitochondrially associating Bax-binding protein) binds UVRAG (a component of the autophagy regulating Class III PI3Kinase complex), and knockdown of Bif-1 suppresses induction of autophagy by starvation. Interplay between autophagy and mitochondrial proteins is often ascribed to mitophagy; however, our data suggest an alternative—mitochondria participate in the formation of autophagosomes. Work co-submitted by Ryu et al. demonstrates that Beclin (a component of the Class III PI3Kinase complex) must be delivered to mitochondrial membranes to efficiently execute starvation-induced autophagy. Ryu et al identified a novel highly conserved mitochondrial targeting sequence in Beclin that is sufficient to target a fusion protein to mitochondria. Deletion of this domain blocked Beclin's ability to induce

autophagy; restoring mitochondrial targeting restored Beclin's activity. The authors further show that *S. cerevisiae* cells expressing the yeast Beclin homolog (Atg6p) lacking the mitochondrial targeting domain died more readily when nitrogen-starved. This work with data presented here argues that mitochondria play a critical role in autophagosome formation during starvation.

Observing early stages of autophagosome assembly has been and remains notoriously difficult, and current models for autophagosome biogenesis remain speculative. Because autophagy must orchestrate formation of multilamellar structures that enclose fluid-phase volumes, involvement of a pre-existing cytomembrane source is appealing. Autophagosomes must assemble around cytosolic fluid and their membranes must favor a unidirectional curvature. A model based on imposing membrane curvature on a preexisting membrane allows for the establishment of asymmetric lipid composition to promote membrane curvature and subsequent capture of cytosol. Based on known activities of core autophagy machinery, kinetics of autophagosome formation, and the data described here, one plausible mechanism for autophagosome biogeneis is the model diagrammed in Figure 21F. We propose that the Vps34 Class III PI3Kinase complex marks an initiation site for autophagosome assembly on the mitochondrial outer membrane. Phosphorylation of the target phosphoinsitide to generate PI(3)P and Bif-1 BAR domain interactions with membrane may modify a local environment on the outer mitochondrial membrane (Figure 19F, leftmost panel). Subsequently, the mApg5/Atg12/Atg16 complex is recruited. Notably, in both yeast and higher eukaryotes Atg16 forms homo-oligomeric complexes likely through coil-coiled

domain interactions (Kuma et al., 2002; Mizushima et al., 2003). This complex may therefore form a transient coat to stabilizes an initiation site. (Figure 19F, middle left panel). Initial membrane curvature or lipid partitioning may next enrich the LC3 lipid target phosphotidylethanolamine (PE). LC3 conjugation to PE at the site could stabilize local high concentrations of PE in the outer leaflet of the mitochondrial and supports continuing outgrowth of a structure. Notably, PE is one of a small set of lipids that imposes a negative radius of curvature to bend a membrane toward an aqueous interface. Such curvature could generate a cup like structure capable of capturing cytosol within its volume (Figure 19F, middle right panel). A double lamellar structure could then be formed if the distal edges efficiently fuse (Figure 19F, right panel). LC3 has been shown to catalyze fusion of homotypic membranes in an *in vitro* system (Nakatogawa et al., 2007). Fusion of these membranes could give rise to a double membrane structure with engulfed cytosol.

4.b. Implications of formation from mitochondria

A little explored aspect of autophagy is its potential role in fluxing lipids through otherwise disconnected cellular compartments. Our photochase data indicates that a significant amount of membrane is moving from the autophagosomal origin to autolysosomes/lysosomes via fusion of outer autophagosomal membranes with lysosomal membranes. The lipid target of LC3—phosphotidylethanolamine—is an abundant ubiquitous cellular lipid that is transferred by autophagosomes. PE is synthesized principally at two sites—in the ER via the CDP-ethanolamine pathway and in the mitochondria via decarboxylation of phosphotidylserine (Vance, 2008). ER synthesis of PE utilizes DAG and exogenous ethanolamine. By contrast, synthesis in

the mitochondria utilizes phosphotidylserine transferred from the ER. Under starvation conditions the sources for exogenous ethanolamine and DAG (produced following growth factor engagement) are limited. These substrates are required for PE synthesis in the ER. Autophagy may counter this by routing mitochondrial derived PE to lysosomes, and subsequently via retrograde and anterograde transport through other membrane systems. Mitochondria contribution to autophagosomal membranes under starvation conditions could then contribute to lipid homeostasis in addition to established roles in nutrient recycling.

As noted above, starvation induced autophagy in the NRK58B line does not result in net loss of mitochondrial mass. In fact, we observe a slight increase in mitochondrial mass with increased incubation time in DPBS (Figure 18D). Other conditions reported to induce autophagy (i.e. Sirt1 overexpression) also increase mitochondrial mass. (Lee et al., 2008). A major source for mitochondrial phospholipids is the ER. Increased rates of lipid transfer to the mitochondria during starvation could underly this increase in mass

Interestingly, Axe et al recently reported that DFCP1, a unique PI3(P) binding protein in the ER, translocates to punctae under starvation (Axe et al., 2008). These punctae are sites where autophagosome formation occurs. The authors observe mApg5 and LC3 autophagosomal markers surrounded by DFCP1, and present a model suggesting autophagosomes form from ER membrane at these sites. Our work suggests that the DFCP1 sites the authors observe may be sites of connection between the ER and mitochondria. MAMs—mitochondrial associated membranes—act as bridges between the mitochondria and ER in both yeast and mammals (Achleitner et

al., 1999; Bozidis et al., 2008). Phosphotidylserine and other phospholipids are known to be transferred from ER to mitochondrial membranes at these sites; and that transfer is required for PS to reach the decarboxylating enzyme in the mitochondria that converts it to PE. Clearly PE is required for autophagosome formation. Tracking the route that it takes—we suggest through the mitochondria—may be a useful next step in understanding autophagosome biogenesis.

Chapter 5: Conclusion

Work presented in the preceding chapters implicates mitochondria in the formation of autophagosomes. In this final chapter I conclude by considering below whether there is precedence for membrane budding from mitochondria, and whether mitochondria membrane is likely to be the only source for autophagosome formation. Finally I consider why understanding how exactly autophagosomes form is important.

The role of mitochondria in the production of energy (i.e., ATP) has been exhaustively studied. Their familiar label--"powerhouse of the cell"—pervades how we think of these organelles. However, a growing body of research implicates mitochondria in many aspects of cell biology. A vast amount of time has elapsed since the purported endosymbiotic event put mitochondria into an ancestral eukaryotic cell. From that perspective, it is counterintuitive to think mitochondria play a single functional role. Clearly mitochondria are integrated into many aspects of cell biology. They act as reservoirs for death signals, participate in cell cycle control, and contribute to lipid homeostasis. At the structural level, proteins that regulate their morphology (e.g. the dynamin-like protein DRP1) also regulate the structure of other organelles (e.g. peroxisomes). Most likely, mitochondria do more than has been appreciated.

1. Is there structural evidence for budding from mitochondria?

An argument against mitochondrial involvement in organelle biogensis is the paucity of examples. In the now long history of electron microscopy studies, budding from mitochondrial membranes has not been reported. Clathrin-coated endocytic buds and vesicles at the trans golgi network are readily apparent in electron micrographs; mitochondrial-derived vesicles are not. That said, we may see budding events throughout the secretory pathway because they are common, because of their particular topologies, and possibly because they tolerate fixation. (Notably, the concentration of proteins in autophagosomal membranes is very low—100 fold less than in lysosomal membranes) (Fengsrud et al., 2000a). Electron microscopy is good at seeing structural detail; it is not good at seeing rare events. Arguably, fluorescence microscopy is a much better tool to detect rare events exactly because of its relative low resolution. You don't need to see much to find a friend at the theater if they have the only flashlight in the hall.

Budding from mitochondrial membranes was in fact recently reported and visualized using fluorescent protein imaging, and we now have some molecular insight into this process. Heidi McBride's group described specific budding events that are regulated by a mitochondrial anchored protein E3 ligase (MAPL) (Neuspiel et al., 2008). MAPL was identified by a bioinformatics screen to identify mitochondria E3 ligases and was subsequently cloned. Overexpression of the protein induces fragmentation of the mitochondria; at lower expression levels it labels small 70 to 100 nm vesicles, some of which target from mitochondria to peroxisomes. The McBride group has biochemically isolated these vesicles and are currently probing them for a

potential role in peroxisomal biology (personal communication). Although the MAPL positive vesicles do not share some significant features with what we report here (i.e., they are much smaller and do not label with LC3), many of these vesicles do appear to be double lamellar--a provocative observation.

2. Is there genetic evidence for budding from mitochondria?

A second argument against mitochondrial budding is the lack of any machinery identified in genetic screens. One simple explanation is that it is simply difficult to imagine what form such genetic evidence would take. Practically nothing is known about what budding events at the mitochondria might do. Nor has there been any visual readout for such a process until recently. Genetic screens may become more tractable if work like that from the McBride group unveils functions that can be screened. A recent report by Chen et al for the first time demonstrated a functional connection between mitochondria and the yeast vacuole (Chen et al., 2008). Such a connection could be mediated by membrane budding events. Chen et al show that crd1 mutants (defective for cardiolipin synthesis in the mitochondria), exhibit swollen vacuoles with increased pH that can be rescued by expression of NHX1, a proton exchanger found principly in endosomes. Notably, although cardiolipin is a mitochondrial-specific lipid, it does appear to make its way to other intracellular structures and the plasma membrane(Sorice et al., 2000). The literature is thin at this point, but such reports raise the possibility that membrane budding from the mitochondria and consequent lipid transfer may occur and play significant roles in the behavior of other organelles. The jury is still out.

3. Are mitochondria the only membrane source for autophagosomes?

The autophagy field has historically envisioned a single dedicated route of autophagosome formation. However, the extent to which autophagosomes have universal characteristics is increasingly debated. In the work above, I compared starvation- and ER stress-induced autphagosomes. The YFP-cb5^{TM} mitochondrial outer membrane marker does not appear on ER stress-induced autophagosomes. Additionally, while both starvation and thapsigargin treatment of the NRK58B cells induce autophagosomes, the structures are morphologically distinct, show different substrate capture, and exhibit different turnover kinetics. One possible explanation for this is the utilization of different membrane sources in the formation of these structures.

Recent studies in *S. cerevisiae* indicate that autophagosomes formed is response to ER stress appear to utilize ER membrane. During ER stress, the ER expands and is subsequently engulfed by an autophagosome dependent process (Bernales et al., 2006). Notably, markers derived from ER are observed on the limiting membranes of these autophagosomes, suggesting that the ER membranes themselves contributed to autophagosome formation. In mammalian cells components of the Class III PI3kinase complex (e.g. Beclin 1) have been localized at the ER in addition to the mitochondria, and PE is abundant in ER membranes. Membrane events like those we proposed in the model above could underlie autophagosome formation from other intracellular membrane systems like the ER. The lipid components are present. Such events would require targeting the machinery to initiate autophagosome formation to different membranes.

4. Is targeting to different membranes plausible?

Strikingly, of the now almost 31 Atg genes that have been identified , almost all are cytosolic proteins (Geng et al., 2008; Xie and Klionsky, 2007). Given that almost all identified critical autophagy machinery is cytosolic and the required lipid precursors for autophagosomes (the Vps34/Beclin Class III kinase target phosphotidylinositol and the LC3 target phosphotidylethanolamine) are ubiquitously present in intracellular membrane systems, it is plausible that AV biogenesis can utilize a variety of membrane sources. Recent work by Douglas Green's lab demonstrates that autophagy machinery can be targeted to plasma membrane derived endosomes, and that targeting requires the PI3Kinase complex and the activity of Atg5 and Atg7 (Sanjuan et al., 2007). Particles designed to activate toll-like receptors on the surface of macrophages are phagocytosed and promptly recruit autophagy proteins. Clearly autophagy machinery is capable of seeing plasma-derived membrane, consistent also with the appearance of autophagy markers on membranes that surround intracellular pathogens like *Legionella pneumophila*.

Given at least some diversity in the membrane targets and the fact that autophagy machinery is nearly all cytosolic, one useful way to conceptualize autophagic machinery may be as a cohort of proteins that can impose membrane curvature on a variety of membrane sources whose identity depends on the specific induction. The location of autophagosome biogenesis may then depend on specific induction conditions that establish target sites for initiation.

5. Are all biogenesis programs the same?

One problem raised by the model I present here is trying to envision how it would explain engulfment of organelles like peroxisomes or mitochondria. Notably, if the membranes of these organelles are themselves used, it is difficult to envision how they might wrap back around without invoking very complicated membrane curvatures.

As previously discussed, at least some features of autophagosome biogenesis must be specific to the activity. In yeast, cytoplasm to vacuole targeting delivers the lysosomal protease Aminopeptidase I to the yeast vacuole via autophagosomal-like structures. Crystalline unprocessed enzyme is surrounded by autophagic membranes that deliver the enzyme to the vacuole lumen. Core autophagy machinery is utilized. However, Cvt utilizes unique components (i.e. Atg19, Atg20), shows substrate specificity, and generates structures that are much smaller than starvation induced autophagosomes; Cvt vesicles are below the resolution of confocal microscopy (Scott et al., 1996).

How can we reconcile this type of process with processes that carry out non-selective bulk capture and degradation (ie. starvation-induced autophagy)? One possibility is that small Atg8-positive vesicles are constitutively formed and present in eukaryotic cells and can assemble to build a double lamellar membrane around substrates for selective autophagy. A likely example of this is the sequestration of aggregated proteins; the protein p62 was recently shown to bind both ubiquitin and the Atg8 homolog LC3, and may act to tether small LC3 positive vesicles around a core of ubiqutinated proteins (Pankiv et al., 2007). How large can this core be?

Interestingly, even large organelles like peroxisomes may be turned over in a p62 dependent fashion; p62 knockdown anecdotally appears to increase the number of peroxisomes (current work I have participated in; submitted by Peter Kim et al).

Such assembly of membrane around a core may underlie the so-called housekeeping function of autophagy. Indeed, NRK58B cells appears to constitutively deliver CFP-LC3 to lysosomes in the absence of DPBS induction and in the absence of resolvable autophagic bodies. Simply inhibiting lysosomal proteases results in the dramatic accumulation of LC3 in lysosomes without formation of detectable autophagosomes in the cytosol.

In contrast to assembly of small vesicles around a solid core, starvation-induced autophagy presents a conceptually more challenging case. Bulk degradation by autophagy is orchestrated by formation of comparatively large multilamellar structures that enclose a fluid-phase volume. How does a large multilamellar structure assemble around cytosolic fluid in the absence of any clear underlying structure? How does a membrane favor a unidirectional curvature? The data here cannot absolutely rule out the rapid assembly of small vesicles at an assembly site at the mitochondria, and lipid sharing between this structure and the mitochondria. However, a model based on imposing membrane curvature and partitioning on a preexisting membrane (the mitochondria) would allow for the establishment of asymmetric lipid composition to promote membrane curvature.

In light of current studies, it is possible that the different outcomes of autophagy may involve a rheostat on the pathway. Possibly constitutive autophagy in mammalian cells, as probably occurs in yeast cells, involves the constitutive

formation of small vesicles that can be tethered and assembled together. However, inducing the pathway causes the pathway to then shift to the formation of much larger vesicles. Interestingly, levels of Atg8 itself appear to play a regulating role in the rate of growth and size of autophagosomes (Geng et al., 2008; Xie et al., 2008).

6. Why does the path of biogenesis matter?

Much effort has gone into trying to understand the process of autophagosomal biogenesis, and indeed it is an ongoing challenge. Does it matter how clearly we understand how these structures form? Clearly we know many effects of autophagosomes without knowing how they form. The recent dramatic growth in our knowledge of autophagy might argue that unraveling how these structures form is a minor aspect of the larger field. However, there is growing interest in using autophagy to treat cancer, neurodegenerative diseases and immune disorders. If for instance ER stress-related autophagy is indeed involved in neurodegenerative diseases, then autophagosomes that specifically capture ER membrane are a more promising target than drugs that activate a different program. Given the interest in utilizing autophagy regulators as pharmaceutical targets, understanding how autophagosomes differ is paramount. And lastly, while the pharmaceutical issues are compelling, to cell biology it is enough that it is simply a remarkable and unique process in the cadre of membrane events that regulate cell behavior.

Chapter 6: Materials and Methods

1. Mammalian Cell culture

1.a. Maintenance in tissue culture incubators

NRK cells were obtained from the American Type Culture Collection and maintained in Dulbecco's Modified Eagle's Medium with 10% fetal bovine serum, 100 units/ml penicillin and 100 g/ml streptomycin. Incubators were maintained at 37 °C / 5% CO_2. Stocks were passaged in vented T25 flasks and split every 48 to 72 hours to maintain confluency at <90%. Adherent cells were split suspended following washing with 2 mL 0.05% Trypsin/0.53 mM EDTA (CellGro, Cat# 25-051-Cl) and reseeded into either T25 flasks (0.2mL transfer) or LabTek chambers (10uL transfer). For live cell imaging, trypsinized cells were seeded into 8-well LabTek chambers containing 350uL DMEM/well and incubated for 16 hours prior to imaging. Maintained stocks were intermittently treated with BM Cyclin (Roche, Cat# 10 799 050 001) to prevent contamination by mycoplasm and other Penn/Strep resistant pathogens.

1.b. Maintenance at the microscope

For transfer to microscope systems, LabTeK chambers were removed from incubators and placed on T75 flasks filled with 37C water to maintain temperature. DMEM was aspirated from the wells and immediately replaced with preheated 37C CO2 independent media (Gibco, Cat# 18045-088) or appropriate media formulations. At the microscopes, temperature was maintained either with temperature regulated air

blowers (Air Stream, NevTek Model ASI 400) or with stage enclosures (Pecon systems, XL-3 LSM 128).

1.c. Stock storage

To aliquot cells for liquid nitrogen storage, cells were trypsinized; subsequently trypsin activity was neutralized by addition of DMEM. The cell suspension was centrifuged at 800 RPM for 10 minutes, resuspended in Fetal Bovine Serum with 10% DMSO, and aliquoted to Cryotubes. Temperature was sequentially dropped to 0 (20 min), -20C (60 min), -80C (16 hours) and -190C. Stocks were kept in liquid nitrogen at -190C.

1.d. Plasmid transfections

For an 8-well chamber, 200ng of DNA and 50 uL of serum-free DMEM were pipetted into separate microcentrifuge tubes. 2 uL of Fugene 6 transfection reagent (Roche) was added to the DMEM. Subsequently, the DMEM/Fugene mixture was pipetted over the DNA and incubated at room temperature for 25 minutes. The transfection mix was added directly to media in seeded LabTek chambers 16 hours post seeding. Transfections were incubated for 16 hours prior to imaging. This protocol was scaled based on surface area for transfections of larger wells or plates.

1.e. Stable Cell Line Selection

For plasmids carrying the Kanamycin resistance gene (conferring G418 resistance in eukaryotes), one day following transfection as above, DMEM in 6cm transfected plates was exchanged for DMEM with 800ug/mL G418. DMEM/G418 media was exchanged every other day for 8 days until well-isolated cell colonies were

visible. Individual clonal colonies were scraped and transferred using a P1000 pipette and sterile filtered tips to separate wells of a 24-well plate with DMEM. 24 hours later, DMEM was replaced with DMEM/G418. Adhering cells were subsequently trypsinized and passaged. To screen cells for genomic insertion of plasmids, cells were trypsinized. 10uL aliquots were transferred to individual 8-well LabTek chambers and evaluated at the microscope for appropriate fluorescence. ($Note_1$: Although low power objectives will detect fluorescent signal in stable lines plated in plastic wells, signal loss through plastic biases the selection toward cells that express at very high levels.) ($Note_2$:clones with PAGFP fluorophores were screened by using a non-conventional filter block with 405nm excitation and 510nm emission band pass peaks.

2. Bacterial Cell Culture

2.a. Stock maintenance

DH5α (methylating) and SCS110 (non-methylating) bacterial stocks were stored at -80C in LB/15%glycerol and grown in LB. Competent cells were generated from DH5α and SCS110 stocks according to instructions in Current Protocols in Molecular Biology.

2.b. Plasmid transformations

For plasmid transformations, 50uL aliquots of competent cells (above) were incubated with 100ng DNA on ice X 20min, transferred to 42C for 45s, returned to ice for 2 min, and outgrown in 400uL SOC media for 1 hour. Suspended transformed

cells were spread on LB plates with appropriate antibiotics and incubated at 37C for 16 hours to obtain isolated colonies.

2.c. Plasmid isolation and handling

Plasmids were isolated from E. coli (transformed as above) using miniprep and midiprep Qiagen Spin kits according to the manufacturers instructions. To amplify low copy plasmids, transformed E. coli were grown to mid log phase (OD600 0.4) and subsequently incubated overnight with vigorous shaking in 170ug/mL chloramphenicol (to stall bacterial protein translation while allowing plasmid replication.) For low yield plasmid preps, concentrations were increased using columns from Qiagen purification kits. PB binding buffer was added to the plasmid solution at 5:1, incubated briefly, and loaded onto the column. The column was washed and the plasmid was subsequently eluted with buffer EB.

3. Molecular Biology

3.a. Plasmid design and construction

Plasmids were constructed using standard protocols. For ligations, Shrimp alkaline phophatase was added to enzymatic digests of the target vector to prevent re-ligation of single cut contaminants. For PCR based cloning, PCR conditions described below were used to amplify fragment segments.

3.b. PCR reactions for site directed mutagenesis and cloning fragment synthesis

For most PCR reactions, PfuTurbo (Stratagene) was used. For 50uL reactions, 50ng DNA, 125ng forward primer, 125ng reverse primer, and 200uM

dNTP (each), were combined with water to a final a final volume of 44.5uL. 5uL of 10X Reaction buffer and 0.5 uL Pfu polymerase were added. PCR parameters were set according to manufacturers instructions.

3.c. Sequencing of plasmids

Plasmids were sequenced at a core facility operating a 3100 Genetic Analyzer from ABI Prism. Sequencing primers (and other primers) were purchased from Operon.

3.d. Plasmid information

Yoshinori Ohsumi provided pEGFP-mApg5(C1) and pEGFP-LC3(C1). The BspE1/Age1 fragment of pEGFP-LC3(C1) was replaced by the BspE1/Age1 fragment from pmCFP C1 to generate pmCFP-LC3. The BspE1/BamH1 fragment of pEGFP-mApg5(C1) was moved into pmVenus C1 (cut with BspE1/BamH1) to generate pmVenus-mApg5(C1). The cytosolic proteins mVenus-LDH (YFP-LDH) and GAPDH-YFP were provided by Eileen Whiteman and Manoj Raje respectively. Richard Youle provided YFP fusions to mitochondrial proteins Mfn1, Mfn2, Beclin 1, and Oct1. Heidi McBride provided YFP fusion to Opa1. Christian Wunder and Peter Kim provided Prohibitin-YFP and YFP-cb5^{TM} respectively. YFP-cb5^{TM}(P115) was made by site directed mutagenesis of pYFP-cb5^{Tm}. The plasmid was amplified using primer AAC TGG GTT ATC GCG GCG ATC TCT GCT CTG and its reverse complement. Following PCR, (methylated) template DNA was digested by the enzyme DpnI. YFP fusion to the tail anchor of mitochondrial targeted Fis1 was generated by PCR cloning using primers (5')TAC CTG TAC AAG GAG CCC CAG

AAC AAC CAG GCC and (3')TAC CTC CGC GGC GAT GGC CCA CTA CGT GAA CC. The BsrG1/SacII fragment PCR amplified from Fis1 in pcDNA3.1 (provided by Peter Kim) was cut and cloned into Venus C1. Plasmids EEA1-YFP, GPI-YFP, YFP-TGN38, GalT-YFP, CD3Delta-YFP, and YFP-HLA A2-CFP arepreviously published.

4. Immunofluorescence

Anti-LC3 was purchased from MBL (Cat# PD012). (IF required methanol fixation using standard protocols.) Cy3 and Cy5 labeled secondary antibodies were purchased from Jackson Immunological. Alexa 488 secondary antibodies were purchased from Invitrogen. Anti-Tom20 was purchased from Santa Cruz (Cat# FL-145). Anti-PI(3)P was purchased from Echelon (Z-P003). Anti-Mfn2 and Anti-Fis1 were gifts from Richard Youle. For paraformaldehyde fixations, cells were fixed with 3.7% (w/v) paraformaldehyde in phosphate buffered saline (PBS) for 15 min at room temperature and subsequently washed. Fixed cells were permeabilized with 0.1% Triton X-100 or 0.4% Saponinin (v/v) in PBS for 15 min and blocked overnight at 4C with either 10% FBS or 10% Goat serum. Blocked cells were washed and subsequently incubated with appropriate primary antibodies diluted in PBS or TBS with 1%FBS at Room temp. Following primary antibody incubations, cells were washed three times and incubated with appropriate secondary antibodies.

5. Live Cell Staining

Nonyl acridine orange, LysoTracker DND99, and Mitotracker RedCMXRos (all from Invitrogen Molecule Probes) were used as cell permeant live cell dyes for Cardiolipin (inner membrane of the mitochondria), lysosomes, and mitochondria

respectively. Dyes were added directly to media at 10nM, 100nM and 150nM respectively, incubated for 10 minutes, washed with DMEM three times and subsequently imaged. Mitotracker green FM was additionally used to assay mitochondrial mass. (Its affinity for mitochondria is independent of mitochondria potential.)

6. Pharmaceutical treatments

3-Methyladenine was purchased from Sigma (Cat M9281-100MG). For a 10mM final concentration, 15mg was dissolved directly in 10mLs of cell culture medium. Low solubility makes this more practical than making a stock solution. Media with 10mM 3-MA can be aliquoted and frozen at -80C for use <1 month later. 3-methyladenine immediately blocked formation of autophagosomes; no drug pretreatment was necessary.

Thapsigargin was purchased from Sigma (Cat T9033) and was used at 25nM final concentration. Autophagy was induced in <2 hours. NRK cells continued to survive and divide in the presence of 25nM thapsigargin for prolonged periods (>24 hours). Washout of Thapsigargin did not result in the rapid disappearance of induced CFP-LC3 labeled structures.

Digitonin was purchased from Calbiochem (Cat 300410) A 6% stock was made in water. When added to NRK cells at 1:1000 for cell permeabilization it readily released free GFP from the cytosol within 1 to 2 minutes. Prolonged exposure to this concentration in KHM buffer perturbed cell architecture. KHM buffer is described in (Lorenz et al., 2006)

Chloroquine and ammonium chloride were purchased from sigma. Stock solutions of 100uM chloroquine (100X final concentration) or 30uM Ammonium chloride (1000X final concentration) were made in water. Addition of either of these drugs caused lysosome swelling. Although they act by increasing lysosomal pH, lysotropic dyes still selectively labeled lysosomes in the presence of the drugs.

Z-VAD-FMK and Staurosporine were purchased from Sigma (Cat# V-116 and S6942 respectively.) Z-VAD-FMK was dissolved in DMSO to make a 100mM stock solution. Cells were pretreated with Z-VAD-FMK for 30 minutes (50uM final concentration). Subsequently Staurosporine was added for 6 hours at 1uM final concentration. After 6 hours, cells were washed three times and media was replaced with media containing only Z-VAD-FMK (50uM) and incubated for 24 hours. Media was replaced again with Z-VAD-FMK containing media. Cells were incubated for an additional 24 hours and subsequently images to assess mitophagy.

7. Media treatments

Starvation was induced by replacement of growth media with either DPBS with D-glucose and sodium pyruvate (Invitrogen SKU# 14287-080), serum-free DMEM , or Hanks Balanced Salt solution (Gibco Cat# 14025).

8. Fluorescence microscopy and imaging.

Single images of CFP/YFP expressing cells or fixed cells were acquired with an LSM 510 laser-scanning confocal microscope with a 63x 1.4 NA Plan-Apochromat oil objective (Carl Zeiss MicroImaging, Inc.). For live CFP/YFP imaging, the 458 nm and 514 nm laser lines of an Argon/Krypton laser (Lasos) were used to excite CFP and YFP. Line interlace scanning (wavelengths alternated

between linescans) was used to minimize artifacts of motion. The pinhole was adjusted to capture non-saturated images of 1um optical slices. Emission filter passes were 470-500 nm for CFP and 535-590 nm for YFP.

For live cell imaging of induction conditions, an LSM 510 laser-scanning confocal microscope with a 40x 1.3 NA Plan-Neofluar oil objective was used. The 458 nm laser line was used to excite CFP. Single plane images were captured from 1.7um optical slices using a 505 nm long pass filter. (Settings to minimize phototoxicity and photobleaching of CFP signal.) Single plane images were captured every 20 to 30 minutes for <12 hours.

For live cell imaging of autophagosome turnover, images were captured as described for induction conditions except the 488 line was used to excite activated PAGFP and the optical slice was increased to 2.0um. For photoactivation, either a the 413 nm line of a Coherent Enterprise II laser or 405 nm diode laser was used to activate signal to <80% of maximal signal. For subsequent bleaching, the 488 nm line was repetitively targeted to a 5X5 micro region in the cell periphery. (See Chapter 3 for detailed description.)

For live cell imaging of autophagosome fusion, tracking GFP-LC3 association with RFP-labeled mitochondrial elements, and photobleaching to assay for autophagosome substrate capture and continuity, a Beta version of the Zeiss LSM DUO with a 63x 1.4 NA Plan-Apochromat oil objective (Carl Zeiss MicroImaging, Inc.) was used at scan zoom < 2 in all cases. For GFP/lysotracker and GFP/RFP tracking, 489 and 561 diode lasers and 495-555 and 575-615 bandpass filters were used during image acquisition.. For CFP/YFP imaging, 440 and 489 diode lasers and

445-505 and 495 long pass emission filters were used. For photobleaching, either 489 nm (YFP) or 561 nm (RFP) laser targeting was used.

For live cell imaging of GFP-mApg5 association with RFP labeled mitochondrial elements, an UltraView ERS 6FO-US system with Photokinesis ERS6 module was used (Perkin Elmer). 490 nm and 561 nm diode lasers and were used to excite GFP and RFP. A 63x 1.4 NA Plan-Apochromat oil objective (Carl Zeiss MicroImaging, Inc.) and Orca-ER CCD camera (Hamamatsu) were used for image acquisition.

For maintenance of focal position over long time periods, the autofocus macro in the Zeiss Multi-time software was used. Prior to each timepoint, a 633 nm laser line was scanned on a line of the sample. Focal plane position was detected by reflection of the laser line at the focal plane. Sample offset from this position was determined before the time was started.

9. Image analysis

Conversion of digital images to numerical arrays was done either with LSM (Carl Zeiss MicroImaging, Inc.) or ImageJ (NIH/public domain) software. Numerical values were imported to Microsoft excel for further evaluations. All images were adjusted for brightness and contrast using Photoshop CS (Adobe).

10. Flow Cytometry

Cells plated on tissue culture dishes were stained with Mitotracker green FM (100nM for 30 mins) and subsequently washed three times with pre-equilibrated media. Cells were then trypsinized, centrifuged at 300g, and washed twice in

medium. Stained cells were diluted in medium and loaded into a BD FACSCalibur FACS flow system (BD Biosciences, San Jose, CA). Forward and side scatter were appropriately adjusted; Mitotracker green FM was excited with the 488-nm laser and detected in the FL1 channel. Data were appropriately gated and analyzed by CellQuest Pro software.

11. Electron Microscopy

Cells were fixed with 2.5 % glutaraldehyde in 0.1 M Cacodylate buffer, and post-fixed in reduced osmium prior to Epon embedding. 70 to 100nm sections were cut and collected on carbon-coated grids and subsequently stained with lead citrate. Grids were imaged with a Tecnai 20 TEM (FEI Company, Netherlands) operating at 120 kV. Images were captured on a 2k × 2k CCD camera (Gatan, Pleasanton, CA, USA). For ImmunoEM, cells were fixed in 4% paraformaldehyde and blocked with 1% bovine serum albumin in PBS. Permeabilized cells (0.05 % saponin in PBS / BSA 1%) were incubated with primary GFP antibody (rabbit anti-GFP; Molecular Probes), washed, and subsequently incubated with nanogold-conjugated secondary antibodies (Nanoprobes). Cells were then fixed with glutaraldehyde, treated with a gold enhancement mixture for 6 min and post-fixed in reduced osmium prior to embedding in Epon. 70 to100 nm sections were cut and stained with lead citrate prior to imaging.

Bibliography

Achleitner, G., et al., 1999. Association between the endoplasmic reticulum and mitochondria of yeast facilitates interorganelle transport of phospholipids through membrane contact. Eur J Biochem. 264**,** 545-53.

Adams, C. L., et al., 1998. Mechanisms of epithelial cell-cell adhesion and cell compaction revealed by high-resolution tracking of E-cadherin-green fluorescent protein. J Cell Biol. 142**,** 1105-19.

Adams, S. R., Tsien, R. Y., 2008. Preparation of the membrane-permeant biarsenicals FlAsH-EDT2 and ReAsH-EDT2 for fluorescent labeling of tetracysteine-tagged proteins. Nat Protoc. 3**,** 1527-34.

Ashford, T. P., Porter, K. R., 1962. Cytoplasmic components in hepatic cell lysosomes. J Cell Biol. 12**,** 198-202.

Axe, E. L., et al., 2008. Autophagosome formation from membrane compartments enriched in phosphatidylinositol 3-phosphate and dynamically connected to the endoplasmic reticulum. J Cell Biol. 182**,** 685-701.

Axelrod, D., et al., 1976. Mobility measurement by analysis of fluorescence photobleaching recovery kinetics. Biophys J. 16**,** 1055-69.

Baier, J., et al., 2006. Singlet oxygen generation by UVA light exposure of endogenous photosensitizers. Biophys J. 91**,** 1452-9.

Bernales, S., et al., 2006. Autophagy counterbalances endoplasmic reticulum expansion during the unfolded protein response. PLoS Biol. 4**,** e423.

Berry, D. L., Baehrecke, E. H., 2007. Growth arrest and autophagy are required for salivary gland cell degradation in Drosophila. Cell. 131**,** 1137-48.

Betzig, E., et al., 2006. Imaging intracellular fluorescent proteins at nanometer resolution. Science. 313**,** 1642-5.

Blommaart, E. F., et al., 1995. Phosphorylation of ribosomal protein S6 is inhibitory for autophagy in isolated rat hepatocytes. J Biol Chem. 270**,** 2320-6.

Bozidis, P., et al., 2008. Mitochondrial and secretory human cytomegalovirus UL37 proteins traffic into mitochondrion-associated membranes of human cells. J Virol. 82**,** 2715-26.

Brostrom, M. A., Brostrom, C. O., 2003. Calcium dynamics and endoplasmic reticular function in the regulation of protein synthesis: implications for cell growth and adaptability. Cell Calcium. 34**,** 345-63.

Bulina, M. E., et al., 2006. Chromophore-assisted light inactivation (CALI) using the phototoxic fluorescent protein KillerRed. Nat Protoc. 1**,** 947-53.

Cao, Y., Klionsky, D. J., 2007. Physiological functions of Atg6/Beclin 1: a unique autophagy-related protein. Cell Res. 17**,** 839-49.

Chalfie, M., et al., 1994. Green fluorescent protein as a marker for gene expression. Science. 263**,** 802-5.

Chen, S., et al., 2008. Cardiolipin Mediates Cross-Talk between Mitochondria and the Vacuole. Mol Biol Cell.

Cole, N. B., et al., 1996. Diffusional mobility of Golgi proteins in membranes of living cells. Science. 273**,** 797-801.

Colell, A., et al., 2007. GAPDH and autophagy preserve survival after apoptotic cytochrome c release in the absence of caspase activation. Cell. 129**,** 983-97.

Cuervo, A. M., 2004. Autophagy: in sickness and in health. Trends Cell Biol. 14**,** 70-7.

Dayan, F., et al., 2006. The oxygen sensor factor-inhibiting hypoxia-inducible factor-1 controls expression of distinct genes through the bifunctional transcriptional character of hypoxia-inducible factor-1alpha. Cancer Res. 66**,** 3688-98.

De Duve, C., Wattiaux, R., 1966. Functions of lysosomes. Annu Rev Physiol. 28**,** 435-92.

Deter, R. L., et al., 1967. Participation of lysosomes in cellular autophagy induced in rat liver by glucagon. J Cell Biol. 35**,** C11-6.

Ding, W. X., Yin, X. M., 2008. Sorting, recognition and activation of the misfolded protein degradation pathways through macroautophagy and the proteasome. Autophagy. 4**,** 141-50.

Doelling, J. H., et al., 2002. The APG8/12-activating enzyme APG7 is required for proper nutrient recycling and senescence in Arabidopsis thaliana. J Biol Chem. 277**,** 33105-14.

Ellenberg, J., et al., 1998. Two-color green fluorescent protein time-lapse imaging. Biotechniques. 25**,** 838-42, 844-6.

Ellenberg, J., et al., 1997. Nuclear membrane dynamics and reassembly in living cells: targeting of an inner nuclear membrane protein in interphase and mitosis. J Cell Biol. 138**,** 1193-206.

Fengsrud, M., et al., 2000a. Ultrastructural characterization of the delimiting membranes of isolated autophagosomes and amphisomes by freeze-fracture electron microscopy. Eur J Cell Biol. 79**,** 871-82.

Fengsrud, M., et al., 2000b. Autophagosome-associated variant isoforms of cytosolic enzymes. Biochem J. 352 Pt 3**,** 773-81.

Fimia, G. M., et al., 2007. Ambra1 regulates autophagy and development of the nervous system. Nature. 447**,** 1121-5.

Fire, A., et al., 1998. Potent and specific genetic interference by double-stranded RNA in Caenorhabditis elegans. Nature. 391**,** 806-11.

Furuta, S., et al., 2004. Ras is involved in the negative control of autophagy through the class I PI3-kinase. Oncogene. 23**,** 3898-904.

Furuya, N., et al., 2005. The evolutionarily conserved domain of Beclin 1 is required for Vps34 binding, autophagy and tumor suppressor function. Autophagy. 1**,** 46-52.

Geng, J., et al., 2008. Quantitative analysis of autophagy-related protein stoichiometry by fluorescence microscopy. J Cell Biol. 182**,** 129-40.

Gutierrez, M. G., et al., 2004. Rab7 is required for the normal progression of the autophagic pathway in mammalian cells. J Cell Sci. 117**,** 2687-97.

Harding, T. M., et al., 1995. Isolation and characterization of yeast mutants in the cytoplasm to vacuole protein targeting pathway. J Cell Biol. 131**,** 591-602.

Hoyer-Hansen, M., Jaattela, M., 2008. Autophagy: an emerging target for cancer therapy. Autophagy. 4**,** 574-80.

Hoyvik, H., et al., 1991. Inhibition of autophagic-lysosomal delivery and autophagic lactolysis by asparagine. J Cell Biol. 113**,** 1305-12.

Ichimura, Y., et al., 2000. A ubiquitin-like system mediates protein lipidation. Nature. 408**,** 488-92.

Jahreiss, L., et al., 2008. The itinerary of autophagosomes: from peripheral formation to kiss-and-run fusion with lysosomes. Traffic. 9**,** 574-87.

Juhasz, G., Neufeld, T. P., 2006. Autophagy: a forty-year search for a missing membrane source. PLoS Biol. 4**,** e36.

Kabeya, Y., et al., 2000. LC3, a mammalian homologue of yeast Apg8p, is localized in autophagosome membranes after processing. Embo J. 19**,** 5720-8.

Kanazawa, T., et al., 2004. Amino acids and insulin control autophagic proteolysis through different signaling pathways in relation to mTOR in isolated rat hepatocytes. J Biol Chem. 279**,** 8452-9.

Kimura, S., et al., 2007. Dissection of the autophagosome maturation process by a novel reporter protein, tandem fluorescent-tagged LC3. Autophagy. 3**,** 452-60.

Kirkegaard, K., et al., 2004. Cellular autophagy: surrender, avoidance and subversion by microorganisms. Nat Rev Microbiol. 2**,** 301-14.

Klionsky, D. J., 2007. Autophagy: from phenomenology to molecular understanding in less than a decade. Nat Rev Mol Cell Biol. 8**,** 931-7.

Klionsky, D. J., et al., 2008a. Guidelines for the use and interpretation of assays for monitoring autophagy in higher eukaryotes. Autophagy. 4**,** 151-75.

Klionsky, D. J., et al., 2008b. Does bafilomycin A(1) block the fusion of autophagosomes with lysosomes? Autophagy. 4.

Klionsky, D. J., Emr, S. D., 2000. Autophagy as a regulated pathway of cellular degradation. Science. 290**,** 1717-21.

Kochl, R., et al., 2006. Microtubules facilitate autophagosome formation and fusion of autophagosomes with endosomes. Traffic. 7**,** 129-45.

Komatsu, M., et al., 2005. Impairment of starvation-induced and constitutive autophagy in Atg7-deficient mice. J Cell Biol. 169**,** 425-34.

Kuma, A., et al., 2004. The role of autophagy during the early neonatal starvation period. Nature. 432**,** 1032-6.

Kuma, A., et al., 2007. LC3, an autophagosome marker, can be incorporated into protein aggregates independent of autophagy: caution in the interpretation of LC3 localization. Autophagy. 3**,** 323-8.

Kuma, A., et al., 2002. Formation of the approximately 350-kDa Apg12-Apg5.Apg16 multimeric complex, mediated by Apg16 oligomerization, is essential for autophagy in yeast. J Biol Chem. 277**,** 18619-25.

Lee, I. H., et al., 2008. A role for the NAD-dependent deacetylase Sirt1 in the regulation of autophagy. Proc Natl Acad Sci U S A. 105**,** 3374-9.

Lee, S. B., et al., 2007. ATG1, an autophagy regulator, inhibits cell growth by negatively regulating S6 kinase. EMBO Rep. 8**,** 360-5.

Levine, B., Klionsky, D. J., 2004. Development by self-digestion: molecular mechanisms and biological functions of autophagy. Dev Cell. 6**,** 463-77.

Levine, B., Kroemer, G., 2008. Autophagy in the pathogenesis of disease. Cell. 132**,** 27-42.

Liang, C., et al., 2006. Autophagic and tumour suppressor activity of a novel Beclin1-binding protein UVRAG. Nat Cell Biol. 8**,** 688-99.

Liang, X. H., et al., 1999. Induction of autophagy and inhibition of tumorigenesis by beclin 1. Nature. 402**,** 672-6.

Liang, X. H., et al., 1998. Protection against fatal Sindbis virus encephalitis by beclin, a novel Bcl-2-interacting protein. J Virol. 72**,** 8586-96.

Lippincott-Schwartz, J., et al., 2003. Photobleaching and photoactivation: following protein dynamics in living cells. Nat Cell Biol. Suppl**,** S7-14.

Lippincott-Schwartz, J., Patterson, G. H., 2008. Fluorescent proteins for photoactivation experiments. Methods Cell Biol. 85**,** 45-61.

Liscum, L., Munn, N. J., 1999. Intracellular cholesterol transport. Biochim Biophys Acta. 1438**,** 19-37.

Lorenz, H., et al., 2006. Fluorescence protease protection of GFP chimeras to reveal protein topology and subcellular localization. Nat Methods. 3**,** 205-10.

Luebke, K. J., 1998. A FLASH of insight into cellular chemistry: genetically encoded labels for protein visualization in vivo. Chem Biol. 5**,** R317-22.

Lukyanov, K. A., et al., 2005. Innovation: Photoactivatable fluorescent proteins. Nat Rev Mol Cell Biol. 6**,** 885-91.

Lum, J. J., et al., 2005. Autophagy in metazoans: cell survival in the land of plenty. Nat Rev Mol Cell Biol. 6**,** 439-48.

Maddox, P. S., et al., 2003. Spinning disk confocal microscope system for rapid high-resolution, multimode, fluorescence speckle microscopy and green fluorescent protein imaging in living cells. Methods Enzymol. 360**,** 597-617.

Manley, S., et al., 2008. High-density mapping of single-molecule trajectories with photoactivated localization microscopy. Nat Methods. 5**,** 155-7.

Mari, M., Reggiori, F., 2007. Atg9 trafficking in the yeast Saccharomyces cerevisiae. Autophagy. 3**,** 145-8.

Meijer, A. J., Codogno, P., 2004. Regulation and role of autophagy in mammalian cells. Int J Biochem Cell Biol. 36**,** 2445-62.

Melendez, A., et al., 2003. Autophagy genes are essential for dauer development and life-span extension in C. elegans. Science. 301**,** 1387-91.

Mijaljica, D., et al., 2007. Different fates of mitochondria: alternative ways for degradation? Autophagy. 3**,** 4-9.

Mizushima, N., et al., 2003. Mouse Apg16L, a novel WD-repeat protein, targets to the autophagic isolation membrane with the Apg12-Apg5 conjugate. J Cell Sci. 116**,** 1679-88.

Mizushima, N., et al., 1998. A protein conjugation system essential for autophagy. Nature. 395**,** 395-8.

Mizushima, N., et al., 2001. Dissection of autophagosome formation using Apg5-deficient mouse embryonic stem cells. J Cell Biol. 152**,** 657-68.

Mizushima, N., et al., 2004. In vivo analysis of autophagy in response to nutrient starvation using transgenic mice expressing a fluorescent autophagosome marker. Mol Biol Cell. 15**,** 1101-11.

Muller-Taubenberger, A., Anderson, K. I., 2007. Recent advances using green and red fluorescent protein variants. Appl Microbiol Biotechnol. 77**,** 1-12.

Nakatogawa, H., et al., 2007. Atg8, a ubiquitin-like protein required for autophagosome formation, mediates membrane tethering and hemifusion. Cell. 130**,** 165-78.

Neuspiel, M., et al., 2008. Cargo-selected transport from the mitochondria to peroxisomes is mediated by vesicular carriers. Curr Biol. 18**,** 102-8.

Nixon, R. A., et al., 2005. Extensive involvement of autophagy in Alzheimer disease: an immuno-electron microscopy study. J Neuropathol Exp Neurol. 64**,** 113-22.

Ogata, M., et al., 2006. Autophagy is activated for cell survival after endoplasmic reticulum stress. Mol Cell Biol. 26**,** 9220-31.

Ohsumi, Y., 2001. Molecular dissection of autophagy: two ubiquitin-like systems. Nat Rev Mol Cell Biol. 2**,** 211-6.

Ott, C. M., Lingappa, V. R., 2002. Integral membrane protein biosynthesis: why topology is hard to predict. J Cell Sci. 115**,** 2003-9.

Paddock, S. W., 2000. Principles and practices of laser scanning confocal microscopy. Mol Biotechnol. 16**,** 127-49.

Paludan, C., et al., 2005. Endogenous MHC class II processing of a viral nuclear antigen after autophagy. Science. 307**,** 593-6.

Pankiv, S., et al., 2007. p62/SQSTM1 binds directly to Atg8/LC3 to facilitate degradation of ubiquitinated protein aggregates by autophagy. J Biol Chem. 282**,** 24131-45.

Patterson, G. H., 2008. Photoactivation and imaging of photoactivatable fluorescent proteins. Curr Protoc Cell Biol. Chapter 21**,** Unit 21 6.

Patterson, G. H., Lippincott-Schwartz, J., 2002. A photoactivatable GFP for selective photolabeling of proteins and cells. Science. 297**,** 1873-7.

Petiot, A., et al., 2000. Distinct classes of phosphatidylinositol 3'-kinases are involved in signaling pathways that control macroautophagy in HT-29 cells. J Biol Chem. 275**,** 992-8.

Pfeifer, U., 1977. Inhibition by insulin of the physiological autophagic breakdown of cell organelles. Acta Biol Med Ger. 36**,** 1691-4.

Pouyssegur, J., et al., 2006. Hypoxia signalling in cancer and approaches to enforce tumour regression. Nature. 441**,** 437-43.

Prendergast, F. G., Mann, K. G., 1978. Chemical and physical properties of aequorin and the green fluorescent protein isolated from Aequorea forskalea. Biochemistry. 17**,** 3448-53.

Presley, J. F., et al., 2002. Dissection of COPI and Arf1 dynamics in vivo and role in Golgi membrane transport. Nature. 417**,** 187-93.

Pyo, J. O., et al., 2005. Essential roles of Atg5 and FADD in autophagic cell death: dissection of autophagic cell death into vacuole formation and cell death. J Biol Chem. 280**,** 20722-9.

Ravikumar, B., et al., 2004. Inhibition of mTOR induces autophagy and reduces toxicity of polyglutamine expansions in fly and mouse models of Huntington disease. Nat Genet. 36**,** 585-95.

Reef, S., et al., 2006. A short mitochondrial form of p19ARF induces autophagy and caspase-independent cell death. Mol Cell. 22**,** 463-75.

Reggiori, F., et al., 2005. Atg9 cycles between mitochondria and the pre-autophagosomal structure in yeasts. Autophagy. 1**,** 101-9.

Reits, E. A., Neefjes, J. J., 2001. From fixed to FRAP: measuring protein mobility and activity in living cells. Nat Cell Biol. 3**,** E145-7.

Romano, A. H., Conway, T., 1996. Evolution of carbohydrate metabolic pathways. Res Microbiol. 147**,** 448-55.

Rubinsztein, D. C., et al., 2007. Potential therapeutic applications of autophagy. Nat Rev Drug Discov. 6**,** 304-12.

Sakaki, K., et al., 2008. Protein kinase Ctheta is required for autophagy in response to stress in the endoplasmic reticulum. J Biol Chem. 283**,** 15370-80.

Sanjuan, M. A., et al., 2007. Toll-like receptor signalling in macrophages links the autophagy pathway to phagocytosis. Nature. 450**,** 1253-7.

Sankaranarayanan, S., et al., 2000. The use of pHluorins for optical measurements of presynaptic activity. Biophys J. 79**,** 2199-208.

Schmidt, K., Nichols, B. J., 2004. A barrier to lateral diffusion in the cleavage furrow of dividing mammalian cells. Curr Biol. 14**,** 1002-6.

Schulz, I., 1990. Permeabilizing cells: some methods and applications for the study of intracellular processes. Methods Enzymol. 192**,** 280-300.

Scott, S. V., et al., 1996. Cytoplasm-to-vacuole targeting and autophagy employ the same machinery to deliver proteins to the yeast vacuole. Proc Natl Acad Sci U S A. 93**,** 12304-8.

Seglen, P. O., Gordon, P. B., 1982. 3-Methyladenine: specific inhibitor of autophagic/lysosomal protein degradation in isolated rat hepatocytes. Proc Natl Acad Sci U S A. 79**,** 1889-92.

Shaner, N. C., et al., 2005. A guide to choosing fluorescent proteins. Nat Methods. 2**,** 905-9.

Snapp, E. L., et al., 2003. Measuring protein mobility by photobleaching GFP chimeras in living cells. Curr Protoc Cell Biol. Chapter 21**,** Unit 21 1.

Sneve, M. L., et al., 2005. Comigration of two autophagosome-associated dehydrogenases on two-dimensional polyacrylamide gels. Autophagy. 1**,** 157-62.

Sorice, M., et al., 2000. Cardiolipin on the surface of apoptotic cells as a possible trigger for antiphospholipids antibodies. Clin Exp Immunol. 122**,** 277-84.

Suzuki, K., et al., 2004. Interrelationships among Atg proteins during autophagy in Saccharomyces cerevisiae. Yeast. 21**,** 1057-65.

Tadini-Buoninsegni, F., et al., 2008. Effects of high-affinity inhibitors on partial reactions, charge movements, and conformational States of the Ca2+ transport ATPase (sarco-endoplasmic reticulum Ca2+ ATPase). Mol Pharmacol. 73**,** 1134-40.

Takagaki, Y., et al., 1983. The membrane-embedded segment of cytochrome b5 as studied by cross-linking with photoactivatable phospholipids. J Biol Chem. 258**,** 9128-35.

Takahashi, Y., et al., 2007. Bif-1 interacts with Beclin 1 through UVRAG and regulates autophagy and tumorigenesis. Nat Cell Biol. 9**,** 1142-51.

Takeshige, K., et al., 1992. Autophagy in yeast demonstrated with proteinase-deficient mutants and conditions for its induction. J Cell Biol. 119**,** 301-11.

Tanida, I., et al., 2005. Lysosomal turnover, but not a cellular level, of endogenous LC3 is a marker for autophagy. Autophagy. 1**,** 84-91.

Tanida, I., et al., 2004. HsAtg4B/HsApg4B/autophagin-1 cleaves the carboxyl termini of three human Atg8 homologues and delipidates microtubule-associated protein light chain 3- and GABAA receptor-associated protein-phospholipid conjugates. J Biol Chem. 279**,** 36268-76.

Tasdemir, E., et al., 2008. Methods for assessing autophagy and autophagic cell death. Methods Mol Biol. 445**,** 29-76.

Teckman, J. H., Perlmutter, D. H., 2000. Retention of mutant alpha(1)-antitrypsin Z in endoplasmic reticulum is associated with an autophagic response. Am J Physiol Gastrointest Liver Physiol. 279**,** G961-74.

Terasaki, M., et al., 2001. Fluorescent staining of subcellular organelles: ER, Golgi complex, and mitochondria. Curr Protoc Cell Biol. Chapter 4**,** Unit 4 4.

Tsukada, M., Ohsumi, Y., 1993. Isolation and characterization of autophagy-defective mutants of Saccharomyces cerevisiae. FEBS Lett. 333**,** 169-74.

Vance, J. E., 2008. Phosphatidylserine and phosphatidylethanolamine in mammalian cells: two metabolically related aminophospholipids. J Lipid Res. 49**,** 1377-87.

White, J., Stelzer, E., 1999. Photobleaching GFP reveals protein dynamics inside live cells. Trends Cell Biol. 9**,** 61-5.

Williams, A., et al., 2008. Novel targets for Huntington's disease in an mTOR-independent autophagy pathway. Nat Chem Biol. 4**,** 295-305.

Willig, K. I., et al., 2006. Nanoscale resolution in GFP-based microscopy. Nat Methods. 3**,** 721-3.

Wolleschensky, R., et al., 2006. High-speed confocal fluorescence imaging with a novel line scanning microscope. J Biomed Opt. 11**,** 064011.

Xie, Z., Klionsky, D. J., 2007. Autophagosome formation: core machinery and adaptations. Nat Cell Biol. 9**,** 1102-9.

Xie, Z., et al., 2008. Atg8 Controls Phagophore Expansion during Autophagosome Formation. Mol Biol Cell. 19**,** 3290-8.

Yamamoto, A., et al., 1998. Bafilomycin A1 prevents maturation of autophagic vacuoles by inhibiting fusion between autophagosomes and lysosomes in rat hepatoma cell line, H-4-II-E cells. Cell Struct Funct. 23**,** 33-42.

Yorimitsu, T., Klionsky, D. J., 2005. Atg11 links cargo to the vesicle-forming machinery in the cytoplasm to vacuole targeting pathway. Mol Biol Cell. 16**,** 1593-605.

Young, A. R., et al., 2006. Starvation and ULK1-dependent cycling of mammalian Atg9 between the TGN and endosomes. J Cell Sci. 119**,** 3888-900.

Zhang, L., et al., 2007. Small molecule regulators of autophagy identified by an image-based high-throughput screen. Proc Natl Acad Sci U S A. 104**,** 19023-8.

Zimmer, M., 2002. Green fluorescent protein (GFP): applications, structure, and related photophysical behavior. Chem Rev. 102**,** 759-81.

Zucker, R. M., Price, O. T., 1999. Practical confocal microscopy and the evaluation of system performance. Methods. 18**,** 447-58.

Zucker, R. M., Price, O. T., 2001. Statistical evaluation of confocal microscopy images. Cytometry. 44**,** 295-308.